THE IMPACT OF CONFUSION ON HI SURVEYS AND THE ENVIRONMENTAL DEPENDENCE OF THE HI GALAXY POPULATION IN THE ALFALFA SURVEY

A Dissertation

Presented to the Faculty of the Graduate School

of Cornell University

in Partial Fulfillment of the Requirements for the Degree of

Doctor of Philosophy

by

Michael Gordon Jones

August 2016

THE IMPACT OF CONFUSION ON HI SURVEYS AND THE ENVIRONMENTAL DEPENDENCE OF THE HI GALAXY POPULATION IN THE ALFALFA SURVEY

Michael Gordon Jones, Ph.D.

Cornell University 2016

The ALFALFA (Arecibo Legacy Fast ALFA) survey is a blind radio survey of neutral hydrogen gas (HI) in nearby galaxies. The latest ALFALFA release is its 70% catalogue which contains over 20,000 high signal-to-noise extragalactic HI sources, the largest catalogue of HI-detected galaxies to date. As HI is detected through a spectral line this immediately provides a redshift for each galaxy, while the line width informs us of the projected rotation velocity, and finally the integrated flux can be used to estimate the total HI mass.

We use the ALFALFA galaxy-galaxy 2 point correlation function to predict the rate of source confusion in current and future HI surveys. Two sources become confused when their spatial extent on the sky overlaps within the observing telescope's beam (or synthesised beam) on the sky, and their line emission overlaps in redshift space. This has the potential to impact all of the parameters determined from these sources, therefore we assess how this may have influenced the current measurements of the HI galaxy mass function (HIMF) and predict how frequent source confusion will be in the next generation of surveys that will be more sensitive and probe out to higher redshifts.

Confusion also has the potential to impact another class of upcoming surveys,

those that aim to extend observations of HI galaxies to redshifts of order unity. Such surveys will likely require the use of stacking of non-detections in order to achieve this goal for normal galaxies, however, when targets are co-added the emission they are confused with is also co-added, creating a mass limit below which stacking cannot proceed. We derive an analytic expression that approximates this limit for a generic deep HI survey and show that this limit is indeed a concern for some planned surveys.

We also use the ALFALFA 70% catalogue to explore the dependence of the HIMF on galaxy environment. Existing studies have frequently found conflicting results, but now with ALFALFA with have a significantly larger sample than ever used before. We find evidence that the 'knee' mass of the Schechter function fit to the HIMF is dependent on local, but not large scale, environment, suggesting that a galaxy's parent halo may be the most important factor influencing its HI mass. We find no evidence of a corresponding shift in the low-mass slope of the HIMF, and discuss how this may be in conflict with some previous results.

Finally, we outline the progress thus far on the APPS (Arecibo Pisces Perseus Supercluster) survey, an ongoing targeted follow-up survey aimed at expanding the ALFALFA catalogue to lower HI masses in the Pisces-Perseus region, in order to map the peculiar velocity field and detect infall onto this linear overdensity.

BIOGRAPHICAL SKETCH

Michael Jones was born in Cambridge, UK, the youngest of four close-knit children. He grew up in the rural county of Norfolk and was initially home educated along with all his siblings, which mostly consisted of making dens and climbing trees. At the age of 7 he began attending the local village school, Eccles Primary, which at the time had a total of 36 pupils. Michael quickly took to maths and science, but much less so to reading and writing, which may occasionally be apparent in what follows. His father, a physics and chemistry teacher, would frequently show him experiments, invariably featuring sparks, flames or explosions, and this undoubtedly encouraged his curiosity in how the physical world works.

Growing up in a rural area meant Michael was always very fond of outdoor activities. He took every opportunity to run, cycle, hike, and play football (the one where you kick a round ball with your foot), and eventually settled on rugby as his primary sport.

At the age of 11, Michael left Eccles Primary and moved on to the local secondary school in Old Buckenham, a bustling hive of almost 500 pupils. After 5 years at Old Buckenham it was time to move on to Diss Sixth Form. At this point Michael was most excited to be leaving behind subjects like English, French and history to focus exclusively on physical sciences and mathematics for two years during his A-levels. After a solid performance in his A-levels and 5 nerve racking interviews, Michael was admitted to Fitzwilliam College, Cambridge, where he matriculated in 2007.

Michael studied for 4 years at Cambridge, obtaining both his bachelor's and master's degrees in natural sciences, with specialisation in astrophysics. Summer and master's research projects reaffirmed his choice continue in this field, and in 2011 he was accepted to Cornell's PhD program in astronomy.

While at Cornell Michael joined the ALFALFA team and became interested in the statistical aspects of the survey and the HI population of galaxies. Working with Profs. Martha Haynes and Riccardo Giovanelli, as well as Dr. Emmanouil Papastergis, Michael completed his PhD in 5 years and is now looking forward to the future and to a significantly warmer climate in Granada, Spain as a post-doctoral researcher with Prof. Lourdes Verdes-Montenegro, where he will focus on contrasting the HI properties of isolated galaxies with those in compact groups.

For my siblings, my oldest friends.

ACKNOWLEDGEMENTS

- Martha – There are many, many things to thank Martha for. I will address a few of the most important ones here. Firstly, I'm grateful that I was allowed to find my own way and choose what projects I wanted to work on; this was an important part of the PhD process for me. Martha and Riccardo also deserve an enormous amount of credit for protecting me and their other students from the mountain of repetitive work associated with a survey like ALFALFA. I played my part, but that part was small enough that it enhanced, rather than detracted from, my experience. Finally, I'd like to thank Martha for always advocating for me and her other students. She is a force to be reckoned with and you can be that bit more confident when you know she's on your side.
- Riccardo – In addition to being my second advisor, I would also like to thank Riccardo for all the source extraction he has done that makes the ALFALFA dataset a reality for everyone else. While many people have contributed to this effort over the years, none can compete with the titanic effort that he has put in, and this is the reason why the rest of us measure our source extraction rate in milli-Riccardos. I would also be remiss if I did not acknowledge Riccardo's incredibly dry sense of humour that always brought a chuckle to every group meeting.
- Luke – Since all the people below graduated, Luke has been my sole officemate for a few years now. We have constantly used each other as sounding

boards to discuss or complain about just about anything, and this is an invaluable resource. He is also to be commended for his appreciation of terrible puns, and has assisted me in educating Michael Lam of their brilliance as well. Between the two of us we always had things to say at group meetings, and I'm sorry I won't be around to do my share next year.

- Manolis – Manolis was the ideal older grad student to have in the group when I arrived. He commands an impressive affinity for clarity and explained a great deal to me before he graduated. He also authored a very detailed appendix to his dissertation that was key to my initial understanding of the HI mass function calculation. In addition to academic advice he also gave me (and continues to give me) plenty of life advice. The "three things" rule (never try to do more than three things simultaneously) is the golden rule for grad school, he was definitely right about that, however, I must still contend that food poisoning is actually a real thing!
- Betsey, Greg and Shan – Although I had less interaction with these three ALFALFA grad students, than with Manolis, they were all good role models and each taught me important things along the way.
- All of the ALFALFA team – Most of my work was based on ALFALFA catalogue which was ultimately made possible by a whole team of people who observed, flagged, extracted sources and matched them to optical counterparts. Without all of this for me to work with none of this dissertation would have been possible.
- Tyler, Jason, Patrick, Everett, Jeremy and Freddy – This group was always

willing to do things with me whether it be play football, go climbing (including ice climbing), or go on camping and hiking trips. These are some of the best times I've had over the past few years.

- Tyler, Michael and Ryan – For the most part, they were pretty good housemates over the past year, but even more than that I think they need acknowledging for being the original C-store crew (our group that made daily coffee and snack trips together). Our time at Cornell would have been quite different if that had never happened.
- Monica – Monica was always cheerful as well as super helpful. If ever I needed help with any grad school related form I always knew she'd be there to help and have a laugh at the same time.
- Other Cornell astronomy grad students – I found Cornell's astronomy department atmosphere to be very welcoming when I first arrived and I think it's excellent that the grad students do so much together. It's a genuinely nice group of people.
- Jim, Becky, Carolyn, Greg and Jackie – These people have really made Ithaca my home away from home. I know they're my family, but they have done so much more than I expected. I wish to thank them for the countless dinners, parties, bonfires, and especially for setting up the only Guy Fawkes party in Ithaca, plus so much more. I will miss all of them greatly.
- Schuyler (and Rosi) – I'm definitely not a dog person, but I have to admit that Schuyler is a pretty awesome animal and the way he lives his life is an inspiration to chill out a little more. And obviously if I mention Schuyler then

Joyce would be rather mad if I didn't also mention Rosi, the much smaller, scruffier, and significantly more uptight, second half of the duo.

- The Cornell Store, Manndible, the Dairy bar, and DP Dough – Thanks for providing snacks and food to help get me through.
- NSF and the Brinson Foundation – For most of my time at Cornell I was funded from Martha and Riccardo's NSF grants (AST-0607007 and AST-1107390), and much of my conference travel was funded by their grants from the Brinson Foundation.
- My parents – This has not been the easiest time for my mum and dad with both me and my brother moving 3,000 miles away, especially given our terrible record at keeping in touch. However, they never complained, never suggested that I shouldn't go, and have always supported me to proceed the way that I want to.
- Joyce – I left Joyce until last because I don't really know how to sum things up in an acknowledgement, so I'll just say this: While at Cornell I learnt so much, made so many friends, and had countless great experiences, but without a doubt Joyce was the most important part of my time here and I know she will be in the future as well.

TABLE OF CONTENTS

LIST OF TABLES

LIST OF FIGURES

CHAPTER 1

INTRODUCTION

The HI spectral line arises from the difference in energy of the quantum mechanical spins of the electron and proton in a neutral hydrogen (HI) atom either being aligned or anti-aligned. This energy difference is minute, releasing a photon of only 1420 MHz (or 21 cm wavelength) when the electron's spin flips from aligned to anti-aligned.

The coefficient of spontaneous emission is incredibly low, giving HI in the high energy spin state a half-life of approximately 10 million years. However, even at astrophysical densities particle collisions still occur on the order of every 100 years. Therefore, the two states of HI generally exist at thermodynamic equilibrium abundances in the interstellar medium. The weak rate of transitions also means that the HI line can only be seen emanating from astrophysical sources, which have enormous quantities of hydrogen, and has never been seen in a laboratory experiment. Detecting such a faint line in extragalactic objects necessitates either a very large telescope or a very long integration time. At present the largest single dish radio telescope in the world is the 305 m Arecibo telescope in Puerto Rico, and my thesis is mostly based on HI data from this telescope.

HI traces a very different portion of a galaxy than optical starlight. The HI line is emitted by neutral hydrogen that is at approximately 1000 K. Substantially below this temperature and the gas will tend to condense into molecular hydrogen;

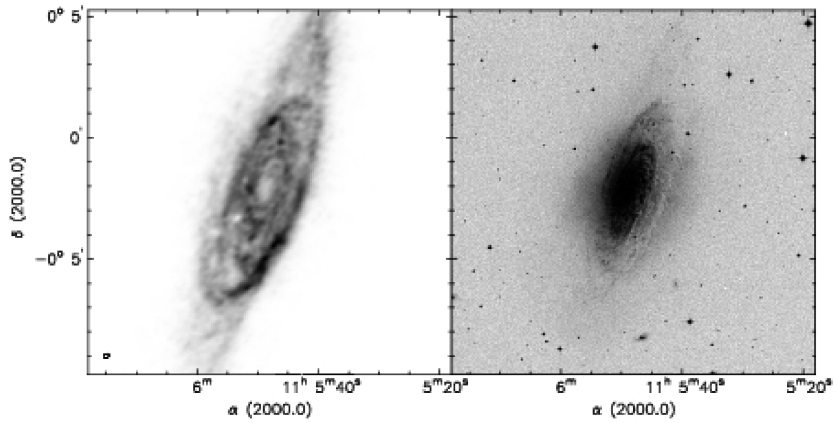

Figure 1.1: *Left*: THINGS HI moment 0 map of NGC 3521. This traces the amount of HI gas throughout the galaxy. *Right*: Optical image of NGC 3521 (from the Digitized Sky Survey) at the same scale. The HI traces the disc much further out than the optical starlight, and it also has a central hole where gas is dense enough to condense into H_2. Figure from Walter et al. (2008).

much above it, and it will become ionised. This neutral gas is effectively the reservoir of gas that a galaxy has to condense into molecular gas and then form stars. Figure 1.1 shows The HI Nearby Galaxy Survey (THINGS, Walter et al., 2008) map of the highly inclined spiral galaxy NGC 3521 (UGC 6150). As is immediately apparent from this image, the spiral structure of the disc can be traced a factor of 2 or more further out, compared to in optical image. There is also a prominent hole in the HI emission at the centre of the disc. This is a typical feature of spiral galaxies, as in this region the HI is typically dense enough and cool enough to form H_2.

The HI map in figure 1.1 has very fine spatial resolution, which allows us to see the detailed structure of the galactic disc. This is because it was taken using an interferometer, in this case the Very Large Array (VLA) in New Mexico, USA. By spacing many smaller dishes over several kilometres, interferometers

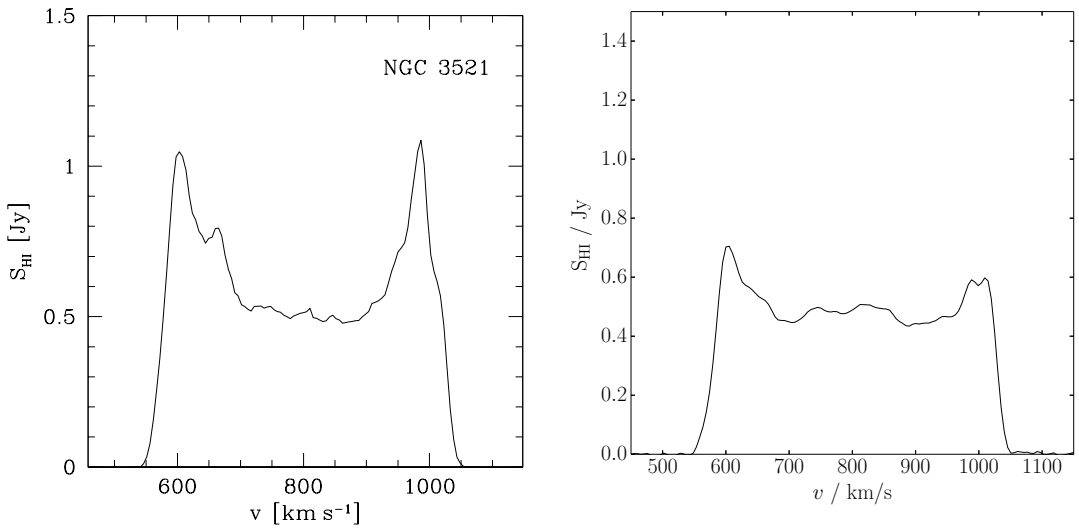

Figure 1.2: *Left*: THINGS HI spectrum of NGC 3521 (Walter et al., 2008). *Right*: ALFALFA HI spectrum of NGC 3521. Both the THINGS and ALFALFA spectra of this galaxy are very similar, however the ALFALFA spectrum took about 80 seconds to collect with Arecibo, whereas the THINGS spectrum took about 21 hours with the VLA.

can achieve very high angular resolution. However, they must observe for a long time to achieve a comparable sensitivity to a large single dish telescope, as sensitivity scales directly with collecting area. Arecibo does not have the resolution to recover the HI density map on the plane of the sky (as THINGS does), however, it can collect spectra of most HI-rich galaxies in the nearby Universe in an observation lasting on the order of a minute. Thus, this extreme sensitivity, provided by its 305 m diameter, allows for blind searches for HI galaxies covering a larger fraction of the sky. Figure 1.2 compares the VLA (THINGS) and Arecibo (ALFALFA, Arecibo Legacy Fast ALFA survey) spectra of NGC 3521. The VLA spectrum is the result of many observations with different dish configurations totalling about 21 hours; the spectrum observed with Arecibo was collected with two ~40 second

passes with the ALFA (Arecibo L-band Feed Array) instrument. The two spectra are very similar, with the most noticeable difference being the smoothing out of the peaks in the Arecibo spectrum (caused by its lower angular resolution). This double horned profile shape is the classic shape formed by a spectral line detected throughout the disc of an inclined spiral galaxy. The lower velocity component is formed due to the Doppler shifted emission from the side of the disc that is rotating towards us, while the higher velocity horn is from the side rotating away from us. Either of these spectra can be used to generate equivalent global HI properties of this galaxy, and in this way a blind HI survey can achieve a census of the HI galaxy population in the local Universe.

The ALFALFA survey is a blind survey covering approximately 1/6th of the sky (Giovanelli et al., 2005), which detects galaxies out to a redshift of 0.06 through the 21 cm radio emission of neutral hydrogen (HI). This survey was carried out over 7 years (2005-2012), a total of 4,742 hours of observing, with the 305 m Arecibo single-dish telescope in Puerto Rico. ALFALFA is the current cutting edge of surveys of its type and constitutes the largest uniform catalogue of extragalactic HI detections by an order of magnitude (~30,000), the principle dataset of my PhD research.

HI surveys offer a different view of the galaxy population compared to other wide area surveys, such as SDSS (Sloan Digital Sky Survey, York et al., 2000) in the optical and 2MASS (2 Micron All Sky Survey, Skrutskie et al., 2006) in the infrared. Some of the largest and brightness galaxies in SDSS and 2MASS are

invisible to ALFALFA due to their lack of neutral gas, whereas some of the faintest galaxies that were missed from those surveys are clear HI sources (e.g. Leo P, Giovanelli et al., 2013). While shorter wavelength surveys predominantly trace the current stellar components of galaxies, HI observations open a window to the reservoir of neutral gas available to fuel molecular cloud formation and star formation in the long term. In order to construct a complete picture of galaxy formation and evolution using simulations and semi-analytic models we must first understand the properties of the galaxy population that exists today. Without surveys like ALFALFA the neutral gas properties of the population produced by galaxy evolution models would be largely unconstrained, and the simulated gas reservoirs would be free to behave in potentially unphysical ways.

Partially due to the low intrinsic brightness of the HI line, the scope of blind HI surveys have lagged somewhat behind those in the optical. The development of feed horn arrays (effectively multi-pixel radio cameras) dramatically improved the survey speed of single-dish radio telescopes and allowed the first wide-field surveys to be carried out in a reasonable length of time. HIPASS (HI Parkes All Sky Survey, Barnes et al., 2001; Meyer et al., 2004), ALFALFA's immediate predecessor, was a blind survey carried out with a 13 pixel feed horn array on the 64 m Parkes radio telescope in New South Wales, Australia. This was arguably the first time that the form of the HI mass function (HIMF) had been tightly constrained[i] (Zwaan et al., 2005). However, due to its low mean redshift ($z_{\rm mean}$ = 0.01)

[i]The HI mass function is the distribution of HI galaxy masses – that is, the intrinsic number density of galaxies of a given HI mass.

HIPASS's measurements were dominated by the local volume, while its low sensitivity meant that very few truly low-mass galaxies were detected. In turn, ALFA (Arecibo L-band Feed Array), Arecibo's 7 pixel feed horn array, allowed Arecibo to survey a large fraction of the sky in years, rather than decades. The superior resolution and sensitivity afforded by Arecibo's diameter and collecting area, and the wider bandpass chosen for ALFALFA, largely resolved these difficulties present in HIPASS, giving a cosmologically fair account of the HI content of the $z \approx 0$ Universe.

The HIMF of the ALFALFA 70% catalogue is shown in figure 1.3 (upper panel), along with the observed source counts (lower panel). Measuring the HIMF with ALFALFA can be thought of as equivalent to performing a census of humans on Earth, where the mass of each person (galaxy) is recorded. While the masses of people on Earth would take the form of a Gaussian distribution, the HIMF takes a Schechter function form: a rising power law towards low masses with an exponential drop off at the highest masses (figure 1.3, upper panel). The slope of this power law reveals how many more galaxies exist at progressively lower HI masses, while the turnover (or 'knee') mass represents the characteristic HI mass of the galaxies that contain most of the HI in the Universe. When inferring the distribution in the upper panel of figure 1.3 from the observed distribution in the lower panel, the real challenge is in correcting for the effects of large scale structure (LSS) in the Universe and the survey's sensitivity. In the human census analogy, imagine that the survey was global, but was based in Washington DC. It might be expected that the fraction of people who respond would decline with

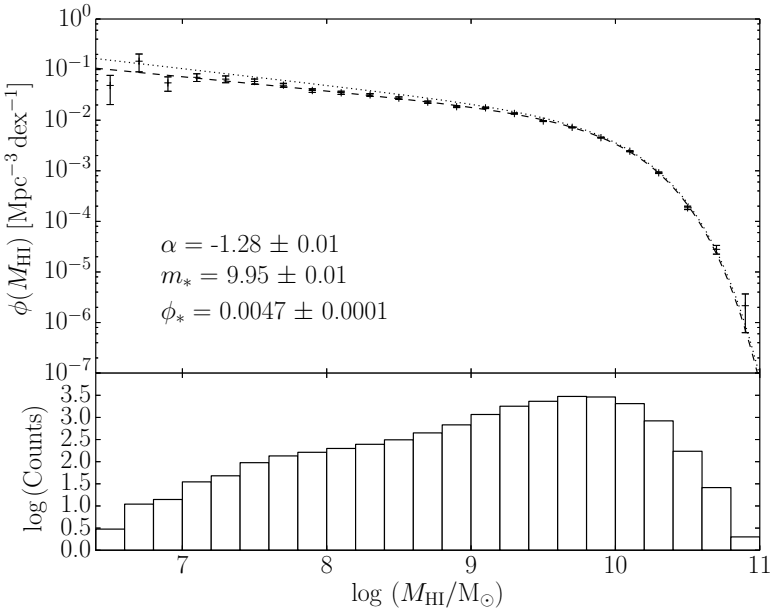

Figure 1.3: *Bottom*: The observed number counts of high signal-to-noise ALFALFA 70% sources in logarithmic bins of their HI mass. *Top*: The inferred intrinsic number density of galaxies as a function of their HI mass (i.e. the HIMF) after observational selection effects are accounted for. The error bars indicate the Poisson counting errors of the data, the dashed line is the Schechter function fit to the data, and the dotted line is the Schechter function fit to the ALFALFA 40% catalogue, which showed a slightly steeper low-mass slope.

increasing distance from Washington. In order to make the census representative of the whole world this response rate effect must be corrected for. Furthermore, it might be particularly difficult to get responses from children (who tend to be much less massive than adults) without expending significant resources that may only be available in the immediate vicinity of Washington. In the case of ALFALFA these effects are simply that the more distant a galaxy is the harder it is to detect, and the less massive it is the harder it is to detect. Therefore, low-mass

and distant galaxies are underrepresented in the observed sample. This effect has a further complication because galaxies in different parts of the Universe are not exactly equivalent, just as the average mass of people in different countries are not going to be exactly the same. In the census the response rate from the Netherlands would likely be much higher than that from Japan (because it is much closer to Washington). Dutch people are on average much taller than Japanese people, so would be expected to be more massive, while Japan is much more densely populated than the Netherlands, so the total number of responses may still be higher. Equivalent effects resulting from dense clusters of galaxies, where many sources are close together, but can remove and destroy each others' neutral gas (thereby reducing their HI mass), must be corrected for as well when calculating the HIMF.

The HIMF is of fundamental importance for our understanding of the galaxy population. In the field in low-mass galaxies HI becomes the dominant baryonic component of a galaxy (Huang et al., 2012a) and quantifying the statistics of this population is vital to understanding how the baryonic portion of a galaxy is associated with its host dark matter (DM) halo in the case of dwarf galaxies, the most numerous galaxies in the Universe. The HIMF at all masses also provides an important constraint, in addition to the galaxy luminosity function, on hydrodynamic cosmological simulations. The populations of galaxies that these simulations produce must simultaneously match not just the stellar properties of real galaxies, but also the distribution of their gas reservoir masses, as well as other properties constrained by HI observations, such as the HI galaxy rotation velocity width function (Papastergis et al., 2011, 2015) and being anti-biased with the DM

halos (Martin et al., 2012). In the near future the scope of the HIMF will be extended to a constraint in 3 dimensions, as with new facilities it will soon become measurable beyond $z \approx 0$.

In addition to evolving over time, the HIMF is also expected to shift form based on galaxy environment. As the HI extent of spiral galaxies is typically much greater (by a factor of a few) than their stellar discs, it is expected that interactions between galaxies would have a marked impact on their HI content, and there are numerous observational examples of HI tidal tails and bridges demonstrating this. However, the environmental dependence of the HIMF remains relatively poorly studied and unclear. Several studied of individual galaxy groups have found their HIMFs to have flat low-mass slopes[ii] (Verheijen et al., 2001; Kovac, Oosterloo & van der Hulst, 2005; Freeland, Stilp & Wilcots, 2009; Pisano et al., 2011), but there are also select studies that find groups with slopes steeper than in the field (e.g. Stierwalt et al., 2009), whereas wide-field studies of environmental trends in the HIMF have found either very little dependence in the low-mass slope (Springob, Haynes & Giovanelli, 2005; Moorman et al., 2014), or a dependence in the opposite direction to what's implied by the studies of groups (Zwaan et al., 2005). Forming a clearer understanding of how the HIMF is impacted by a galaxy's environment will not only provide additional constraints for simulations and models of galaxy evolution, but will also provide a more complete picture of how a gas-rich galaxy may transform and lose it gas reservoir over the course of

[ii]The low-mass slope determines the relative abundance of progressively lower mass galaxies. A flat slope corresponds to a uniform distribution over all low masses, whereas a steep slope means lower mass galaxies are much more common.

its life.

In the coming years HI surveys will be revolutionised once again by the development of phased array feeds and the construction of SKA-pathfinder (Square Kilometre Array) facilities. The currently proposed surveys will be carried out using the APERTIF instrument (APERture Tile In Focus) on WSRT (Westerbork Synthesis Radio Telescope) in the Netherlands, MeerKAT in South Africa, the ASKAP (Australian SKA Pathfinder) telescope, and the VLA (Very Large Array) in New Mexico, USA. The proposed blind HI surveys fall into three categories:

1. Shallow, wide area surveys that will cover many thousands of deg^2 and have sensitivities a few times that of ALFALFA. Examples are WALLABY (Wide-field ASKAP L-band Legacy All-sky Blind surveY) and WNSHS (Westerbork Northern Sky HI Survey). These surveys will extend the census of HI galaxies that ALFALFA has performed to map almost the entire sky and will begin to detect low-mass HI galaxies outside of the local volume for the first time in a blind survey.

2. Medium-deep surveys that will cover hundreds of deg^2 and have sensitivities an order of magnitude better than ALFALFA. Examples are DINGO (Deep Investigation of Neutral Gas Origins) with ASKAP and the medium-deep survey with APERTIF. The improved depth and sensitivity of these survey will detect many low-mass galaxies in targeted regions outside the local volume and will begin to be capable of measuring the evolution in the shape of the HIMF with redshift.

3. Ultra-deep surveys that will cover a few deg^2 (usually just a single pointing) and aim to detect HI galaxies out to a redshift of order unity. Examples are CHILES (Cosmos HI Large Extragalactic Survey) with the VLA (the only one currently in progress), LADUMA (Looking At the Distance Universe with MeerKAT), and DINGO UDEEP.

A key goal of these surveys will be to constrain how the HI content of the Universe changes with redshift, and to understand what are the corresponding changes to the form of the HIMF as the galaxy population evolves between $z \approx 1$ and $z \approx 0$. This will transform the existing constraint of HI galaxy population from the existing present day constraint, to one that varies as a function of the age of the Universe. Such a constraint will further inform galaxy evolution models by providing them with a target as they progress, rather than simply an end goal that may be reached through a number of evolutionary paths.

A potential difficulty that these surveys may face is that of source confusion, the blending together of adjacent sources which are closer together in angular separation than a (synthesised) beam width and with HI line emission that overlaps in velocity (redshift) space. The impact of confusion on HI surveys has been little studied as is usually considered an almost negligible effect. Even for surveys like HIPASS and ALFALFA, only a few percent of the sources were confused. However, as HI surveys become more sensitive and probe higher redshifts, it is non-trivial to assess whether this will remain the case. In Chapter 2 we investigate how frequent source confusion will be for the first two classes of surveys listed above,

and estimate what impact confusion already has on our low redshift constraints on the HIMF from ALFALFA and HIPASS. Chapter 3 focuses on the third class of upcoming HI surveys. Due to the intrinsic faintness of the HI line these surveys will need to integrate on a single pointing for thousands of hours, and even then will likely still require stacking of non-detections to be capable of detecting normal HI galaxies at $z \sim 1$. We develop an analytic model based on the ALFALFA correlation function to predict the contribution of confusion to a stacked spectrum and assess at what point this will limit a generic survey's capabilities.

In Chapter 4 we return to the original motivation, the HI mass function, and investigate its environmental dependence in the ALFALFA 70% catalogue. We define environment based on the neighbour density around ALFALFA sources in both SDSS and 2MRS (2MASS Redshift Survey, Huchra et al., 2012), giving local and larger scale definitions of environment. In Chapter 5 we describe the ongoing APPS (Arecibo Pisces-Perseus Supercluster) survey, of which I am PI. This survey is making a deeper catalogue of HI sources (than ALFALFA) in the exceptional environment of the Pisces-Perseus filament, which stretches for tens of degrees across the sky. Using this dataset we aim to make a robust measurement of the infall onto this filament and in doing so obtain an accurate measurement of its dynamical mass. Finally, in Chapter 6 we summarise the conclusions and outline future directions in Chapter 7.

CHAPTER 2

SPECTROSCOPIC CONFUSION: ITS IMPACT ON CURRENT AND FUTURE EXTRAGALACTIC HI SURVEYS

2.1 Introduction

Source confusion is an issue for all galaxy surveys as blended sources lead to incorrect fluxes, masses, sizes, velocity widths and of course, number counts. In the submillimetre, source confusion is common as the surveys typically have poor resolution (compared to optical) and are at high redshift where source density is much higher; as a result submillimetre sources frequently overlap on the sky, often multiple times (e.g. Nguyen et al., 2010). In optical surveys, the high angular resolution and relatively low redshift (compared to submillimetre) makes confusion much less common, with it usually only occurring in the direction of clusters or in interacting systems (where the confusion is physical, not due to survey limitations).

If an optical survey had the resolution of a single dish HI survey, it would be impossible to pick out individual galaxies, every source would be confused, multiple times. It is only because HI astronomy is intrinsically spectroscopic that such 21cm surveys are possible, and confusion is actually uncommon. In this sense HI surveys present a unique variant of confusion.

This chapter is an adapted version of the published article Jones et al. (2015).

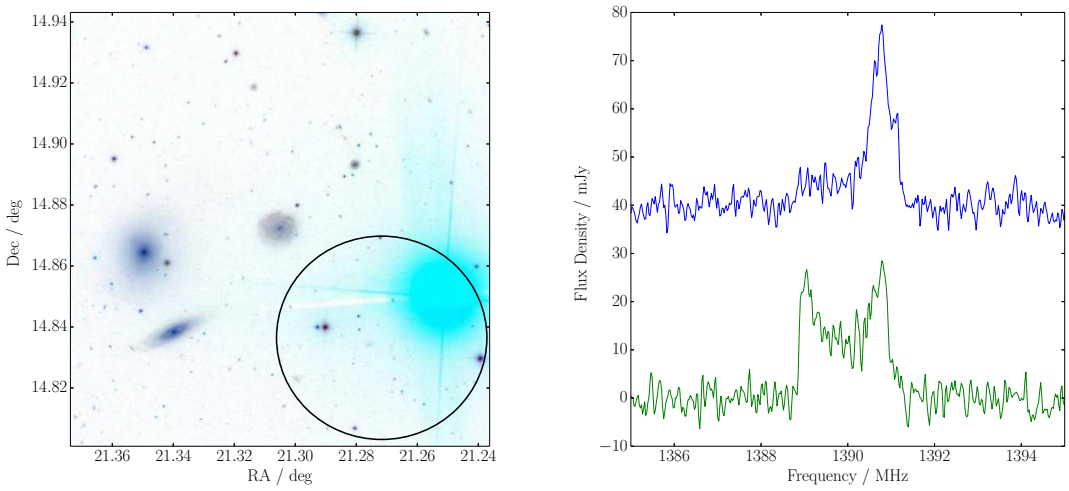

Figure 2.1: The optical image (left) from the SDSS DR10 (http://skyserver.sdss3.org/dr10/en/tools/chart/image.aspx, Ahn et al. (2014)) shows three galaxies; UGC978 and UGC983, with their respective ALFALFA spectra (right), and an early-type galaxy to the east, which ALFALFA does not detect. UGC978 is the central, face on spiral, its spectrum is the upper (blue), narrow profile, vertically offset by 40 mJy. UGC983 is the edge-on late-type galaxy to the south-east, associated with the lower (green), broad spectrum. The dark circle represents the ALFA beam on the sky (here taken to be a conservative 4'). Low levels of confusion are clear in the spectrum of UGC978, where there is excess emission over the velocity range of UGC983.

Unlike in the optical or submillimetre, galaxies are essentially transparent to 21cm radiation (e.g. Giovanelli et al., 1994). This means that 2-dimensional overlap on the plane of the sky is not a sufficient condition for sources to be confused. As well as overlap on the sky, the emission must overlap in redshift space. That is to say, that the sum of the observed velocity widths of the sources must be greater than twice their separation in redshift. As in most cases HI galaxies subtend an angle smaller than the telescope beam, a conservative condition for overlap on the sky would be if the two sources are within a beam diameter of each other. If both

these conditions are met then the two sources will be confused to some degree.

Depending on the severity of the blend, confused sources may be extracted as single, or separate sources. However, in both cases this will introduce bias. When extracted as one source, that one source will have the flux (mass) of the combined sources, the velocity width may be increased, and the position of peak emission may be altered, potentially effecting the redshift and misleading the process of identifying a counterpart at other wavelengths. When extracted separately, all the same issues are possible to a lesser degree, as flux can bleed from one source to another. This also introduces an additional bias, as some flux (mass) is counted multiple times.

These biases can potentially influence the global data products of such surveys; correlation functions (CF), HI mass functions (HIMF), and HI velocity width functions (WF). While the CF will only be affected on small scales, the effect on the HIMF and WF is less straightforward. Furthermore, as the rate of confusion will depend on the physical size of the telescope beam at a given redshift, as well as the channel width, such biases will be dependent on redshift and survey instrument, likely leading to different surveys harbouring different biases in these functions used to describe and test cosmology and the growth of structure.

Recent works such as Moorman et al. (2014), Zwaan et al. (2005), and Springob, Haynes & Giovanelli (2005) have begun to look for environmental dependence of the HIMF. Such a dependence would be expected from a ΛCDM model of structure growth, as voids are expected to have an excess of low mass halos relative to

filaments (e.g. Peebles, 2001). However, confusion will likely also be influenced by environment, with more blends occurring in high density regions. It is necessary to have a more complete understanding of confusion in order to be sure any trends observed are really cosmological in origin.

With the commissioning of Square Kilometre Array precursors, many large area, blind surveys are expected. While there have been some estimates of confusion for these surveys (e.g. Duffy, Moss & Staveley-Smith, 2012; Duffy et al., 2012), it has primarily (as with current surveys) been ignored under the assumption that it will not have a significant impact. Duffy, Moss & Staveley-Smith (2012) (hereinafter DMS12) used a 1-dimensional CF and a fixed velocity range to make an estimate of the rate of confusion around the 'knee'-mass of the HIMF, while Duffy et al. (2012) used semi-analytic models to populate halos from N-body simulations with HI gas, from which they derived an array of predictions for upcoming ASKAP (Australian Square Kilometre Array Pathfinder) surveys, including estimates of confusion. However, neither of these studies estimated the potential impact on the measurement of the HIMF.

Here we take an alternative approach, using both the 2-dimensional CF and mass-velocity width function (MWF) to derive an integral expression for the rate of confusion at a given distance, for any survey based on its resolution, depth and rms noise level. Present and future surveys are also simulated by drawing HI masses and velocity widths from the MWF, while neighbour separations are drawn from the 2D CF, allowing us to calculate the HIMF for confused and un-

confused cases.

Our primary dataset, from which we derive the properties of our model, consists of the 40% (α.40) catalogue (Haynes et al., 2011) from the Arecibo Legacy Fast ALFA (Arecibo L-band Feed Array), or ALFALFA, survey (Giovanelli et al., 2005), but we also make extensive use of the HI Parkes All Sky Survey (HIPASS, Barnes et al., 2001), to test our model and make comparisons. The ALFALFA survey, which has now completed data acquisition, covers approximately 6900 sq deg of sky, detects HI galaxies out to a redshift of 0.06, and was carried out using the 305m Arecibo telescope in Puerto Rico. Observations were completed in October 2012, with an average 'open shutter' time efficiency of greater than 95% including all startup, shutdown and calibration procedures. The ALFALFA team are currently reducing and extracting sources from the remaining dataset. HIPASS was carried out with the 64m Parkes telescope in New South Wales, and covers a greater area of sky than ALFALFA (approximately a hemisphere), but is less deep, detecting galaxies out to a redshift of 0.04. The α.40 catalogue contains 11,941 high S/N extragalactic sources, almost all of which have optical counterparts identified in the Sloan Digital Sky Survey DR7 (Abazajian et al., 2009), and the HIPASS catalogue HICAT (Meyer et al., 2004; Zwaan et al., 2004) contains 4,315 sources.

The following section describes the model used to predict confusion rates for general surveys, and discusses how the relevant properties are determined from the α.40 catalogue. In section 2.3 we display the results of our model, compare them to existing surveys, explore the effect confusion has on the HIMF, discuss

predictions for proposed upcoming surveys, and evaluate the limitations confusion places on single dish telescopes. Finally, section 2.4 outlines our conclusions and recommendations for dealing with confusion.

2.2 Modelling Confusion

Unlike optical or submillimetre surveys, in HI radio surveys confusion must be spectroscopic; it requires overlap both on the plane of the sky and in velocity space. An example of two confused sources from the α.40 catalogue is shown in figure 2.1. The galaxy in the centre of the frame is a face on spiral galaxy (UGC978), with a narrow profile (due to the projection), however there is a clear excess contribution (at lower frequency than the main peak of emission) that is coincident in frequency with the profile of another nearby galaxy (UGC983) within the beam. If the two galaxies were separated by an angular distance greater than the diameter of the beam, they would not be confused as flux could not be simultaneously received from both sources (ignoring the possibility of flux entering from spatial sidelobes). They would also not be confused if their redshifts were different by an amount larger than half the sum of their velocity widths, as then their emission would not be overlapping in frequency. This would still be true even if they were in contact on the plane of the sky.

The model of confusion will be explained by beginning with an idealised case and replacing each component until a realistic model is reached. The details of

the fits used to describe the correlation function, mass-width function and the detection limit can be found in the appendix.

To model how frequently this kind of dual overlap occurs, consider a Universe where all galaxies are the same mass (M_0), with the same projected velocity width (W_0), and are distributed randomly in 3D space with a mean number density n_0. In order for two galaxies to be blended in a survey they would need to be both closer together in projected linear distance (κ) than the linear diameter of the beam at the distance to the galaxies, $D_{\text{beam}}(d)$, and closer together along the line-of-sight (β) than the effective radial separation, W_0/H_0 (where H_0 is the Hubble constant, $\sim 70\,\text{km}\,\text{s}^{-1}\,\text{Mpc}^{-1}$).

The diameter of the telescope beam, rather than its radius, is used because the surveys considered are blind, meaning that in general a source can be anywhere within the beam, and so other emission from anywhere within a beam's width of that source could potentially contribute to its measured flux. The maximum line-of-sight separation, W_0/H_0, results from the requirement that the velocity (or equivalently, redshift) difference between the two sources must be less than half the sum of their velocity widths, in order for their velocity profiles to overlap (see figure 2.1). Thus, the criteria for two sources to be confused are:

$$\kappa < \Theta_{\text{beam}} d \tag{2.1}$$

$$-\frac{W_0}{H_0} < \beta < \frac{W_0}{H_0} \tag{2.2}$$

where Θ_{beam} is the angular diameter of the telescope beam, and d is the comoving distance to the central source. Here the phrase "central source" refers to the source

at the centre of the cylindrical volume being considered, this does not necessarily imply that it was at the centre of the beam when detected.

According to the Poisson distribution, the probability of a blend occurring (i.e. one or more galaxies lying in the cylindrical volume defined by equations 2.1 & 2.2) is:

$$P(\text{blend}) = 1 - e^{-\langle N \rangle}, \tag{2.3}$$

where $\langle N \rangle$ is the average number of additional sources expected to be found within the relevant cylindrical volume around the central source. In this model $\langle N \rangle$ can be found simply by multiplying the number density of sources by the cylindrical volume:

$$\langle N \rangle = 2\pi n_0 \Theta_{\text{beam}}^2 d^2 \frac{W_0}{H_0}. \tag{2.4}$$

Within this uniform model $\langle N \rangle$ grows quadratically with distance, as the volume increases with the square of the physical size of the beam.

This is the most basic model of spectroscopic confusion, and in order to construct a more comprehensive model each component must be realistically accounted for. Firstly, to address the fact that the Universe is not uniform on the scale of galaxy neighbour separations we must employ the correlation function (CF), the excess probability (above random) of two galaxies being separated by a given distance. Papastergis et al. (2013) measured the CF of the $\alpha.40$ dataset, which is plotted in figure 2.2 along with our 2D fit. The κ-direction corresponds to linear separations perpendicular to the line-of-sight, and the β-direction corresponds to separations along the line-of-sight, both are measured in Mpc.

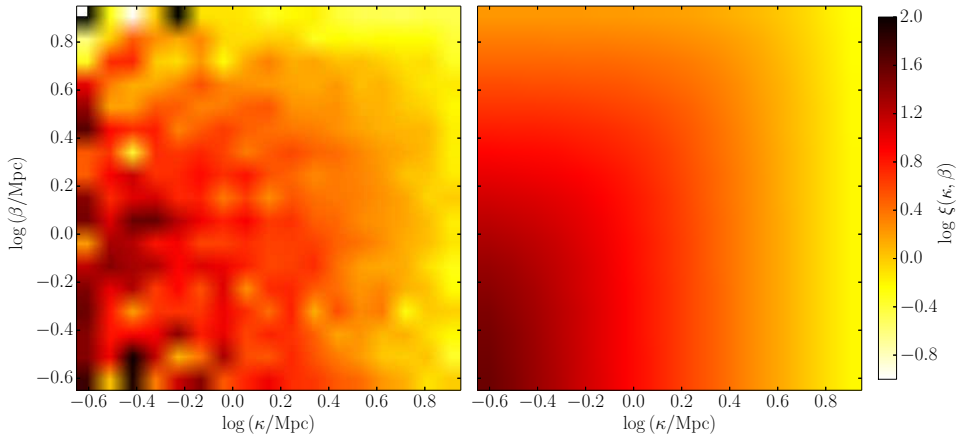

Figure 2.2: The 2-dimensional correlation function of the ALFALFA 40% sample (left), calculated by Papastergis et al. (2013), and our fit using an elliptical shaped function in the projected separation - line-of-sight velocity (κ-β) plane (right). The slight elongation in the velocity direction indicates a weak 'finger of god' effect.

The inclusion of the CF, $\xi(\kappa,\beta)$, alters the calculation of the occurrence rate, $\langle N \rangle$. When evaluating the integral over the volume defined by the beam and maximum possible line-of-sight separation given the velocity widths, the probability that a galaxy will be found at any given point is now multiplied by $1+\xi(\kappa,\beta)$. This gives the occurrence rate as

$$\langle N \rangle = 2n_0 \int_0^{\frac{W_0}{H_0}} \int_0^{\Theta_{\rm beam} d} 2\pi\kappa \, (1 + \xi(\kappa,\beta)) \, {\rm d}\kappa \, {\rm d}\beta. \tag{2.5}$$

Next, consider galaxy masses and velocity widths. Rather than fixed values they should be drawn from distributions representative of the intrinsic properties of HI galaxies. For masses this distribution is the HIMF ($\phi(M)$), and for velocity widths it is the WF. However, since the two properties are not independent

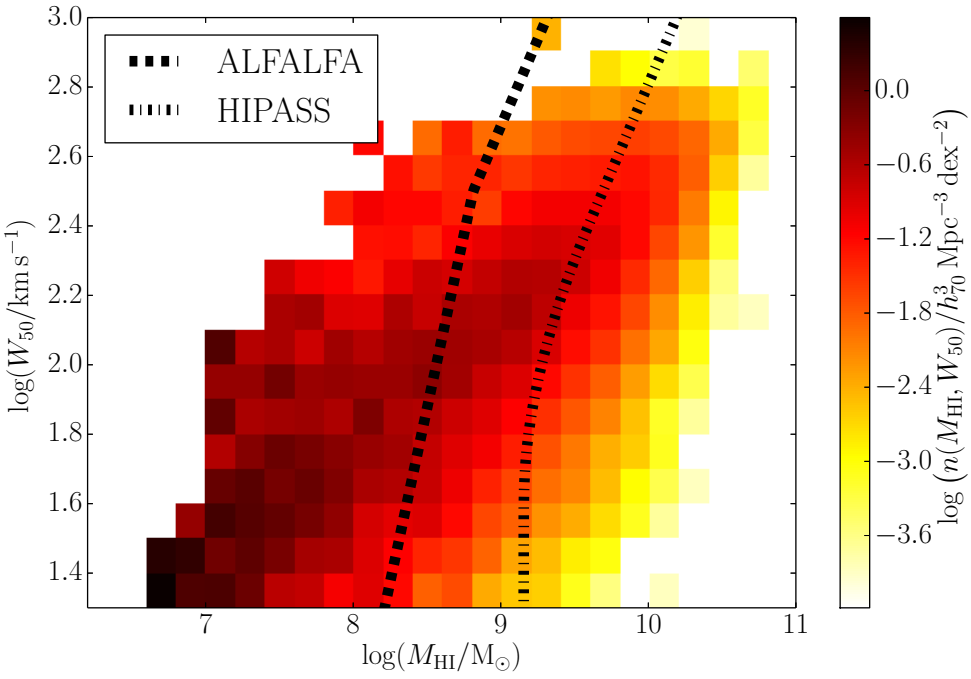

Figure 2.3: The ALFALFA mass-width function (see appendix of Papastergis et al. (2015)). Each pixel represents the intrinsic number density of HI galaxies with those mass and velocity width properties. The HIMF is the integral through all velocities, and the mass conditional velocity width function (MCWF), is a vertical slice at the relevant mass. The ALFALFA and HIPASS 50% completeness limits at 50 Mpc are shown as dashed and dot-dash lines, respectively (Haynes et al., 2011; Zwaan et al., 2004). Integrals over all detectable sources cover all the space to the right of these lines.

the mass conditional velocity width function (normalised such that it integrates to unity over all widths) $p(W|M)$, is the appropriate distribution to use. We use the ALFALFA HIMF as calculated by Martin et al. (2010), and follow a similar procedure to the appendix of that paper to calculate the mass conditional width function (MCWF), the details of which can be found in the appendix.

The ALFALFA mass-width function (MWF) is shown in figure 2.3. The HIMF

is this function integrated through all possible velocity widths, whereas the MCWF can be thought of as a slice through all velocities, at a particular mass. The ALFALFA 50% completeness limit (Haynes et al., 2011) at a particular distance (50 Mpc) is shown as the dashed black line, and the equivalent limit for HIPASS is the dash-dot black line Zwaan et al. (2004). When integrating over all detectable masses and velocity widths, as we will do below, the integral simply covers everything to the right and below the appropriate line.

Now that there are a range of possible masses and velocity widths for the second galaxy, instead of multiplying by n_0 in the expression for $\langle N \rangle$, all possible masses and widths, weighted by the probability of them occurring, must be integrated through. Thus, the occurrence rate now becomes

$$\begin{aligned} \langle N \rangle &= 2 \int_{W_{\min}}^{W_{\max}} \int_{M_{\lim(d,W_2)}}^{M_{\max}} \phi(M_2) p(W_2|M_2) \\ &\quad \int_0^{\frac{W_1+W_2}{2H_0}} \int_0^{\Theta_{\rm beam} d} 2\pi\kappa \, (1 + \xi(\kappa, \beta)) \\ &\quad \mathrm{d}\kappa \, \mathrm{d}\beta \, \mathrm{d}M_2 \, \mathrm{d}W_2, \end{aligned} \tag{2.6}$$

where W_1 and W_2 are the velocity widths of the central galaxy and the galaxy it is potentially blended with, and M_2 is the HI mass of this second galaxy. $W_{\min}$ and $W_{\max}$ are the limiting velocity widths, taken to be 15 and 1000 km s^{-1} respectively, $M_{\max}$ is the maximum HI mass considered (10^{11}M$_\odot$), and $M_{\min}(d, W)$ is the minimum detectable mass for a given velocity width, at a given distance (although an absolute minimum is set at $10^{6.2}$M$_\odot$). As before, $\langle N \rangle$ can be used to estimate the probability of a blend: $P(\text{blend}) = 1 - e^{-\langle N \rangle}$.

Implementing realistic values of mass, velocity width, and the detection limit have two important effects. The line-of-sight separation that can result in confusion will now be dependent on the velocity widths of each pair of galaxies that might be confused. Thus, similarly to equation 2.6 we must integrate through all possible masses and widths for the central galaxy, with each mass and width weighted appropriately, and again truncating the integral at the detection limit. This gives our final model as:

$$P(\text{blend}|d) = \frac{1}{n_{\text{Det}}(d)} \int_{W_{\min}}^{W_{\max}} \int_{M_{\lim}(d,W_1)}^{M_{\max}} \phi(M_1)\, p(W_1|M_1) \left[1 - e^{-\langle N(d,W_1)\rangle}\right] \mathrm{d}M_1\, \mathrm{d}W_1. \tag{2.7}$$

Here the normalisation, $n_{\text{Det}}(d)$, is the number density of detectable sources at a given comoving distance, d. This is calculated by integrating the MWF over the detectable region of HI mass and velocity width (see figure 2.3).

The above equation represents the specific case of confusion between detectable sources only, which will be the blends that are noticeable in the final dataset of a survey. However, sources may also be blended with objects that are below the detection limit. To assess how frequently such blends occur the exact same framework can be used, but instead of setting the lower bound of the integration over M_2 (in the expression for $\langle N \rangle$) by the detection threshold, it should be set as the minimum mass object considered as a source of confusion. In section 2.3.3 we consider various different prescriptions for what minimum mass object constitutes a significant source of confusion.

Although this model now encompasses realistic masses and velocity widths, as

well as the distribution of sources on the sky and in redshift space, it still assumes (as in equations 2.1 & 2.2) that both the beam response and the velocity profiles of galaxies are top-hat functions, clearly this is a crude simplification. However, as we show in the following section, this simple model reproduces the observed rate of confusion in both ALFALFA and HIPASS, and can be used to make an estimate of the upper limit of the impact this has on the shape of the HIMF.

In general this model cannot be evaluated analytically, and so we carry out a Monte Carlo integration to estimate the rate of confusion as a function of redshift. While the data itself could be used to describe the HIMF, MCWF and 2D CF, we instead make analytic fits to each of these (described in detail in the appendix) in order to produce a more accessible model and to reduce computation time.

2.2.1 Catalogue Simulation

In order to evaluate the impact confusion has on the HIMF, it is necessary to explicitly simulate a catalogue of blended and non-blended HI detections, so that an HIMF can be derived for both cases.

The survey volumes were simulated by drawing masses and widths from the HIMF and MCWF (described in the appendix), placing them randomly in space with the average number density associated with the ALFALFA HIMF, and then eliminating anything below the detection limit of the relevant survey.

Confusion was assessed for each source by drawing the number of neighbours within 1000 km/s and the beam width from the expression for $\langle N \rangle$ (equation 2.6), and then assigning their positions (relative to the central) galaxy by drawing from the 2D CF in the same range. Masses and widths were then drawn as for any other galaxy (but all were retained, even those below the detection limit), at which point it can be assessed whether they are blended with the central galaxy.

2.3 Results & Discussion

This comprehensive model of confusion must now be tested against existing blind HI surveys. Good agreement with ALFALFA and HIPASS is demonstrated before this model is used to make predictions for upcoming surveys.

2.3.1 Existing Surveys: Rate of Confusion

To test the validity of the model described in section 2.2, we wish to compare its results to those of existing blind HI surveys, in this case HIPASS (Meyer et al., 2004) and ALFALFA's 40% sample, α.40 (Haynes et al., 2011).

Both surveys are modelled based on their published detection limits. For ALFALFA this corresponds to setting a sharp cut off at 50% completeness (as defined in Haynes et al. (2011), however the HIPASS completeness surface is more com-

plicated (Zwaan et al., 2004), being a function of both peak and integrated flux. Thus, HIPASS is only simulated directly (as described in section 2.2.1), rather than run through our integral models. The detection limit used here is cut at 50% completeness, and above that the completeness function of each source is treated as a probability of detection. Here we note that this formulation, based on the ALFALFA MWF and the published completeness limits, produces appropriate number counts, HI mass and velocity width distributions for both ALFALFA and HIPASS, despite the fact that the published HIMFs of the two surveys are different.

In order to make a fair comparison with the data, the occurrence rate of blends between detectable sources only, was calculated. The equivalent value for the real data sets can be measured by counting the number of sources that are within a beam's width of another detected source, and within half the sum of their velocity widths of each other in velocity space. We carry out this measurement for the α.40 catalogue, and use an equivalent flag set in the HIPASS source catalogue (HICAT). The estimated rates from the surveys are shown as the bars in figure 2.4, the model is the magenta line, and the green line represents the simulated catalogue. The same colour scheme is used in figure 2.5 to show the observed and modelled number counts as a function of redshift.

It can be seen that the models are reasonable fits to α.40 and HIPASS confusion rates, though the deviations are larger for the α.40 volume. The reason for this discrepancy is that α.40 contains significant background density variations

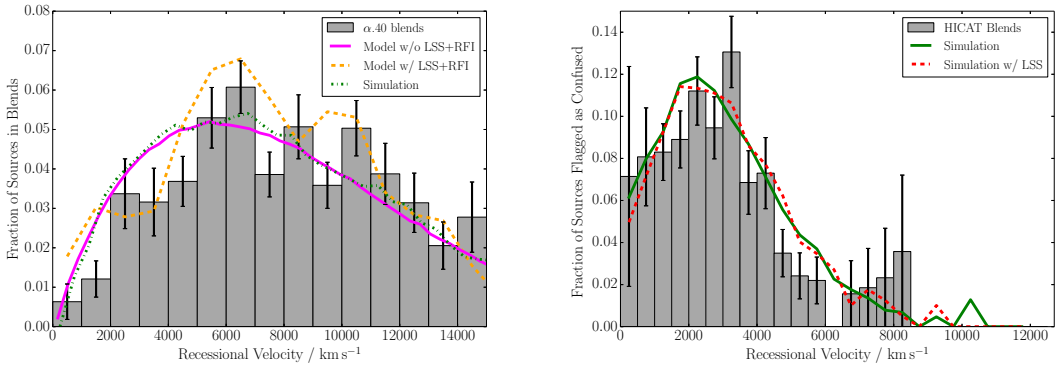

Figure 2.4: The observed rates of blended sources in ALFALFA (left) and HIPASS (right), compared to the model of confusion between detectable sources only (solid magenta), and confusion in a simulated population (dot dashed green). The ALFALFA data is binned in bins that are 1000 km s^{-1} wide, and is cut off at 15,000 km s^{-1}, beyond which a significant band of RFI makes the completeness of the survey difficult to model. The HIPASS blends are binned in 500 km s^{-1} wide bins. The fit to ALFALFA is improved by including weighting for LSS (from 2MRS) and RFI (dashed orange), though there are still discrepancies which are discussed in the text. The LSS correction has little impact in the case of HIPASS (dashed red), indicating that it was a small bias to begin with. The plotted error bars include only counting errors. ALFALFA detects a number of blends between nearby galaxies and tidal debris, we make no attempt to model these complex systems, and such sources are not included here.

due to large scale structure (and radio frequency interference), whereas the larger sky area of HIPASS effectively averages out this bias. The ALFALFA confusion rate is plotted in wider bins in order to smooth the effects of large scale structure (LSS), but in addition we also account for LSS[i] by weighting the background density of HI sources using a full sky 3D overdensity map from the 2MASS Redshift Survey (2MRS), calculated by Erdoğdu et al. (2006) (provided by P. Erdoğdu and C. Springob via private communication). The fraction of the survey volume

[i]LSS impacts the rate of confusion because at certain distances from the Milky Way there are overdensities where galaxies are far more numerous than on average. The correction we apply simply alters the number density of galaxies in each radial velocity bin to reflect the overdensity calculated from 2MRS.

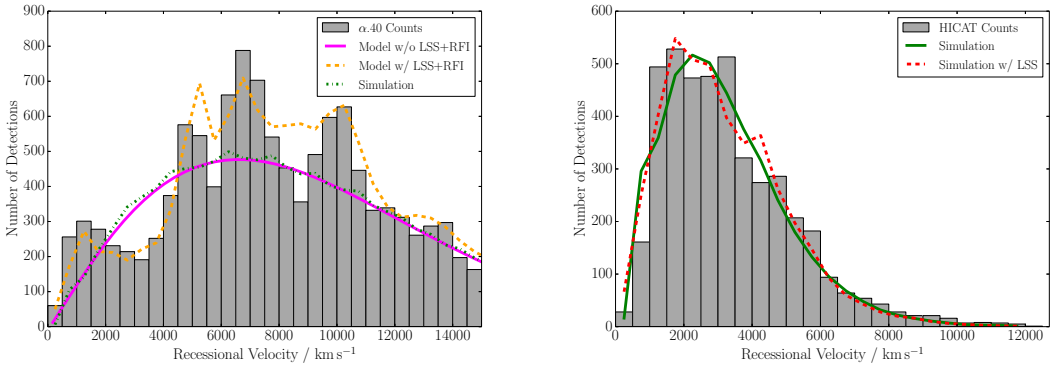

Figure 2.5: The observed detection number counts in 500 km s^{-1} wide bins for ALFALFA (left) and HIPASS (right). The solid magenta line shows the equivalent number counts from our model and the green lines show the number counts from simulations, both without corrections for LSS or RFI, and the dashed orange line shows the model with those corrections for ALFALFA, while the dashed red line shows the HIPASS simulation with the LSS correction.

eliminated by radio frequency interference (RFI) as a function of redshift was calculated in Papastergis et al. (2013) (their figure 6), and in addition to weighting by LSS we also weight the intrinsic number density by the fraction of the volume available in the presence of RFI.

The ALFALFA-like model with weighting for LSS and RFI now fits somewhat better (see figures 2.4 & 2.5), but there are still a few discrepancies. The largest of these discrepancies occurs at approximately 1,500 km s^{-1}, where there is an over prediction of blends in the model. This can be explained by the presence of the Virgo cluster. While this represents a significant overdensity, leading to an excess of detections, it does not produce the corresponding excess of blends. Given Virgo's proximity it is possible to detect galaxies in HI much closer to the centre of the cluster than with any other cluster, which leads to very large peculiar ve-

locities, making confusion less likely than predicted by a model without this level of complexity. In addition, galaxies in Virgo are HI-deficient (Solanes et al., 2002) which could decrease their observed HI velocity widths, also reducing the chance of confusion.

In addition to reproducing the observed rate of blends between detections, it is also important to check that the model and simulations can reproduce the observed detection counts of the surveys, as a function of redshift. Not only is this a critical criteria for accurately modelling a survey, it is also one of the most important quantities in determining the blend rate. As can be seen in figure 2.5, both the number counts of ALFALFA and HIPASS are approximately reproduced, though ALFALFA requires a LSS and RFI correction to achieve a convincing match.

As objects are often studied in classes defined by mass (for example dwarfs, or M_* galaxies), an understanding of the relative rates of confusion across such classes is of interest. Figure 2.6 shows the rate of confusion of simulated ALFALFA sources with another galaxy at least 10% of the central's HI mass, binned by mass. This represents only the blends where there is the potential for a non-negligible alteration of the observed mass. The highest rate of confusion occurs around the 'knee' of the HIMF function, with it dropping off approximately exponentially in either direction in mass. Essentially identical behaviour was seen in all our simulations, only the amplitude varied from survey to survey.

The above behaviour can be understood as follows: occurrences of confusion will become more likely as mass increases, because galaxy velocity widths grow

with mass. This greatly increases the cylindrical volume available to confusion, as an increase in velocity width of 70 $\mathrm{km\,s^{-1}}$, increases the depth of the cylinder by approximately 2 Mpc, whereas typical angular scales will correspond to tens or hundreds of kpc. In addition, the 'finger of god' effect causes there to be more power in the line-of-sight direction (compared to the perpendicular direction), than would be expected from a model using a 1D CF. However, once beyond the 'knee' of the mass function the availability of other sources of comparable mass, drops precipitously, and the increase in velocity width begins to stagnate, leading to a decline in the occurrence of these blends in the most massive sources.

2.3.2 Existing Surveys: Bias in the HI Mass Function

Figures 2.4 & 2.5 give a strong indication that this model is valid, as it is able to simultaneously reproduce the detection rate of both surveys with redshift, and the observed rate of confusion. However, as well as knowing how much confusion is present in a survey it is important to understand what effect this has on the measured quantities, such as the HIMF. To do this we make use of the simulated catalogues of each survey (see section 2.2.1).

The HIMF is calculated using the $1/V_{\mathrm{max}}$ method (as there is no LSS included). For the non-confused HIMF only detectable galaxies are considered, but for the confused HIMF all sources confused with their central (detectable) object are considered together as a single source. The exact details of how the flux and velocity

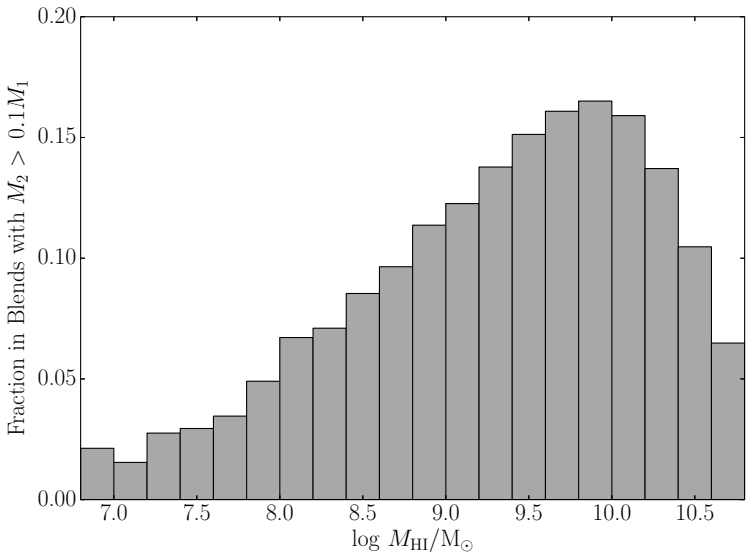

Figure 2.6: The fraction of simulated ALFALFA detections in blends with other galaxies above 10% of their own HI mass (regardless of detectability), in logarithmic bins of width 0.2 dex. The peak rate of confusion occurs around the 'knee'-mass of the HIMF. Below this mass the velocity widths of galaxies drop, making blending less likely, and above this mass the number density of sources with appropriate masses drops exponentially with mass.

width are affected in a blend will depend strongly on the separation and geometry. Here we aim to estimate upper limits on the influence of confusion, so we make the extreme assumption that the velocity width of the central source is unchanged, but the flux (mass) becomes the sum of all objects that are blended together.

Figure 2.7 shows the simulated HIMF, the solid grey lines are non-confused, and the dashed red are confused. The general action of confusion is to increase the mass of a given object, and potentially push it in to a higher mass bin. Its higher apparent mass fools you in to thinking it is detectable over a larger volume than

it is. Therefore the overall influence on the shape is to decrease the HIMF in the original bin and enhance it in the apparent bin. The most noticeable effect occurs around and beyond the 'knee', where the net result of these competing effects switches from the former to the latter. Galaxies just below M_* can become blended together, causing the HIMF to be suppressed immediately before the 'knee', and enhanced immediately after it, where the more massive, blended sources now fall and true sources become scarce.

The alterations to the HIMF's shape can be measured by the deviations in the parameters of Schechter function fits. The faint end slope, α, shows a slight decrease of less than 2σ (compared to published random errors for the ALFALFA and HIPASS HIMFs) in both the simulations. For ALFALFA this decrease was 0.03, and for HIPASS it was 0.04, which corresponds to a 1-2σ deviation in both cases. However, there was large variance between the values calculated in the 20 HIPASS simulations, whereas the 20 ALFALFA simulations were very consistent. The estimate of a decrease of 0.04 in faint end slope of HIPASS' HIMF corresponds approximately to the scale of the systematic error estimated by Zwaan et al. (2004). M_*, the 'knee' mass, was more severely altered, showing a 2-3σ increase, or 0.06 dex for both ALFALFA and HIPASS. In this case the alteration was more than double the previously estimated systematic error in the HIPASS HIMF.

As the parameters of the Schechter function are highly covariant we also estimated the alteration to the faint end slope by fitting a straight line (in log-log space) to all mass bins below $10^9 M_\odot$. Though these results were significantly more

noisy, the mean values were similar to those quoted above, giving decreases of 0.015 and 0.06 for ALFALFA and HIPASS, respectively.

The larger beam of the Parkes telescope compared to the Arecibo observatory leads one to expect that HIPASS would suffer much greater adverse effects of confusion, however the impact on the HIMF has many competing factors and is a non-linear function of the rate of confusion. The alteration of the faint end slope depends on relative, rather than absolute confusion, that is, the slope is dependent on the relative amount of confusion in adjacent bins. In other words, a more confused survey does not necessarily have a more altered faint end slope, so long as the suppression is nearly uniform along it. The 'knee' mass is more simply related to the rate of confusion; it will always increase with increasing confusion (assuming the survey is not artificially truncated in redshift extent, see section 2.3.4). The reason that HIPASS' M_* is not significantly more impacted than it is for ALFALFA, is likely due to there being similar rates of total confusion (not just with other detections) at the respective distances where most of their M_* galaxies are detected ($\sim$ 50 and $\sim$ 150 Mpc).

The overall effects of confusion are to slightly steepen the faint end slope (α), though this is a weak effect, and increase the value of M_*, the position of the 'knee'. This means that ALFALFA's 0.1 dex higher M_* value, compared to the more confused HIPASS (Martin et al., 2010; Zwaan et al., 2005), cannot be explained by confusion. However, given the variance in the HIPASS simulations, its steeper faint end slope could be a result of increased confusion.

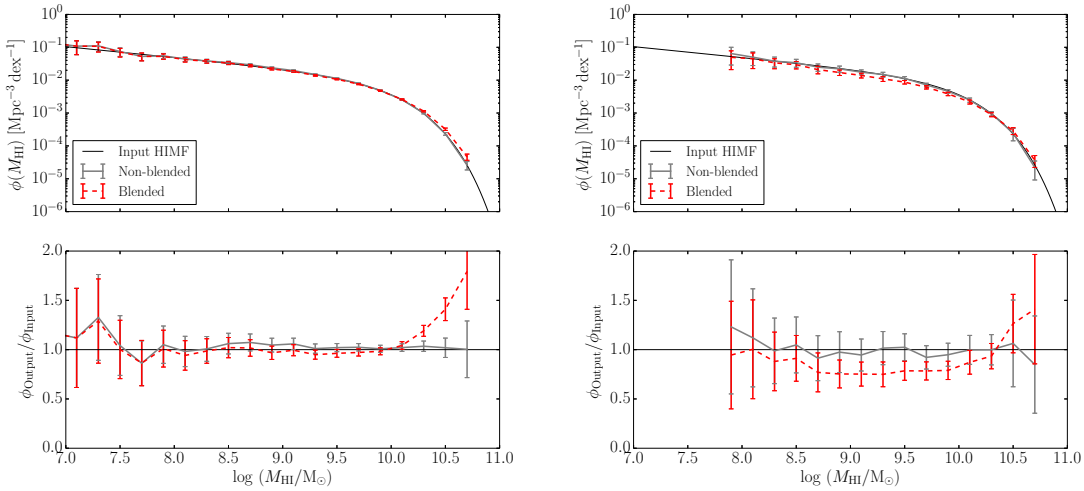

Figure 2.7: Example HIMFs (top row) for simulated ALFALFA (left) and HIPASS (right) surveys, and their fractional deviations from the simulation's input HIMF (bottom row). The thin black line represents the input HIMF, the thick grey line is the calculated HIMF in the absence of confusion, and the dashed red line is the HIMF with confusion. The error bars are errors purely from counting noise, as these simulations contain no LSS or RFI. The effect of confusion is to depress the faint end slope and enhance the values beyond the 'knee'. This results in measuring a marginally steeper faint end slope and a greater 'knee' mass, in the case where confusion is present.

At this stage the reader should recall that these estimates are intended to be conservative, in that they aim to estimate the worst case scenario. Implementing realistic source angular sizes and velocity profiles, along with the beam response function would likely reduce the impact on the shape of the HIMF. Additionally, careful source extraction probably mitigates some of the biases caused by confusion.

Finally, an encouraging point is the relative insensitivity of the faint end slope to spectroscopic confusion. Although studies looking for environmental depen-

dence of the HIMF (Springob, Haynes & Giovanelli, 2005; Zwaan et al., 2005; Moorman et al., 2014) are likely to include biases in the faint end slopes they derive, due to differing levels of confusion intrinsic to the regions being compared, a detection of a 3σ deviation from ALFALFA's faint end slope would still be robust against the effects of confusion. However, caution should be used when comparing M_* in different environments, as this is more noticeably biased by confusion.

2.3.3 Predictions for Future Surveys

A number of blind HI galaxy surveys have been proposed recently, primarily as part of Square Kilometre Array (SKA) precursors, these include medium-depth surveys out to a redshift of about 0.25, and very deep surveys aiming to detect HI at redshifts of order unity. The Australian SKA Pathfinder telescope (ASKAP) plans to undergo two medium depth surveys, the Widefield ASKAP L-band Legacy All-sky Blind surveY (WALLABY - PIs: B. Koribalski & L. Staveley-Smith) and the Deep Investigation of Neutral Gas Origins (DINGO - PI: M. Meyer), whist the Westerbork Synthesis Radio Telescope (WSRT) intends to carry out its own survey similar to WALLABY, but in the northern hemisphere, called the Westerbork Northern Sky HI Survey (WNSHS - PI: G. Józsa). The deep surveys are COSMOS (Cosmological Evolution Survey) HI Large Extragalactic Survey (CHILES - PI: J. van Gorkom), currently underway at the Very Large Array (VLA), and the proposed Looking At the Distance Universe with MeerKAT survey (LADUMA - PIs: S. Blyth, B. Holwerda & A. Baker). In this section we ask how confused these

next generation, deeper survey will be, and how this will affect their ability to measure the HIMF and its evolution with redshift.

Duffy et al. (2012) published predictions of the rms noise and channel widths of ASKAP and WSRT with Phased Array Feeds (PAFs) installed, as well as survey areas and redshift ranges for WALLABY, DINGO and WNSHS. The relevant information is reproduced in table 2.1. WNSHS and WALLABY have quite similar specifications, so we choose to focus on WALLABY here in the knowledge that any findings transfer almost directly to WNSHS. The ambitious depth of LADUMA and CHILES represent somewhat different challenges regarding confusion, from the the medium deep surveys, and we leave the discussion of these to a later study.

Our theoretical detection limit model (described in the appendix), assuming a signal to noise (S/N) threshold of 5.75, fits very closely to ALFALFA's measured 50% completeness limit. We assume this form of detection limit for both WALLABY and DINGO, and make use of the properties listed in table 2.1 to estimate confusion in these upcoming surveys.

Figure 2.8 displays four different measures of confusion: confusion with other detections (as plotted above for ALFALFA and HIPASS), confusion with any other HI galaxy (above $10^{6.2}\mathrm{M}_{\odot}$), confusion with HI galaxies that are above a tenth of M_* in HI mass, and confusion with other HI galaxies above a tenth of the HI mass of the central galaxy. The first of these represents the amount of confusion that would be apparent in the data, whereas the other three are different measures of

Survey Name	Area (deg^2)	Resolution	σ_{rms} (mJy/15 km s^{-1})	Redshift Range	Time (hr)
HIPASS	21,350	15.5′	12	$z < 0.04$	4,300
ALFALFA	~6,900	4′	2.0	$z < 0.06$	4,742
WALLABY[1]	30,940	30″	0.81	$z < 0.26$	9,600
WNSHS[1]	10,313	13″	0.48	$z < 0.26$	16,900
DINGO[1]	150	30″	0.10	$z < 0.26$	2,500

Table 2.1: The parameters of current and proposed wide area, blind, HI surveys presented in this table are used throughout this chapter to simulate the results of these surveys. [1]Values predicted by Duffy et al. (2012) assuming system temperatures of 50 K (although it now seems likely that the final phased array feed systems will fall short of this temperature goal, and thus these numbers will need to be revised).

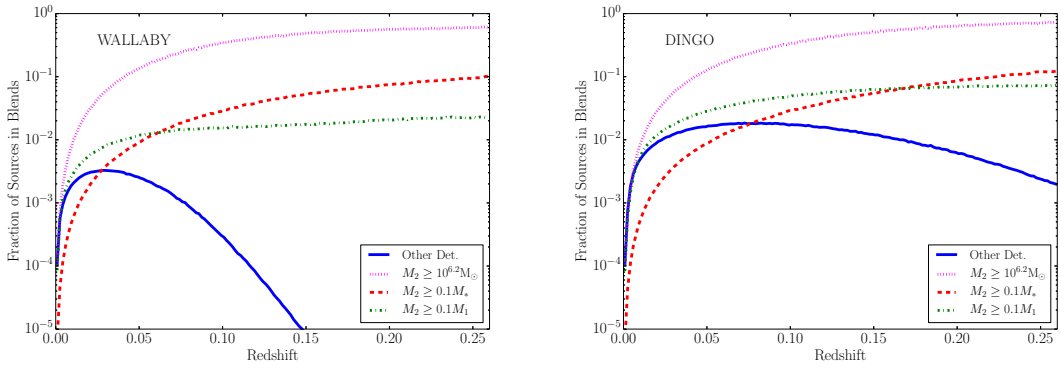

Figure 2.8: Predictions of the rate of confusion in the proposed HI surveys WALLABY (left) and DINGO (right). The blue lines show the rate of confusion with other detected sources (equivalent to figure 2.4), the red dashed lines indicate confusion with galaxies with masses above a tenth of M_*, the dotted magenta line indicates confusion with any HI galaxy (above an HI mass of $10^{6.2}$ $M_\odot$), and the green dash-dot line indicates confusion with any other galaxy above a tenth of the mass of the central galaxy. All of these values lie well below those for ALFALFA or HIPASS.

the underlying amount of confusion (regardless of detectability).

At small distances the second definition of confusion is most appropriate, however at large distances where only high mass galaxies are detected this measure is largely irrelevant. Although most galaxies detected at large distance will be blended with at least one other galaxy, that other galaxy will typically be hundreds or thousands of times less massive.

The third measure of confusion is closely related to that used by DMS12, where confusion was defined as the central source being within 30 arcsec (ASKAP synthesised beam), and a fixed velocity range (600 km/s) of another source, that was above 0.1 M_*. Using this method they estimated the peak fraction of confused sources in WALLABY and DINGO, would be less than 5%. This approximation effectively ignores any confusion at lower masses. However as we have already seen, in a survey with little confusion the most noticeable effects occur around the HIMF 'knee'. Using our almost equivalent definition of confusion we find the peak fraction to be 10% and 12%, for WALLABY and DINGO respectively. [ii]The value for DINGO is slightly larger as it can detect galaxies with wider profiles at the same redshift, making blending more probable than in WALLABY.

At first glance these numbers may seem to be growing worryingly large, however the equivalent peak value for ALFALFA is ~30% (note that this is a different

[ii]The discrepancy between these values and those estimated by DMS12(~5%) is due to the combination of a typographical error and potential numerical instability in the solution found in that paper (A. Duffy - private communication), and the different CFs used (although this acts to reduce, rather than increase, our answer). The results reported here have been checked to be stable (see appendix).

measure of confusion to those plotted in figures 2.4 & 2.6). Thus, either WALLABY or DINGO would suffer less confusion bias than the currently available large area, blind surveys.

The final measure of confusion is probably the most appropriate for most situations (except when it approaches unity). This measure estimates how frequently a random (detected) galaxy will be blended with something more than a tenth its own mass, and thus potentially introduce a significant error in the measured flux and mass. As it is always significantly below 1, clearly multiple blends are not a concern, even though some of the previous measures may have suggested otherwise. This measure also tends to level out to an almost constant, maximum value beyond a certain redshift. For WALLABY that maximum value is 2%, and 7% for DINGO. This indicates that measuring confusion with other sources above 0.1 M_* (red dashed line in figure 2.8), rather than above a tenth the mass of each central source (green dash-dot line in figure 2.8), erroneously implies that WALLABY and DINGO will be equivalently impacted by confusion (10% and 12% peak values, respectively). The reason for this is that WALLABY's most distant detections are the most extremely HI-rich galaxies only, where as in DINGO, galaxies near M_* are still detectable. This results in their predicted detections being blended at a similar rate with sources above 0.1 M_*, but sources above a tenth of the mass of the central source are much more uncommon for WALLABY's most distant detections, than for DINGO's.

As before, this measure of confusion indicates that WALLABY, or any inter-

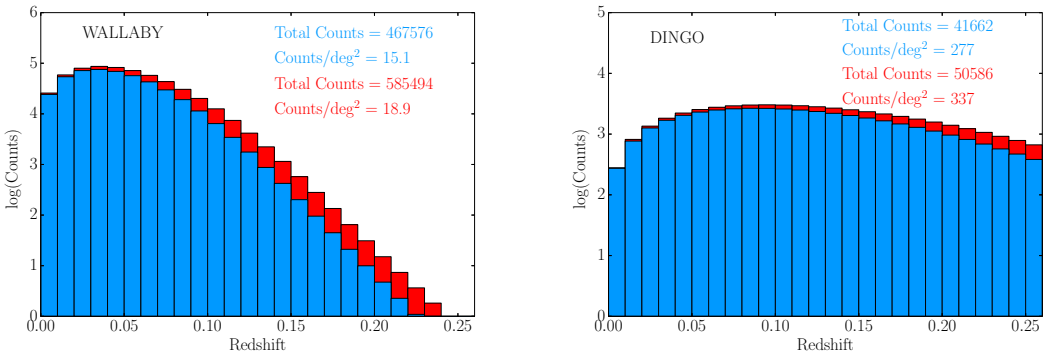

Figure 2.9: Predicted detection number counts of WALLABY (left) and DINGO (right), within redshift bins of width 0.01. The blue bars correspond to a S/N threshold of 5.75 using our detection model, while the red bars assume a straight detection threshold at a S/N of 5 (as in Duffy et al. (2012)).

ferometric HI survey of similar depth, will not suffer any global adverse effects due to confusion. DINGO falls in a similar regime to ALFALFA, where confusion is not currently a significant concern, but it would likely become so if the survey were deeper. In addition, one of the aims of DINGO is to measure the evolution of M_*, and confusion (being a function of redshift also) is likely to be a significant contributor to the error budget of any such measurement.

It should be noted that this analysis is somewhat generous to WALLABY, as it calculates the confusion within one synthesised beam width, whereas ~90% of its sources will be resolved into at least 2 beams (Duffy et al., 2012). However, even if we assume that the beam is actually 1 arcminute across, only 5% of WALLABY's sources will be confused with galaxies greater than a tenth their own mass, at the outermost redshift where it is likely to detect galaxies (z = 0.15). This value is still multiple times smaller than the equivalent value for ALFALFA or HIPASS.

In addition to computing confusion estimates, a byproduct of our model is estimates of the number of galaxies detected as a function of z (assuming no evolution of the HIMF with redshift). Figure 2.9 shows the predictions for the number of detections WALLABY and DINGO would make. The blue bars show the expected number counts, assuming a source extraction process equivalent to ALFALFA's (modelled as a kinked threshold at 5.75σ - see figure 2.3), and the red bars show the expectation if a straight detection threshold at 5σ is used (as in Duffy et al., 2012).

This model predicts number counts that are approximately 60% and 75% of those estimated in Duffy et al. (2012), for WALLABY and DINGO respectively. Relaxing the detection limit to what was used in that paper only recovers an additional 15%. The remaining 10-25% discrepancy must be due to differences between a model based solely on the HIMF (this chapter) and one based on populating simulated dark matter halos with HI gas via semi-analytic models. It is not clear which on these is the more reliable approach, however the model presented here accurately reproduces the two currently available wide area, blind HI surveys. However, those surveys are at low redshift and our model does not incorporate any evolution of the HIMF.

In addition, it should be noted that the above discussion entirely neglects the issue of resolving out sources, which Duffy et al. (2012) estimate will remove 15% of WALLABY's sources (though not DINGO's). Finally, as our detection model is based on ALFALFA's pipeline, where every potential source identified by the

automated extractor is also examined by hand (a feat that would not be possible for WALLABY, barring a citizen science project), it seems unlikely that WALLABY would be able to match the detection limit assumed here. However, even with all these concerns, WALLABY is still sure to detect more extragalactic HI sources than all current such sources combined.

2.3.4 What is the limit of a single dish?

Arecibo is the largest single dish telescope in the world, and with the advent of SKA-precursors and new wide area, blind HI surveys, it is appropriate to ask whether single dish telescopes, like Arecibo and the Five hundred metre Aperture Spherical Telescope (currently under construction in China), have a further role to play in this endeavour. One can easily envisage an ALFALFA-like survey that is deeper, however due to the time necessary for such a survey it is likely it would only be carried out if a new 40 beam phased array feed (PAF) were commissioned for the observatory.

At this point another question becomes relevant: when does the increased confusion, associated with increased depth, prevent accurate measurement of the HIMF with a single dish telescope? To address this question we simulated such surveys with integration times equal to 1, 2, 4, and 8 times that of ALFALFA, but assumed the survey would be truncated at $z = 0.05$. For each simulation we calculated a confused and unconfused HIMF, fit Schechter functions to them, and

Survey	Σ ($\deg^{-2}$)	Survey time (hr)	Survey time w/ PAF40 (hr)	$\Delta\alpha$	Δm_* (dex)	$z_{\max}$
ALFALFA 1	~4	4,800	840	-0.03	0.06	0.05
ALFALFA 2	~5	9,600	1,680	-0.03	0.09	0.05
ALFALFA 4	~8	19,200	3,360	-0.03	0.12	0.05
ALFALFA 8	~11	38,400	6,720	-0.01	0.15	0.05
HIPASS	0.2	4,300		-0.04	0.07	0.04
WALLABY	~15	9,600		-0.002	0.003	0.26
DINGO	~280	2,500		-0.007	0.02	0.26

Table 2.2: The predicted survey timescales and confusion biases for imagined ALFALFA-like surveys with greater integration times (but truncated at z = 0.05) if Arecibo were to with upgraded to a 40 beam PAF. We assume that such a PAF would be cooled to 30 K, and have a sensitivity equivalent to ALFA. Source density on the sky has been denoted as Σ, and $\Delta\alpha$ and Δm_* (where $m_* = \log M_*$) indicate the deviation in the faint end slope and the 'knee' mass (in dex) due to confusion. The full HIPASS and the proposed ASKAP surveys are included for comparison. The final column indicates the maximum redshift at which a 21 cm detection could possibly be made given the (assumed) bandwidth. All source density and deviation values (except for HIPASS) assume a detection threshold of 5.75σ.

tabulated the deviation in table 2.2.

Table 2.2 shows the estimated completion times for surveys over the ALFALFA sky (~7000 $\deg^2$), if Arecibo were to be upgraded to a 40 beam PAF. The survey names correspond to the factor increase in integration time. The comparison to other surveys is not quite fair as all the ALFALFA-like simulations are truncated at $z = 0.05$. For clarity, a depth equivalent to WALLABY occurs between 4 and 8 times the integration time of ALFALFA. The reason for this truncation is twofold: firstly, Puerto Rico has serious RFI concerns beyond a redshift of ~0.05, making accurate determination of the completeness difficult, and secondly because confusion will potentially dominate the uncertainty in M_* for a survey deeper than

ALFALFA with Arecibo's resolution, thus any such survey must focus on the faint end slope, and the relevant galaxies will not be detected beyond this redshift.

It should be noted that the survey times given in table 2.2 correspond to the factor gained due to having 40 beams rather than 7, only. The exact completion time of any such deeper survey would depend on the beam pattern and how the drifts are tiled on the sky. We also assume that a 40 beam PAF at Arecibo would be cooled to 30 K (as is ALFA), whereas the PAFs on ASKAP are assumed to be at 50 K. Cooling PAFs on an interferometer presents a more complex engineering challenge, compared to cooling a similar device on a single dish telescope, as each antenna must be have its own cooling system. As the noise level scales linearly with the system temperature any increase in the assumed temperature will result in the relevant survey losing sensitivity by the same factor, unless its timescale were to be increased by that factor squared.

As can be seen in table 2.2 the deviation of the faint end slope (α) due to confusion, is not a simple function of survey depth, and in fact is smaller in the simulations of 2 and 4 times the integration time of ALFALFA, than for the original simulation. The reason for this is because we are dealing with a fixed volume. In a fixed volume, as the survey becomes deeper, the galaxies above M_* are quickly all detected, thus the mass where the effect of confusion transitions from suppressing a bin to enhancing it, decreases. As the transition point shifts to before the 'knee', the deviation of M_* stagnates, and confusion begins to lift the more massive end of the faint end slope, flattening, rather than steepening it. Neither of these effects

would occur in a survey with unlimited bandwidth.

Although the effects described are expected to occur to some degree, the results of these simulations should be approached which caution. The deviations calculated are intended to be upper limits, but in the fixed volume case they may be sensitive to the simplistic assumption that confusion merely combines the flux (mass) of two objects. This is because the position of the transition point is entirely governed by the relative impact of confusion on adjacent bins. To better understand this, a more realistic model of how the flux of one source blends in to another, and how this influences both the measured flux and velocity width, would be required. Despite this, the general result still stands, that the faint end slope measured by a deeper survey in a fixed volume, is not necessarily more impacted by confusion.

Finally, when considering the extreme of the faint end slope a key advantage of single dish telescopes over interferometers is that they have poor resolution. Almost no extragalactic source will be resolved out by any single dish telescope, regardless of its mass or proximity. This simplifies the statistical corrections required to accurately measure the faint end slope. However, it is at present unclear what impact this effect will have on the ability of surveys like WALLABY and WNSHS to probe very low mass galaxies.

If Arecibo were to focus on a certain region of sky, rather than repeating all the ALFALFA sky, one such volume of interest might be the Pieces-Perseus supercluster (PPS) ridge, spanning a 4° strip in declination (from 28° to 32°), between about

22 and 3 hours right ascension. ALFALFA currently has ~900 detections within 9,000 $\mathrm{km\,s^{-1}}$ in this strip, and simulations indicate that a 4 times longer survey would increase this to ~1,500.

In this direction there is a deep foreground void, where ALFALFA only detects tens of galaxies, out to 3,000 $\mathrm{km\,s^{-1}}$. However, the PPS overdensity between 4,000 and 8,000 $\mathrm{km\,s^{-1}}$ is so strong, that the overall surface density of detections in this strip is one and a half times that of the rest of ALFALFA. A deeper map of this volume would thus allow the HIMF to be investigated both in void and supercluster environments, open the door for peculiar velocity studies around these structures (as few redshift have been measured in this region), and create a sample of low mass void galaxies, all with one dataset. Such a survey would require an additional 525 hours with ALFA, or a total of 160 hours with a 40 beam PAF. On the practical side, Arecibo's limited steer-ability and the need for night-time observing would restrict the window for observations to the period between Aug 15th and Dec 1st, and thus such a survey would likely take several years to be executed.

In summary, interferometric surveys aim to trace HI out to greater redshifts, probe any redshift evolution of the high mass end of the HIMF, and will be capable of entering a parameter space that confusion may obscure from single dish telescopes. However, a convincing detection of environmental dependence of the faint end slope has yet to be made, although it is expected from ΛCDM (Peebles, 2001; Tinker & Conroy, 2009). Thus, if future single dish HI surveys are to remain

competitive in this field, they should play to their strengths and focus on studying the environmental dependence of the HIMF (particularly the faint end slope), and nearby, extremely low mass galaxies.

2.4 Conclusions

In general we found that confusion acted to alter the HIMF in the same ways: steepening the faint end slope (α) and increasing the 'knee' mass (M_*). The influence of confusion on the shape of the HIMF is non-linear, and can be counter-intuitive. The reason for this is that the shape of a function depends on the relative shifts occurring in adjacent bins, as well as the absolute change, which in turn depend on both the survey resolution and its depth. Meaning that the shape of an HIMF from a more confused survey is not necessarily more impacted by confusion.

We have developed a comprehensive model to describe the rate at which HI sources will be spectroscopically confused in a given survey, as a function of redshift. This model shows good agreement with the observable confusion present in the ALFALFA survey and HIPASS. Our simulations indicate that neither of those surveys have serious biases stemming from confusion, and that, of the differences in their HIMFs, only the faint end slope might be attributed to confusion bias. The upper limits of the alterations to the Schechter function parameters that describe their HIMFs, are placed at 3σ (based on published random errors), and in reality

could be significantly smaller.

Encouragingly, α, was the parameter most resilient against the influence of confusion. Studies searching for environmental dependence of the HIMF by using the ALFALFA and HIPASS datasets should therefore focus on this parameter. Detection of a 3σ deviation from the slopes of the published $\alpha.40$ or HIPASS HIMFs would be robust against the effects of confusion, however a similar deviation in M_* may not be.

Simulations of proposed medium depth upcoming SKA precursor experiments (WALLABY and DINGO) indicated approximately a factor of 2 more confusion than had previously been predicted, however they would still be less confused than either HIPASS or ALFALFA. For WALLABY the maximum potential bias from confusion was found to be smaller than the random counting errors, and for DINGO it was of the same order as the random errors. Surveys that go deeper than DINGO, but with equivalent resolution, will once again be in the regime of ALFALFA and HIPASS, where a deeper survey with the same telescope will not necessarily return a more accurate HIMF.

Our model also predicts that the ASKAP surveys will detect around 60-75% of the number of sources that had previously been estimated, however this would still be over an order of magnitude greater than ALFALFA and HIPASS combined. A small fraction of this discrepancy can be explained by the different detection limits assumed, however the bulk of it is likely due to differences between a model based on the mass-width function, and one based on semi-analytic models and

halo catalogues.

As in the coming years interferometer based surveys will have far better confusion statistics than single dish surveys, and due to modern phased array feeds, will have vastly improved survey speeds, it begs the question "where can single dishes still be competitive in surveying extragalactic HI?" Other than projects carrying out HI intensity mapping (a whole other field in itself), the answer likely lies in deeper (but fixed volume) surveys that focus on environmental dependence and the lowest mass galaxies, two fields where much is still to be done. The shallow redshift would prevent excess confusion, allowing studies of the faint end slope to remain robust against confusion, while their lower resolution would prevent systematic biases due to the angular extent of nearby, low mass galaxies; which together would permit single dish telescopes to probe an area of cosmology and galaxy evolution that would be more difficult with any other type of instrument.

CHAPTER 3

WHEN IS STACKING CONFUSING? THE IMPACT OF CONFUSION ON STACKING IN DEEP HI GALAXY SURVEYS

3.1 Introduction

The upcoming construction and commissioning of SKA Phase 1 will bring with it a slew of blind HI surveys to be carried out by precursor facilities. While many of these surveys will be shallow or medium depth, wide area surveys, there are several ultra deep single pointing and small field surveys that aim to probe HI galaxies out to unprecedented redshifts.

Stacking has become a key tool for HI astronomers in recent years as measurements of the evolution of HI density with redshift have been attempted (Lah et al., 2007; Delhaize et al., 2013; Rhee et al., 2013), and low mass and HI-deficient galaxies have been studied at low redshift (e.g. Fabello et al., 2011a,b, 2012). As surveys push to increasingly high redshifts, stacking will become an evermore invaluable tool in the attempt to study normal HI galaxies out to a redshift of order unity and beyond.

As surveys become deeper, both in terms of their sensitivity and redshift range, confusion becomes an increasing concern. Longer integration times mean surveys are sensitive to less massive galaxies, but this also means that background

This chapter is an adapted version of the published article Jones et al. (2016a).

emission makes up a larger fraction of the signal detected. Probing HI at higher redshift causes an increasingly large number of objects to be contained in an individual beam width, as the physical size of the beam grows with redshift and therefore encloses more volume. When undetected target objects are stacked this low level emission from the surrounding galaxies will also be coadded. Eventually, when the survey data is deep enough, this confused emission will contribute a significant fraction of the final stacked spectrum and create a bias in the results. The scale of this bias should be estimated so that it can be anticipated and potentially corrected for.

A small number of measurements and predictions of confusion have been made, that are applicable to very deep HI surveys. Duffy et al. (2008) made predictions for potential FAST (Five hundred metre Aperture Spherical Telescope) surveys, using a similar approach to that used here, but assumed a uniform universe (i.e. neglected the correlation function). As we shall show this leads to an order of magnitude underestimation of the signal due to confusion. Delhaize et al. (2013) took a different approach by estimating the contribution of confusion in a stack that was known to be heavily confused, based on the optical parameters of the galaxies in the field. This provides a means to interpret a stacked spectrum with confusion, but could also be used to predict the amount of confusion. However, as this would require the specific (optical) input catalogue, and we intend to produce a general tool to assess a generic survey's confusion, this approach will not be discussed in detail in this chapter.

In this chapter we make use of the currently available HI correlation function (CF) and measurements of the mean ($z = 0$) HI density to predict how much HI mass will be contained in a stacked spectrum, in addition to that of the intended targets. This is intended to be a universal tool which can be used to calculate a realistic, but computationally cheap, estimate of the impact of confusion on any HI survey. Section 3.2 briefly outlines the upcoming surveys for which predictions will be made. Section 3.3 describes how the analytic model is derived, as well as its caveats and limitations. In section 3.4 we present our results and their implications are discussed in section 3.5.

3.2 Deep Surveys

In the coming years a host of new HI galaxy surveys will begin as part of the precursors to the SKA. In Jones et al. (2015) we assessed the impact of confusion on shallow and medium depth surveys, whereas this chapter focuses on the three deepest of upcoming surveys, LADUMA (Looking At the Distant Universe with MeerKAT), CHILES (COSMOS HI Large Extragalactic Survey) and DINGO UDEEP (Deep Investigation of Neutral Gas Origins - Ultra Deep). We also briefly discuss FAST in a more general sense as the specifics of the surveys it will perform have yet to be determined.

LADUMA (Holwerda, Blyth & Baker, 2012) intends to integrate a single pointing with MeerKAT for 5,000 hours. This makes the total field of view of the survey

simply the primary beam of a single dish, 0.9 deg^2 at $z = 0$. MeerKAT will have a maximum baseline of 8 km, potentially allowing the synthesised beams to reach down to sizes of ~10 arcsec. The bandwidth of the survey will in theory permit detections of HI sources out to a redshift of ~1.5.

CHILES (Fernández et al., 2013), which recently began taking data with the VLA (Very Large Array), is also a single pointing survey, with an integration time of 1,000 hours. Due to the longer baselines of the VLA, the minimum synthesised beam is 5 arcsec across, while the larger dishes reduce the field of view to 0.25 deg^2 at $z = 0$. The narrower bandwidth that CHILES adopts (compared to LADUMA), sets its maximum possible redshift for HI detection at 0.45.

Unlike the two deepest planned pathfinder surveys DINGO UDEEP (Meyer, 2009; Duffy et al., 2012) will not be a single pointing. ASKAP (Australian Square Kilometre Array Pathfinder) will survey 60 deg^2 over the redshift range 0.1-0.43. The survey is intended to be 5,000 hours, and should detect tens of thousands of HI sources. However, due to the computational demands of forming multiple beams (from ASKAP's phased array feeds) and correlating all the signals over this wide bandwidth, it is not yet certain whether ASKAP will achieve a resolution of 10 or 30 arcsec for this survey.

FAST is a single-dish telescope (the only one in this list) currently under construction in China. The 305 m Arecibo observatory in Puerto Rico is the only existing telescope of a comparable size and design. However, unlike Arecibo's fixed reflector, FAST's segmented 500 m primary reflector will be deformable, and

the instrument platform will be movable, allowing for zenith angles up to 40°, which is double the sky area observable from Arecibo. While FAST is observing, a 300 m segment of the reflector will be deformed into a parabola (Nan, 2006), giving it a resolution of approximately 3 arcmin for 21 cm radiation, compared to almost 4 arcmin for Arecibo. FAST's larger area will produce greater sensitivity than Arecibo, while its proposed 19 feed horn array (compared to the 7 horn Arecibo L-band Feed Array, or ALFA) will increase its survey speed to a factor of a few faster than Arecibo. Assuming that FAST's feed array has a system temperature of 31 K (as does ALFA) the figure of merit (FoM), which effectively measures a telescope's sensitivity divided by the time taken to map a given area, is 37 for FAST, compared to 4.6 for ALFA on Arecibo (on a scale where 1 pixel with a system temperature of 25 K on Arecibo has a FoM of 1). Although the exact surveys that FAST will carry out have yet to be defined, it has been suggested (e.g. Duffy et al., 2008) that it might probe HI galaxies out to a redshift of ~0.5.

In addition to these upcoming ultra deep surveys, we will reference the two currently available large area, blind HI surveys, ALFALFA (Arecibo Legacy Fast ALFA) and HIPASS (HI Parkes All Sky Survey). The ALFALFA survey (Giovanelli et al., 2005) covers approximately 6,900 $\deg^2$, with a mean source density of 4 $\deg^{-2}$ and a mean redshift of 0.03. The HI properties and functions used throughout this chapter (Martin et al., 2010; Papastergis et al., 2013) were derived from the α.40 catalogue (Haynes et al., 2011), which covers 40% of the nominal sky area. HIPASS (Barnes et al., 2001; Meyer et al., 2004) covers approximately a hemisphere of sky area, but is less deep than ALFALFA, with a mean redshift of 0.01

and a mean source density of 0.2 deg^{-2}.

3.3 Determining the Confusion in a Stack

In order to assess how confused a stacked spectrum is, it is necessary to calculate the relative contributions from the target objects versus those they are confused with. The signal due to confusion is found from the total HI mass there is (on average) in a given stack, in addition to that of the target objects. If this mass is negligible in comparison to the mass of the target sources, then clearly it is not a concern. However, if it is comparable in mass, then the spectral profile of this confused emission is also of interest, as this will determine how it alters the appearance of the stacked spectrum in practice. The following subsections outline how each of these quantities can be calculated.

3.3.1 Confused Mass in a Stack

When creating a stack, the angular (or physical) size of the 'postage stamps' (or 'cut outs') must be chosen. This defines a scale on the sky, and the smallest it can meaningfully be is the size of the beam (or synthesised beam, for interferometers); which is what we shall assume. For simplicity, the fact that the final maps will be made up of pixels is ignored, and the 'cut outs' are assumed to be circular. The same analysis could be done with square 'cut outs', but given the other uncertain-

ties (see section 3.3.4) this factor of order unity is unimportant.

Next, a velocity range in the spectrum must be chosen in which the relevant signal is believed to reside. The broadest HI galaxy velocity widths are around 600 km/s, so with an accurate input redshift, a velocity slice of ± 300 km s^{-1} is a conservative choice, and is what will be used here. The results are less sensitive to this choice than might be expected, because the correlation function (CF) causes the signal to be strongly peaked around zero relative velocity.

Together these dimensions define a cylinder in redshift space that is centred on the target being stacked. The amount of HI mass, in addition to the central source, that is within this volume (on average) determines the strength of the confusion signal in the final stacked spectrum, and we will refer to it as the "confused mass".[i]

In order to calculate the mean confused mass in a stack, two things must be known: the expected number of HI galaxies residing in the cylinder surrounding the target object, and the mean HI mass of an HI-selected galaxy. The first of these can be calculated from the CF, and the second by the integral of the HI mass function (HIMF).

The CF is the excess probability (above random) of two sources being separated by a given distance, here denoted by $\xi(\kappa, \beta)$, where κ is the separation perpendicular to the line of sight, and β is the separation along it. In general it is not symmetric with respect to κ and β, as distance along the line of sight is usually de-

[i]We will also use the phrase "confused sources" throughout this chapter to mean the sources that a target object is confused with, not including the target object itself.

termined from redshifts, and so peculiar velocities alter the derived separations. Although these distortions along the line of sight are not physical, in the sense that the galaxies may not be separated by the distances calculated, they are directly applicable to this scenario as the depth of the cylinder is also a pseudo-distance (a velocity divided by the Hubble constant). Thus, we make use of the 2D CF for HI sources, as calculated in Papastergis et al. (2013), and for convenience, will use the simple analytic fit from Jones et al. (2015) to approximate it:

$$\xi(\kappa,\beta) = \left(\frac{1}{r_0}\sqrt{\frac{\kappa^2}{a^2}+\frac{\beta^2}{b^2}}\right)^{\gamma}, \tag{3.1}$$

where $ab = 1$, $r_0 = 9.05$ Mpc, $a = 0.641$, and $\gamma = -1.13$.

Integrating $1 + \xi$ over the cylinder defined by the choice of 'postage stamp' size and velocity range, and multiplying by the mean HI source number density, gives the expected number of additional HI sources within the volume. Finally, multiplying by the mean HI mass of an HI source (Martin et al., 2010), returns the total mass in these sources within the beam on average, $M_{\rm conf}$.

$$\begin{aligned} M_{\rm conf} &= 4\pi\Omega_{\rm HI}\rho_{\rm c}\int_0^{\beta_{\rm sep}}\int_0^{\kappa_{\rm sep}}\kappa\left[1+\xi(\kappa,\beta)\right]{\rm d}\kappa{\rm d}\beta \\ &= 2\pi\Omega_{\rm HI}\rho_{\rm c}a\left[\frac{\beta_{\rm sep}\kappa_{\rm sep}^2}{ba^2}+I\right], \end{aligned} \tag{3.2}$$

where

$$I = \frac{2\frac{\beta_{\rm sep}}{b}\left(\frac{\kappa_{\rm sep}}{a}\right)^{\gamma+2}(\gamma+3)}{(\gamma+2)(\gamma+3)r_0^{\gamma}}\left[{}_2F_1\left(\frac{1}{2},-\frac{\gamma}{2}-1;\frac{3}{2};-\frac{a^2\beta_{\rm sep}^2}{b^2\kappa_{\rm sep}^2}\right)-2\left(\frac{\beta_{\rm sep}}{b}\right)^{\gamma+3}\right] \tag{3.3}$$

and ${}_2F_1$ is the Gaussian hypergeometric function, $\beta_{\rm sep}$ is the velocity half range, in this case 300/70 Mpc, $\kappa_{\rm sep}$ is the physical radius of the beam in Mpc at the distance

of the target object, and $\Omega_{\rm HI}$ is the background density of HI ($\rho_{\rm HI}$) relative to the critical density ($\rho_{\rm c}$) in $\mathrm{M}_\odot\,\mathrm{Mpc}^{-3}$ (equivalent to the mean source number density times the mean source mass). We adopt $\Omega_{\rm HI} = 4.3 \times 10^{-3}$, as found by Martin et al. (2010). Refer to Jones et al. (2015) for the full details of the fit to $\xi(\kappa, \beta)$ and how to evaluate its integral.

The above equation for the confused mass is independent of the shape of the HIMF, because the quantity of HI in a given volume only depends on its integral. However the variance of the confused mass is dependent on the shape of the HIMF. This can be understood by considering where most of the HI mass in the Universe resides, which at present is in M_* galaxies. If the faint-end slope was steeper and most of the HI mass resided in highly abundant dwarf galaxies, then the variance in the confused mass would be small (ignoring the environmental dependence that would likely be present in such a universe) as the Poisson noise in the number counts within the cylinder would be low. Alternatively if the faint-end slope were to be very flat and the knee mass very high, then although the integral could be identical, most of the HI mass would be contained in exceptionally rare, highly massive systems. As a result the Poisson noise associated with the counts of such galaxies would be very large, leading to high variance in the confused mass.

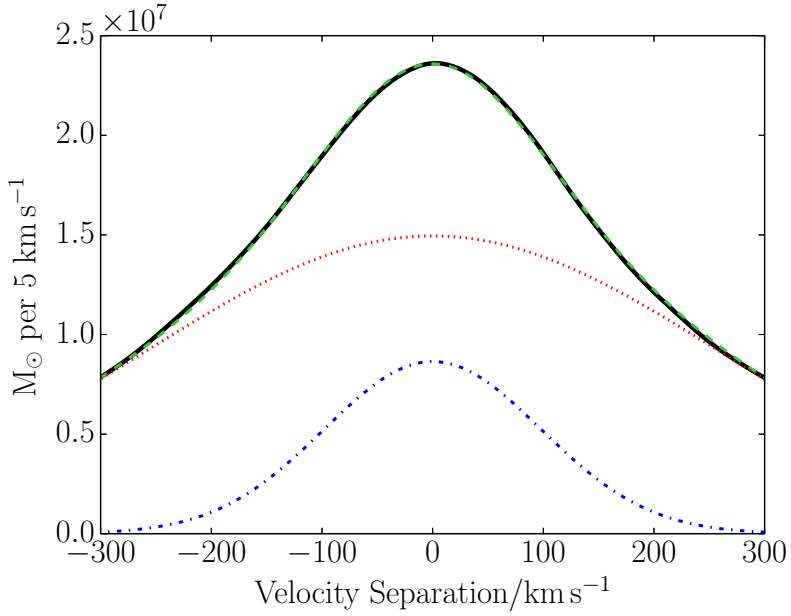

Figure 3.1: The solid black line shows a simulated stack of the average spectral profile contributed by confused sources only (target sources have been removed), in a stack at $z = 0.029$ for a survey with a beam size of 15.5 arcmin (at $z = 0$), intended to mimic the Delhaize et al. (2013) experiment with HIPASS. The green dashed line shows the double Gaussian fit to the black profile, while the red dotted and blue dash-dot lines show the two separate components of the fit.

3.3.2 Spectral Profile of Confusion

If all the additional mass in the cylinder was uniformly distributed in velocity space then it would not pose a problem to deriving physical properties from the stacked spectrum, as the confusion signal would just represent a DC shift in the baseline. However, if the confusion signal is peaked around the central frequency, then it can contribute an unknown amount to the final flux, or worse, make up all of the flux and give a false positive (in the event that the central sources are not detected even in the stacked spectrum).

The spectral shape of the confusion signal (which we will refer to as the "confusion profile") can be calculated using a similar method to that in section 3.3.1, which reveals it takes a double Gaussian form. However, this method neglects the velocity widths of each galaxy contributing to the confusion signal. Therefore, we have estimated the confusion profile using mock stacks (see section 3.3.3), shown by the solid black line in figure 3.1. The inclusion of velocity widths broadens the confusion profile, however it maintains a double Gaussian shape (see figure 3.1). The two components arise from the peak in the CF at zero velocity separation, and the uncertainty in the input catalogue of target redshifts. For the latter we assume a Gaussian distribution centred on zero with a width of 35 $\mathrm{km\,s^{-1}}$, as found by Toribio et al. (2011).

Here it should be reiterated that figure 3.1 includes only the stacked emission of the confused sources, with emission from the target galaxies removed. The profile is well fit by a double Gaussian with a narrow and a broad component, which highlights that caution must be used when interpreting heavily confused stacks, as this profile shape is similar to what might be expected for a stack detection on top of confusion noise, not just from confusion alone.

3.3.3 Mock Stacks

In order to help assess our findings and potential strategies to mitigate confusion, we make use of simulated HI stacks. Our approach is similar to that of Maddox

et al. (2013), which used the template HI profiles of Saintonge (2007), however our mock stacks are intentionally noiseless and the masses and velocity widths are drawn randomly from a fit to the α.40 mass-width function (Papastergis et al., 2015; Jones et al., 2015).

When simulating the signal from confusion, galaxy masses and widths are drawn from the mass-width function. A lower HI mass bound (of $10^{6.2}$ $M_\odot$, the lowest that ALFALFA can measure the HIMF to) must be set, and only masses greater than this are selected. However, the results are insensitive to this bound as most of the HI mass in the Universe is contained in much more massive systems. The number of confused sources to be included (around each target object) is chosen from a Poisson distribution with an expectation equal to $M_{\rm conf}/\bar{M}_{\rm HI}$, where $\bar{M}_{\rm HI}$ is the mean HI mass of a galaxy, and $M_{\rm conf}$ is the confused mass as calculated in equation 3.2. The galaxy masses and widths are then drawn from the mass-width function and are placed at angular and velocity separations (away from the central target) drawn from the 2D CF (equation 3.1). Finally, the profiles are added to the stack at the appropriate frequencies (the angular information is ignored except when non-uniform beam weightings are consider in section 3.5.1).

To simulate the contribution of the target objects, we make the assumption that all the targets have the same mass and then draw only the velocity width (for the relevant mass) from the mass-width function. A redshift error is added to the profile, drawn from a Gaussian of width 35 $\mathrm{km\,s^{-1}}$, and then it is added to the stacked spectrum. All stacked targets are assumed to be the same mass

for simplicity and generality, however information about the mass distribution of targets, which might be available when modelling a particular survey, would be straightforward to incorporate. This assumption has no impact on the amount of confused mass we calculate, but could alter ratio of confusion to target signals.

3.3.4 Modelling Limitations

The model and simulation methods described above have a number of caveats and shortcomings which are outlined in this section. A general note is that this methodology only applies to the average values present in a large stack. This will require on the order of 1,000 spectra in a given stack, such that extreme cases and small number statistics are not dominant.

Redshift Evolution

Although there is some evidence for z-dependence of $\Omega_{\rm HI}$ from stacking, damped Lyman-α observations and HI intensity mapping experiments (e.g. Rao, Turnshek & Nestor, 2006; Lah et al., 2007; Prochaska & Wolfe, 2009; Chang et al., 2010; Freudling et al., 2011; Delhaize et al., 2013; Rhee et al., 2013; Hoppmann et al., 2015), there is no observational data describing how the shape of the HIMF may evolve, or how the HI CF evolves. Due to these limitations we choose to display our results for two separate assumptions: constant $\Omega_{\rm HI}$, and $\rho_{\rm HI} \propto (1+z)^3$, with both using the $z = 0$ CF throughout. The first case will likely under predict the

confused mass at high redshift as the observations indicate a factor of ~2 increase in $\Omega_{\rm HI}$ by $z = 1$, while the second case actually appears to overestimate the increase of HI density with redshift. Thus, barring a major shift in the HI CF, we expect the true value to lie between these two cases.

Sharp Edges & Point Sources

The response of the telescope beam is assumed to be a step-function. When stacking based on 'cut outs' from a uniform survey map, where the shape of the beam response has already been accounted for, this is the simplest choice. In section 3.5.1 we discuss the possibility of using a different weighting as a way to reduce confusion.

When simulating stacks to verify the analytic results and test mitigation strategies (section 3.5.1), the confused sources, which in reality would be galaxies with their own velocity widths and spatial patterns, are modelled with realistic HI profile shapes (Saintonge, 2007) in frequency space, but as point sources on the sky. Given the simplistic weighting of the beam, modelling sources as points (spatially) is sufficient. However, as the finite velocity widths inevitably broaden the profile of any confusion signal (see figure 3.1), it might be expected that the total mass within a ± 300 km s^{-1} window might differ from the value derived via equation 3.2. This has been explicitly checked for in our mock stacks, and while the spectral profile of the confusion signal becomes broader, it maintains a double Gaussian shape and the total confused mass is consistent with the analytic model.

Redshift Error Distribution

In order to stack non-detections an input (presumably) optical catalogue of positions and redshifts must be used. When calculating the profile of the confusion signal a Gaussian distribution with a width of 35 $\mathrm{km\,s^{-1}}$ is assumed to represent the deviations between the HI and optical redshifts. In practice the scale of this dispersion is dependent on the quality of the spectra in the input catalogue. Maddox et al. (2013) found a smaller dispersion between SDSS and ALFALFA when only including the highest S/N ALFALFA detections, while Delhaize et al. (2013) quoted the uncertainty in their input redshifts as 85 $\mathrm{km\,s^{-1}}$. Although the value we chose to adopt changes the width of our resulting profile, it does not alter the qualitative results.

For a particular survey there may be more knowledge about how these redshifts differ from each other which, when available, should be used instead. Alternatively, the bias from confusion could be estimated by calculating the cross correlation function between the HI and optical catalogue when possible, and use this in place of equation 3.1.

Model Uncertainties and Variance

There is an error associated with our choice of the parametric forms used to fit both the 2D CF (equation 3.1) and the mass-width function (see Jones et al., 2015), as well as the exact ranges we chose to fit them over. As this is a single choice

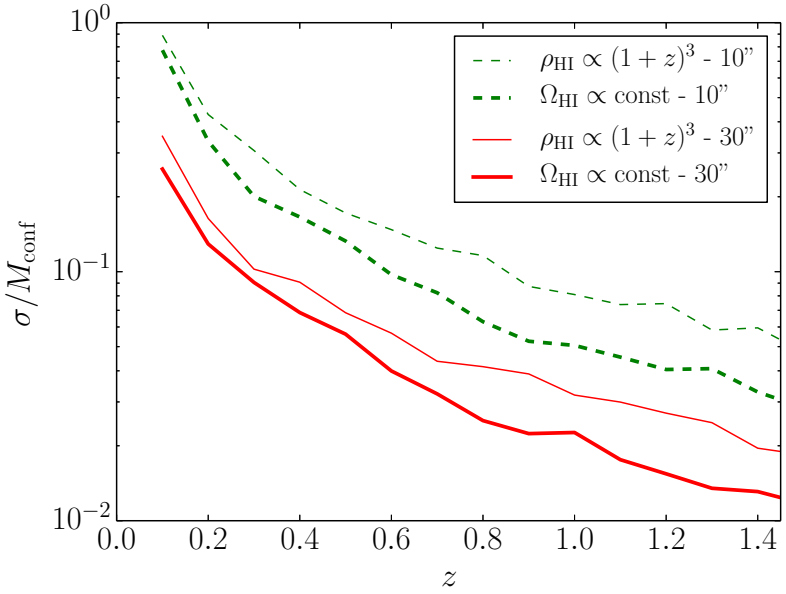

Figure 3.2: The fractional uncertainty in the confused mass (standard deviation divided by mean value) estimated by simulating 100 stacks, each of 1,000 targets, at each redshift and beam size. The bold lines indicate those mocks which assume $\Omega_{\rm HI}$ is constant, and the standard weight lines are for a $\rho_{\rm HI} \propto (1+z)^3$ model. The solid (red) lines represent a beam size of 30 arcsec, and the dashed (green) lines a beam size of 10 arcsec. These are estimates of the 1-σ fractional uncertainties in the red (second from top) and green (second from bottom) solid lines in figures 3.3 & 3.4.

that involves the judgement of the individual performing the fit, it is very difficult to estimate a quantitative error for. Thus, rather than quoting an error we have chosen to a) demonstrate that the model we use is consistent with both the number counts and the observed rate of confusion between detections in the ALFALFA data set (Jones et al., 2015), and b) present arguments (sections 3.3.4 and 3.5) that the two extremes which we adopt for any redshift evolution, likely bracket the true value.

The above concerns aside, there is still another uncertainty that is important. Equation 3.2 gives the confused mass that is present *on average* in a stacked spectrum. As alluded to previously (section 3.3.1) the variance of this quantity depends on the shape of the HIMF, and the more top-heavy it is, the higher the variance in $M_{\rm conf}$. In addition to the shape of the HIMF, the variance of $M_{\rm conf}$ also depends on the number of spectra being stacked, the angular size of the 'cut outs', and the redshift of the stack. To estimate the scale of the variance we ran 100 realisations of stacks of 1,000 targets at redshifts 0.1 to 1.4 (in increments of 0.1), for two beam sizes, 10″ and 30″ (at $z = 0$). Figure 3.2 shows the fractional uncertainties (standard deviation divided by the mean) in the confused mass calculated from these realisations. While the uncertainty for the mock stacks with a 30 arcsec beam quickly (by $z \sim 0.3$) drop to less that 10%, for the stacks using a 10 arcsec beam the uncertainty starts off at almost 100% and does not fall to 10% until between a redshift of 0.5 and 1 (depending on the assumed evolution of $\Omega_{\rm HI}$). This indicates that accounting for confusion in a statistical way will be difficult for surveys with small beam sizes, as the variance in any individual stack will be so large. However, as is shown below confusion will turn out to be only a minor concern for surveys achieving beam sizes of 10 arcsec.

3.4 Results

Before proceeding with predictions for upcoming surveys the CF model was tested against an existing study of HI stacking in a highly confused regime by Delhaize et al. (2013). In that chapter HIPASS non-detections were stacked based on Two-Degree-Field Galaxy Redshift Survey (2dFGRS) positions and redshifts. The mean redshift of their sample was 0.029, and the stacked spectrum has a mass of $3 \times 10^9\, h_{70}^{-2}\, \mathrm{M}_\odot$ between velocities ± 300 km s^{-1}. They also estimated that each source was confused with three others (on average), which increased the effective luminosity of the stacked sample by a factor of 2.5. Assuming a constant mass-light-ratio, this means that the contribution of confusion to the stack was approximately $1.8 \times 10^9\, h_{70}^{-2}\, \mathrm{M}_\odot$. A higher redshift sample of targeted follow-up was also stacked, giving a mean mass of $1.4 \times 10^{10}\, h_{70}^{-2}\, \mathrm{M}_\odot$ at a mean redshift of 0.096, of which $1.1 \times 10^{10}\, h_{70}^{-2}\, \mathrm{M}_\odot$ was estimated to be due to confusion.

Using our framework (and assuming constant Ω_{HI}) to estimate the confused mass in a stack at a redshift of 0.029 in HIPASS data returns a value of $1.9 \times 10^9\, \mathrm{M}_\odot$ for a beam size of 15.5′, and $3.3 \times 10^9\, \mathrm{M}_\odot$ for a beam size of 21.9′. The Parkes telescope beam size is 15.5′ for a wavelength of 21 cm, but the weighting used in Delhaize et al. (2013) produces an effective beam size of 21.9′ (and 21.2′ for the higher z sample). We quote results for both beam sizes as our model does not incorporate the beam profile weighting they assume. For the higher redshift sample we estimate a confused mass of between 1.3 and $2.0 \times 10^{10}\, h_{70}^{-2}\, \mathrm{M}_\odot$ for beam sizes 15.5′ and 21.2′ respectively. Both of these results appear approximately consistent,

although the exact confidence is not possible to assess (see section 3.5).

The confused mass present, on average, in a stack made from a generic survey at a given redshift, was estimated based on the integral of the 2D CF over the telescope beam and ± 300 km s^{-1} in redshift space (see section 3.3.1). Figures 3.3 & 3.4 show the results for various telescope resolutions, each solid line represents a different angular resolution: 5, 10, 20, 30 arcsec and 3 arcmin (at $z = 0$), from bottom to top. The dashed lines represent the confused mass that would be present if the Universe were perfectly uniform, and the faint dotted lines are the results obtained using the projected CF (Papastergis et al., 2013), which removes the difference in the physical and velocity directions. The two figures are identical except that figure 3.3 assumes $\Omega_{\rm HI}$ does not change from its value at $z = 0$, while figure 3.4 assumes $\rho_{\rm HI}$ grows like $(1 + z)^3$.

Below we outline the results relevant to each upcoming survey. Wherever a value is quoted for the constant $\Omega_{\rm HI}$ case, the $\rho_{\rm HI} \propto (1 + z)^3$ value will immediately follow in parentheses (if different at the stated precision).

3.4.1 CHILES

CHILES has a resolution of 5 arcsec, so the solid blue (lowest) lines in figures 3.3 & 3.4 are the appropriate estimates of the confusion in stacked CHILES data. Even at the maximum redshift (0.45) the confused mass within one synthesised beam, and ± 300 km s^{-1}, will still only be $\sim 10^7$ M$_\odot$, indicating that CHILES will have no

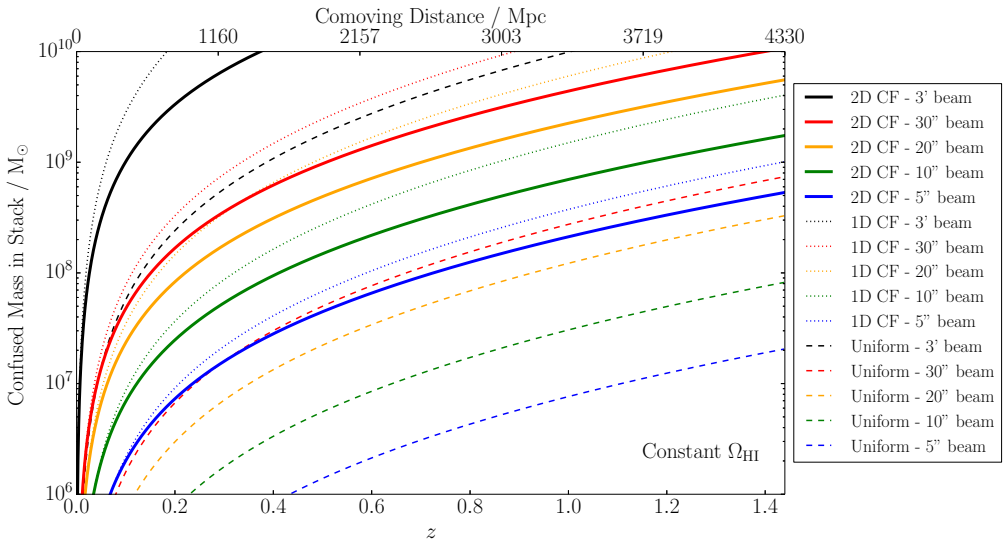

Figure 3.3: The predicted average HI mass due to sources of confusion in a stacked spectrum as a function of the redshift (distance) of the stack, assuming Ω_{HI} is fixed at its zero redshift value. The line styles indicate the method used to generate the estimate, with solid lines representing the 2D correlation function, dotted lines the projected (or 1D) correlation function, and dashed lines assume the Universe is uniform in HI. The blue, green, orange, red and black lines use beam sizes of 5, 10, 20, 30 arcsec, and 3 arcmin (at $z = 0$) respectively, or equivalently smallest to largest beam going bottom to top.

major concerns due to confusion when stacking sources. However, as CHILES will spatially resolve almost all the sources it detects, a more appropriate measure of the confused mass can be derived by choosing a constant physical scale for the 'postage stamp' cut out of a galaxy in a stack. To be overly conservative we choose 100 kpc (diameter), which gives a confused mass of 1×10^8 $M_\odot$ at $z = 0$, which increases to 1.6×10^8 $M_\odot$ (3.1×10^8 $M_\odot$) at $z = 0.45$. In other words, CHILES would only encounter non-negligible amounts of confusion bias if very low mass objects (presumably at lower redshift) were to be stacked, which seems unlikely given the that CHILES is a pencil beam survey.

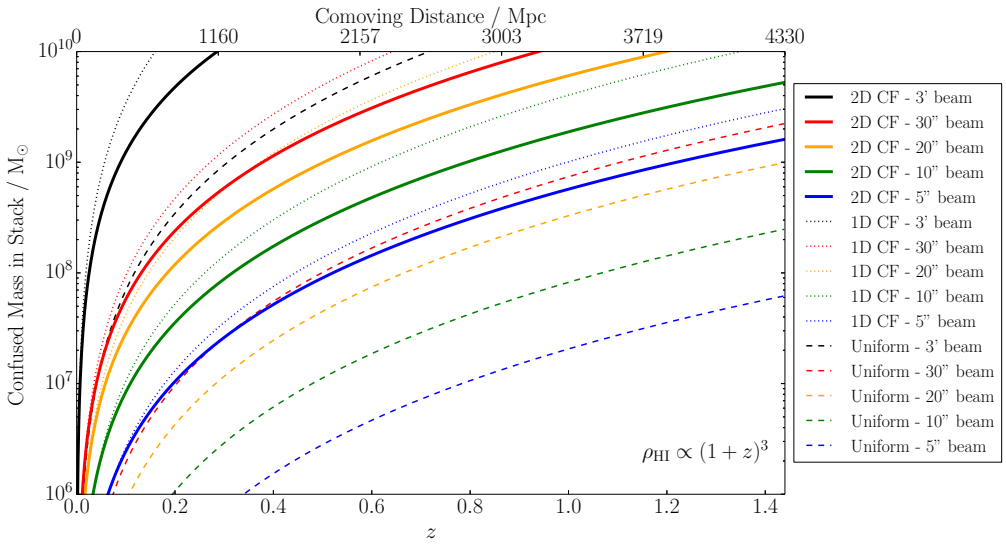

Figure 3.4: Identical to the figure above except ρ_{HI} increases in proportion to $(1 + z)^3$ from its zero redshift value.

3.4.2 LADUMA

For LADUMA the angular size of the minimum synthesised beam is still not set, however as MeerKAT's maximum baseline will be smaller than the VLA's B-configuration baseline, here we assume LADUMA will have a resolution of 10 arcsec. This is represented by the solid green (second lowest) line in figures 3.3 & 3.4. As mentioned above, in reality the confused mass is unlikely to ever drop much below 10^8 $M_\odot$ even at low redshifts, as the physical size of the sources (rather than the size of the beam) will determine the 'postage stamp' size.

Again this indicates that LADUMA will be safe from the impact of confusion when stacking sources significantly more massive than 10^8 $M_\odot$, at least up to intermediate redshifts. By the outer edge of LADUMA's bandpass (z = 1.45) the mass

in confusion will have risen to 1.8×10^9 $M_\odot$ (5.4×10^9 $M_\odot$), potentially large enough to influence the stacking of M_* galaxies.

However, if LADUMA were to be unable to achieve its intended synthesised beam size, then things would look quite different. The orange (third lowest) lines show the case for a 20 arcsec beam, which at the outermost redshift (1.45) would contain over 5×10^9 $M_\odot$ (1.5×10^{10} $M_\odot$) of confused HI, and even by $z\sim0.5$ would contain 5×10^8 $M_\odot$ (1×10^9 $M_\odot$). Preliminary estimates of LADUMA's detection capability (A. Baker, private communication) suggest that at $z\sim0.5$ targets down to masses of 3×10^8 $M_\odot$ might be detectable via stacking, and by the outer edge of the survey this will have increased to 3×10^9 $M_\odot$. In both cases, if LADUMA were to have a beam size of 20 arcsec rather than 10, then these stacks would contain more mass in confused HI than in the target objects. While this may not prevent progress via stacking, it would add a strong additional bias and a new level of complexity to the process that would require careful consideration, compared to if the survey achieves its target resolution.

3.4.3 DINGO UDEEP

Similarly to CHILES, if ASKAP is able to achieve 10 arcsec resolution then the stacking capabilities of DINGO UDEEP will be limited by the physical size of objects, rather than the survey's angular resolution, throughout most of its redshift range (0.1-0.43). Whereas, if only a 30 arcsec resolution can be achieved then, as

the red (second highest) line in figures 3.3 & 3.4 shows, the confused mass will soon rise well above 10^8 $M_\odot$, complicating the interpretation of any stacks of objects of comparable mass. Although stacking of objects above 10^9 $M_\odot$ should still be relatively unimpeded, as the confused mass does not reach 10^9 $M_\odot$ until $z \sim 0.4$ and, as will be discussed in section 3.5.1, the confusion signal can be effectively removed until it becomes comparable to the target signal.

Using the Jones et al. (2015) expression for a general survey detection limit and assuming an order of magnitude improvement from stacking, we estimate that DINGO UDEEP will be capable of detecting an object with an HI mass of 3×10^8 $M_\odot$ via stacking at $z = 0.2$, but at that redshift the predicted confused mass is 1.7×10^8 $M_\odot$ (2.4×10^8 $M_\odot$) for a 30 arcsec beam. At $z = 0.4$ the situation is slightly worse, with the confused mass becoming 6.2×10^8 $M_\odot$ (1.1×10^9 $M_\odot$) and the mass detectable via stacking being 1×10^9 $M_\odot$.

3.4.4 FAST

Unlike the other telescopes discussed here FAST is a single dish, and thus will have a much poorer resolution. The black solid (highest) line in figures 3.3 & 3.4 shows the expected confused mass for a FAST based survey, which rises above 10^9 $M_\odot$ by a redshift of ~0.1 and by 0.4 (0.3) even the most HI massive galaxies will be severely impacted by confusion. FAST's vast collecting area will mean it might be capable of directly detecting HI galaxies in a survey out to $z = 0.2$ or greater,

and would certainly by capable of doing so via stacking, but regardless of how these sources might be detected they will still be subject to considerable bias from confusion.

3.5 Discussion

The approximate agreement shown between the estimates of the confused mass from stacks of Parkes data (Delhaize et al., 2013) and our model is an encouraging validation. However, both our predictions are somewhat higher than the estimates from that paper. The significance of this is difficult to assess as the values quoted from Delhaize et al. (2013) are not given with errors at the relevant stage of their calculation. The simplest potential explanation might be that this is variance between the average value and two particular examples, however using similar multiple realisations of mocks stacks to those in section 3.3.4 it is clear that this cannot be the explanation, as we measure only a standard deviation of approximately a percent between equivalent simulated stacks.

If this offset is real then the reason for it is uncertain; one possibility is that this model uses the HI auto-correlation function, whereas the HI-optical cross-correlation function might be the most appropriate. As shown in Papastergis et al. (2013) the correlation function of SDSS blue galaxies is almost indistinguishable from that of an HI population, but HI-rich galaxies are much less likely to be found in regions with high densities of red galaxies. Therefore, an input sample that

contains any red galaxies will have less confused HI mass around those targets than would targets based on an HI selected sample. Another possible explanation is that the assumption of a constant HI mass to light ratio across the target and confused sources might not be valid at the level of the discrepancy.

Assuming that the upcoming interferometric HI surveys can achieve their desired beam sizes they should have minimal amounts of confusion when making stacks throughout most of their bandpass ranges. However, due to its beam size, confusion is considerably more worrisome for FAST. Duffy et al. (2008) estimated the contribution of confusion to a FAST survey and found that even for very long integration times (over 15 hours) it would not be a concern until beyond a redshift of 0.5. The dashed black (highest) line in figure 3.4 shows the confused mass calculated assuming a uniform universe for a FAST sized beam (3 arcmin). This is equivalent to how the confused mass was defined by Duffy et al. (2008), but our value of $\Omega_{\rm HI}$ is 16 percent larger. As can be seen here the inclusion of the CF (solid black line), compared to assuming a uniform background, increases the confused mass by more than an order of magnitude (over the relevant redshift range). This will severely limit FAST's ability to probe HI galaxies much beyond $z = 0.1$, which reiterates the conclusion of Jones et al. (2015), that future blind HI surveys with single dish telescopes should focus on the nearby universe where their larger beam sizes are a strength rather than a hindrance.

To show how confusion may affect a stack of data from a FAST survey we have simulated two stacks of galaxies with target objects of 3×10^9 $M_\odot$, at redshifts 0.1

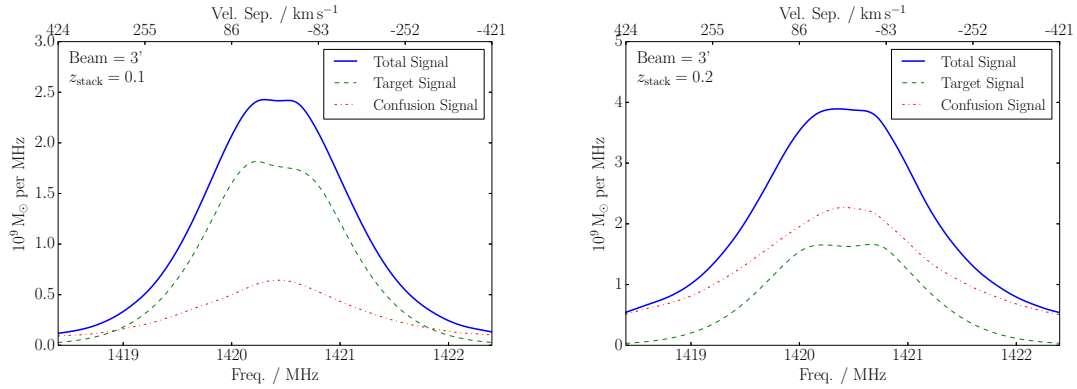

Figure 3.5: Simulated noiseless stacks of 1,000 galaxies of HI mass 3×10^9 M$_\odot$, showing the contributions from the target galaxies (dashed green lines) and from confusion (red dash-dot lines). Both plots assume a zero redshift beam size of 3 arcmin (as expected for FAST). The left plot is for a stack at $z = 0.1$, and the right at $z = 0.2$. Both assume $\rho_{\rm HI} \propto (1+z)^3$.

and 0.2 (see figure 3.5). If the total signal is (incorrectly) assumed to be made up of two Gaussian components, a broad one due to confusion and a narrow one due to the target signal, the mean target masses are found to be 3.3 and 4.4×10^9 M$_\odot$ respectively at $z = 0.1$ and 0.2. The excess signal that is incorporated into the narrow Gaussian component originates from the fact that the confusion profile is itself a double Gaussian, and is therefore not adequately subtracted by the broad component alone. In fact the overestimation would be worse, but some of the target signal is clipped (by the ±300 km s^{-1} boundary), and some is incorporated into the broad Gaussian along with the confusion signal.

A major uncertainty in our predictions is redshift evolution, which due to the current lack of data is inadequately modelled. We argued in section 3.3.4 that the two cases presented for the evolution of HI density likely bracket the true evolution in that quantity, however the impact of the change in the HI CF is more

difficult assess. Hartley et al. (2010) find that the correlation length of blue galaxies in the UKIDSS Ultra Deep Survey increases by approximately a factor of 2 going from $z = 0$ to 1.5. At $z = 0$ blue galaxies and HI-rich galaxies are proxies for each other. Therefore, it is reasonable to assume that the HI CF would also be raised with increasing redshift, meaning the curves shown in figure 3.3 would represent lower limits on the confused mass in stacks.

The two models of the evolution of $\rho_{\rm HI}$ unsurprisingly give similar results at low redshift, but start to diverge at larger redshift, leaving LADUMA with the most uncertain measure of confused mass. The shape of the confused mass versus redshift curve for the constant $\Omega_{\rm HI}$ model (figure 3.3) is qualitatively similar to the shape of a model detection limit for an HI survey. Fabello et al. (2011a) found that an order of magnitude below the detection limit is the most that could be gained by stacking, before non-Gaussian noise became dominant (although Delhaize et al. (2013) indicates that deeper stacks might be possible with very well characterised noise). Therefore, assuming that at all redshifts there are sufficient stacking targets available that are approximately an order of magnitude below the detection limit, we arrive at the somewhat counter intuitive result that the ratio of the mean mass of these targets to the confused mass in their stack, is almost independent of redshift.[ii] It should be noted however that this will break down at the lowest redshifts because, as stated previously, in practice the physical

[ii] Note that this may appear to be in conflict with the Delhaize et al. (2013) experiment, however that is because their two datasets have very different integration times, allowing them to probe lower masses than would otherwise be possible in their higher redshift sample, and thus making the stack more confused.

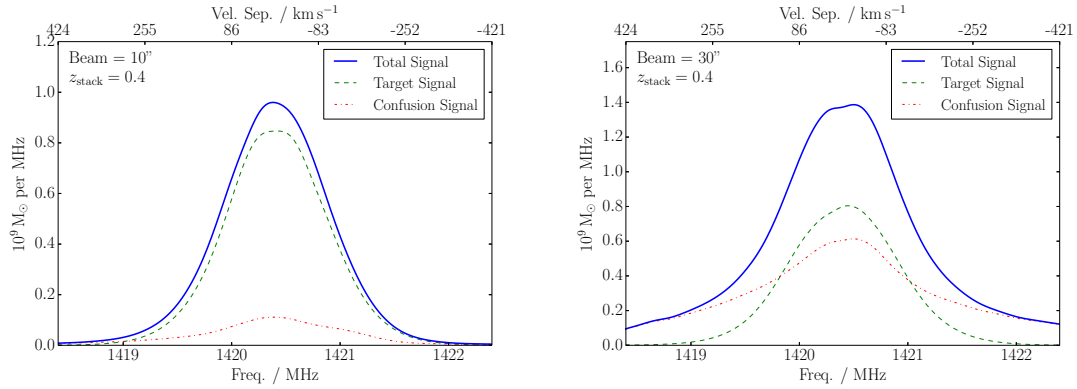

Figure 3.6: Simulated noiseless stacks of 1,000 galaxies of HI mass 10^9 $M_\odot$, showing the contributions from the target galaxies (dashed green lines) and from confusion (red dash-dot lines). Both plots are for a stack at $z = 0.4$ and assume that $\rho_{HI} \propto (1 + z)^3$, but the left has a zero redshift beam size of 10 arcsec, while the right has a 30 arcsec beam.

size of galaxies will prevent the confused mass ever dropping much below 10^8 $M_\odot$. In the case where ρ_{HI} increases with the Universe's decreasing volume (figure 3.4) the confused mass rises much more steeply with redshift, producing much more severe confusion at higher z. While this might seem like the most conservative model to use, the currently available data (Rhee et al. (2013) and references within) indicate that ρ_{HI} does not increase this quickly with redshift.

Regardless of which evolution model is assumed to be correct, the results show that for surveys like LADUMA and DINGO UDEEP, where the synthesised beam size is not yet fixed, there is much to be gained in terms of the stacking performance by pushing to a lower beam size (in this case 10 arcsec). The difference in confused mass between a beam size of 10 and 30 arcsec is approximately an order of magnitude. For DINGO UDEEP a 30 arcsec beam would mean that a large fraction of the mass in stacks (probing the lowest possible HI masses) will

be contributed by confusion, at all redshifts; whereas with a 10 arcsec beam the contribution would be almost negligible. For LADUMA there is little option but to use a ~10 arcsec beam if stacking is going to be a viable option. Even with a 20 arcsec beam the smallest masses that are in theory detectable via stacking would likely always be below the level of the confused mass, but with a 10 arcsec beam this would not be the case until the very largest redshifts.

Figure 3.6 shows the contributions of confusion in two simulated stacks at approximately the outer edge of DINGO UDEEP's bandpass ($z = 0.4$) for beam sizes of 10 and 30 arcsec (at $z = 0$). The target galaxies have HI masses of 10^9 $M_\odot$, the lowest that will likely be detectable via stacking with this survey at $z = 0.4$. While the 30 arcsec beam introduces 1.1×10^9 $M_\odot$ of confusion, the 10 arcsec beam only introduces 1.5×10^8 $M_\odot$. In this case naively splitting the resulting total signal into two Gaussian components gives a mean target mass of 1.3 and 1.0×10^9 $M_\odot$, for the 30 and 10 arcsec beams respectively.

For regimes where the confused mass in a stack is comparable to the anticipated mass of the targets, the spectral profile calculated in section 3.3.2 indicates that caution must be used. The profile of confusion alone appears to be well fit by a double Gaussian, where the two components arise from the width of the velocity space CF and the distribution of redshift uncertainties in the input catalogue. This is precisely the profile that might be expected from a stack detection with a small amount of confusion, a narrow Gaussian (presumed from the target objects) superimposed on a broader Gaussian (presumed to be from confusion). Thus, in

a severe case it is possible that confusion alone could be misidentified as a detection and confusion. In a more moderate case, where there is a real detection, it is desirable to minimise the amount of confused mass and to understand how much it still contributes to the final stack. Strategies to accomplish this are discussed below.

3.5.1 Mitigation Strategies

In any stacking experiment where a significant contribution from confusion is anticipated (not limited to the surveys discussed here), there are two approaches that can be taken to improve the outcome: either strategies to remove confused mass can be implemented, or the amount of the final signal that is contributed by confusion can be estimated.

As a first approximation the model presented in this chapter can be used to predict how much confusion there is in a stack, however there are a number of situations where this might give a poor estimate. For example, a stack with a small number of targets, at high redshift, or with an input catalogue of galaxies not selected for HI content. In such cases other strategies might be necessary. One approach could be to explore the properties of such stacks in a simulation, another is to attempt to mitigate the impact of confusion when extracting the final parameters from a stack, which is the approach we discuss below.

Double Gaussian Decomposition

As figure 3.1 shows, a large fraction of the signal from confusion is expected to be in a broad Gaussian component, whereas most of the target emission should be in a narrow component. Although there is also a narrow component to the confusion profile, removing the broad component will help to alleviate much of the confusion.

This approach was tested by simulating the confusion in a stack using representative HI line profile shapes (Saintonge, 2007), positions from the CF, and assuming the $z = 0$ value of HI density (Martin et al., 2010). The narrow Gaussian component of the total profile was found to reproduce the mean target mass well (within ~10%) in the cases where the confused mass was less that about 2/3 of the target mass, although results were marginally worse for more massive, broader targets. Presumably the portion of the target signal that is excluded from the narrow Gaussian is approximately made up for by the inclusion of some of the narrow component of confusion. However, when the confused mass becomes almost as large as the target mass, the narrow Gaussian integral begins to diverge from the mean target mass.

Thus, this straightforward method is very successful for stacks with low levels of confusion, but cannot adequately separate target signal and confusion when the confusion is more severe.

Beam Weighting

In the regime where the telescope beam (or synthesised beam) is considerably larger than the target source, the weighting of the pixels can be tapered away from the target. This will have little impact on the target flux (presumably concentrated in the central pixel), but will give lower weight to the surrounding confusion signal.

This approach was tested using mock stacks, as before. For stacks with physical beam sizes of 100-600 kpc, assuming 4 pixels across a beam width and a Gaussian weighting scheme, the confused mass was reduced by approximately 25-30% compared to a uniform weighting. However, for larger beam sizes there are diminishing returns as in addition to the target, many of the confused objects also lie within the central pixel.

Inclusion and Exclusion of Confused Targets

Possibly the most obvious solution to confusion is to simply excluded the stacking targets that are likely to be heavily confused. Most of the HI mass in the Universe is contained in M_* systems, which are likely to be visible in the optical input catalogue. Targets that are in close proximity to M_* galaxies (provided they have optical redshifts) could in principle be removed from the input catalogue. As most of the HI mass is contained in these galaxies, this would remove most of the confused mass from the stack.

This approach has some promise for the cases where low mass galaxies are being stacked at low redshift and M_* galaxies are uncommon, but for higher redshifts where the beam sizes become larger, many targets are confused, often multiple times (Delhaize et al., 2013; Jones et al., 2015). Thus, it becomes impractical to remove them.

The approach taken by Delhaize et al. (2013) was to include such targets, but to note the presence of likely sources of confusion. By assuming a constant HI mass to light ratio they were able to estimate the fraction of the stack mass that was contributed by confusion. As shown in section 3.4 our results are roughly consistent with their findings. This procedure could be taken further by using HI scaling relations with stellar mass or disc size to improve the estimate of the confused galaxy masses (Toribio et al., 2011; Huang et al., 2012a).

Exclusion in Velocity Space

Weighting the beam cuts confusion by eliminating sources spatially, but this can also be done in velocity space. Fabello et al. (2011a) used the Tully-Fisher relation (TFR) to remove the section of the spectrum containing the intended target, in order to estimate the rms noise in the rest of the spectrum. The same method could be used to stack just the region of the spectrum that is likely to contain emission from the target galaxy, thereby removing additional sources in front or behind the target that would otherwise contribute to a stack made with a conservative ±300 $\mathrm{km\,s^{-1}}$ cut.

This method was simulated as before, but with each contributing spectrum cut off at $\pm(W_{TF}/2 + \sigma_{\rm input})$ away from the target redshift. Where W_{TF} is the target's simulated velocity width (W_{50}) with 0.2 dex of scatter introduced (designed to emulate the TFR), and $\sigma_{\rm input}$ is the standard deviation of the redshift uncertainty in the input catalogue (35 km s^{-1}). This gave approximately a 60% reduction in confused mass when stacking targets in the mass range 10^8 - 10^9 M$_\odot$, and a 45% reduction for targets in the range 10^9 - 10^{10}. However, it also typically removed 30-35% of the flux from to the target objects, with the higher mass stack more effected.

3.6 Conclusions

We created a model to predict the average amount of HI mass contributed by confused sources to a stack from a generic survey. The analytic expression of our model (equation 3.2) is derived in the general case, allowing for different beam sizes, velocity ranges, HI background densities or fits to the CF to be used to make quick estimates of the amount of confusion in any HI survey. This model, based on the ALFALFA correlation function, shows agreement with estimates of the confusion present in stacks of Parkes data (Delhaize et al., 2013), and predicts approximately an order of magnitude more confused HI than found from assuming a uniform universe (Duffy et al., 2008).

The largest uncertainty in the predictions comes from our relative ignorance

of the redshift evolution of HI-rich galaxies. However, we argued that the true values likely fall between the two idealised cases presented here, and that the smaller of the two is in fact a lower limit.

The results for upcoming SKA precursors surveys, like LADUMA and DINGO UDEEP, reveal that it would be highly advantageous if these surveys could achieve their initially intended resolutions (10 arcsec), as any resolution substantially poorer than this would lead to stacks that are dominated by confusion, rather than their target objects.

Confusion was the most concerning for FAST; its larger (single dish) beam size results in the mass in confusion rapidly overtaking even that of M_* galaxies, as redshift increases. This will prevent a FAST based blind HI survey from probing individual galaxies much beyond $z = 0.1$ with either stacking or direct detections. Similarly to the findings of our previous work (Jones et al., 2015) this indicates that single dish telescopes should focus their HI galaxy studies on the local Universe.

When simulating stacks with a large component of confusion we had limited success in implementing mitigation strategies. Weighting pixels in a Gaussian pattern reduced the confused mass by about 30%, but is only suitable when one pixel is larger than the angular extent of the targets. Using the TFR to exclude regions of the spectrum beyond the target's emission was even more successful at removing unwanted confusion, however it also removed around 30% of the target emission. Simply decomposing the total spectrum into broad and narrow Gaussian components was very successful at estimating the mean target mass with even moderate

levels of confusion, despite it not being an accurate model of the profile shape of targets combined with confusion. However, when the confused mass approached that of the targets, the results began to diverge from the true values. Thus in the event of of heavily confused stack, the best approach will likely be not to try to exclude sources of confusion, but to use optical data or simulations to model and account for their HI properties.

CHAPTER 4

ENVIRONMENTAL DEPENDENCE OF THE HI MASS FUNCTION IN THE ALFALFA 70% CATALOGUE

4.1 Introduction

The HI mass function (HIMF) is the density distribution of HI masses of galaxies in the Universe and represents a key component in understanding how collapsed structures form. HI surveys are complementary to optical surveys, and the galaxy luminosity functions they deliver, because they have fundamentally different selection effects and thus detect a different component of the underlying galaxy population. Together the luminosity functions and mass functions that these surveys calculate offer important constraints on the population of galaxies that simulations of structure formation generate.

Detailed studies of the HIMF have only become possible in the last decade or so, as previously sample sizes were too small and selection effects too poorly understood. With the advent of wide area, blind surveys like HIPASS (HI Parkes All Sky Survey; Barnes et al., 2001) and ALFALFA (Arecibo Legacy Fast ALFA survey; Giovanelli et al., 2005) precise determination of the HIMF in the local Universe has become possible, with both HIPASS and ALFALFA (Zwaan et al., 2005; Martin et al., 2010) indicating that the HIMF is well fit by a Schechter function (an analytic expression for the mass distribution of collapsed objects in an expanding

This chapter is an adapted version of the published article Jones et al. (2016b).

universe, Press & Schechter, 1974; Schechter, 1976), with a low-mass slope of approximately -1.3 and a 'knee' mass of almost 10^{10} $M_{\odot}$. The large area and source counts of these surveys have also allowed studies of environmental dependence that are not restricted to 10s or 100s of objects and a handful of nearby groups.

Although many studies looking for environmental dependence have been carried out (for example Rosenberg & Schneider, 2002; Springob, Haynes & Giovanelli, 2005; Zwaan et al., 2005; Stierwalt et al., 2009; Moorman et al., 2014), it is still important to ask why any environmental dependence is expected at all? There are many processes and properties that are known to depend on a galaxy's environment, here we will briefly discuss a few that we expect to be the most influential on a galaxy's HI content. First, due to their mass and tendency to cluster, more massive dark matter (DM) halos are generally found in more overdense regions. Thus, the 'knee' mass (M_*) of a Schechter function fit to the HIMF, would be expected to increase towards more dense regions of the Universe. Secondly, voids can be considered as more slowly evolving sections of our Universe (Peebles, 2001; Tinker & Conroy, 2009). This means that by isolating the void galaxies in a sample, you are effectively probing the HIMF at a previous time, where systems are likely to be lower mass and more numerous, assuming a hierarchical model of galaxy formation. Therefore, it would be expected that the low-mass slope would steepen within lower density regions. In addition to these two effects, in the most dense regions (galaxy clusters) galaxies will be unable to retain their neutral gas due to the harassment and ram pressure stripping they experience, and so might be expected to be HI-deficient with respect to galaxies in the field; while galaxies

in voids are likely more prone to background UV heating than those in the field (Hoeft et al., 2006). Given all of the above, some environmental dependence in the shape of the HIMF is expected, however there are numerous competing affects, making the exact nature of the dependence difficult to predict. To complicate matters further, most studies have thus far produced marginal and/or conflicting results.

Using the Arecibo Dual Beam Survey (ADBS; Rosenberg & Schneider, 2000) Rosenberg & Schneider (2002) found that the HIMF low-mass slope (α) was flatter in Virgo than the ~-1.5 value found in the rest of the survey. However, the paper points out that small number statistics and distance errors make their results somewhat uncertain. Springob, Haynes & Giovanelli (2005) also found (at low significance) that both α and M_* decrease in high density environments, from their analysis of an optically selected sample from the Arecibo General Catalog (Springob et al., 2005). However, more recently, Stierwalt et al. (2009) used an early ALFALFA release to show essentially the opposite result, that the low-mass slope in the dense Leo region was steeper than other measurements of the HIMF at the time (though, given the quoted error, is now consistent with that of the global ALFALFA HIMF; Martin et al., 2010). There are also a number or other results from surveys of individual groups (Verheijen et al., 2001; Kovac, Oosterloo & van der Hulst, 2005; Freeland, Stilp & Wilcots, 2009; Pisano et al., 2011) which generally imply that the low-mass slope is flatter in galaxy groups.

Zwaan et al. (2005) concluded that α steepened in high density environments,

based on data from HIPASS. However, unlike all other studies, the proximity to other HI galaxies was used to define environment (rather than an optically selected reference catalogue). HI surveys are known to be incomplete for galaxies in the densest environments, which combined with the fact that HIPASS is not a volume limited catalogue, makes a comparison with this result difficult; but we note that attempting to perform a similar experiment with ALFALFA did not result in any apparent environmental dependence in the HIMF. Most recently Moorman et al. (2014) used the 40% ALFALFA catalogue (α.40) to search for environmental dependence based on void and wall regions defined using the method devised by Hoyle & Vogeley (2002). They found no evidence of any change in α, but contrary to Springob, Haynes & Giovanelli (2005) M_* was found to increase in denser regions. This represents the most statistically significant result of large scale environmental dependence in the HIMF to date, which is in part due to the greatly larger sample size that ALFALFA provides. Since that study, data from 30% more of ALFALFA's nominal area (~7,000 deg^2) have been reduced, and ~7,000 additional high signal-to-noise HI sources have been extracted.

In this chapter we choose to focus on a local definition of galaxy environment, rather than defining voids, walls and clusters, for two reasons. First, because the majority of the additional 30% added to the ALFALFA catalogue since the Moorman et al. (2014) study is not within the SDSS (Sloan Digital Sky Survey) spectroscopic footprint, making defining voids problematic; and secondly because related optical and theoretical works (Berlind et al., 2005; Blanton et al., 2006; Tinker & Conroy, 2009) find that galaxy properties are most closely related

to a galaxy's host halo, and may even be almost independent of its large scale environment. Obviously the two are not independent, but if a galaxy's properties depend mostly on its host halo mass rather than its "assembly bias" (the idea that haloes of a given mass, but which assemble at different times, will cluster differently, e.g. see Wechsler et al., 2006), then the strongest signal of any change in the mass function would presumably arise from a measure of local environment, rather than large scale structure (LSS).

We use a combination of SDSS data release 8 (Aihara et al., 2011) and the 2MASS Redshift Survey (2MRS; Huchra et al., 2012) as reference catalogues to define the local density of ALFALFA galaxies based on the separation of their projected nearest neighbours in these catalogues. This allows us to split the HI sources into quartiles of differing environment and calculate the HIMF for each environment separately. 2MRS allows us to make use of the full ALFALFA 70% sample, while the superior depth of SDSS permits smaller scale environments to be probed.

In the following section we give a brief overview of the ALFALFA survey, in §4.3 we describe our definitions of environment, §4.4 outlines how the HIMF is calculated, and our results are presented in §4.5. The implications of these results are discussed in §4.6, and finally we draw our conclusions in §4.7.

4.2 The ALFALFA sample

Observations for the main ALFALFA survey were completed in October 2012 after over 7 years of observing with the 305 m Arecibo radio telescope in Puerto Rico. The final ALFALFA footprint covers approximately 6,900 deg^2 on the sky, and is broken up into two contiguous regions: one ranges from ~7.5 hr RA to ~16.5 hr RA in the Arecibo Spring sky, and the other from ~22 hr RA to ~3 hr RA in the Arecibo Fall sky. While the Spring ALFALFA region has almost complete overlap with SDSS spectroscopy, in the Fall sky there are only a few stripes where spectra are available. The drift scan observing strategy of ALFALFA proved extremely successful with over 95% of observing time spent with the "shutter open", including all start-up, shutdown and calibration procedures. A matched filtering algorithm (Saintonge, 2007) is used to help identify sources, but all ALFALFA spectra are ultimately extracted by a person, and the current progress is over 70% complete, yielding over 20,000 high signal-to-noise (S/N) sources and counting. Over 99% of these HI sources have identified optical counterparts (with matching redshifts where optical spectra exist).[i]

In order to calculate the HIMF it is essential to have HI masses for the ALFALFA sources, which in turn necessitates distance measurements for every source. ALFALFA uses a flow model developed by Masters (2005) to convert recessional velocities below 6,000 km s^{-1} to distances. Distances to galaxies beyond 6,000 km s^{-1} are calculated instead assuming Hubble flow, with H_0 = 70

[i]The ALFALFA 70% catalogue is publicly available at http://egg.astro.cornell.edu/alfalfa/data/index.php

$\mathrm{km\,s^{-1}\,Mpc^{-1}}$. In addition, 303 sources are assigned to regions of the Virgo cluster by matching to the VCC (Virgo Cluster Catalog; Binggeli, Sandage & Tammann, 1985), 1,130 sources are assigned to groups from 2MRS (Crook et al., 2007) and given the mean velocity of the group members, and 63 (1,646) sources are given their primary (secondary) distances from the literature. Note that in this article we only consider galaxies in the 70% ALFALFA catalogue within the range of distances 1,000-15,000 $\mathrm{km\,s^{-1}}/H_0$.

Once distances to ALFALFA galaxies have been calculated, their HI masses can be computed through the usual equation:

$$\frac{M_{\mathrm{HI}}}{\mathrm{M}_\odot} = 2.356 \times 10^5 D^2_{\mathrm{Mpc}} S_{21} \quad . \tag{4.1}$$

In the equation above, D_{Mpc} is the distance to the galaxy in Mpc and S_{21} is its integrated flux in Jy $\mathrm{km\,s^{-1}}$.

4.3 Quantifying Environment

The term 'environment' has no objective definition, and different studies have used drastically different methods to describe it quantitatively. On one extreme we can find techniques that characterise the environment based on the morphology of the cosmic web, classifying galaxies as void, wall, and filament objects (e.g. Hoyle & Vogeley, 2004; Rojas et al., 2004; Hoyle et al., 2005). On the other extreme, it is possible to characterise the most immediate surroundings of a galaxy based

on its status as a central or satellite galaxy (e.g. Carollo et al., 2013). In this article we choose to study the dependence of the HIMF on the *local* environment of ALFALFA sources, as traced by the proximity of neighbouring galaxies. More specifically, we employ the widely-used nearest neighbour (NN) and fixed aperture (FA) methods to quantify the environment (e.g. Muldrew et al., 2012). The former method calculates a local density based on the distance between the target galaxy and its N^{th} nearest neighbour. The latter is instead based on the number of objects found within a region of fixed size surrounding the target galaxy.

Each method of environment characterisation has its own set of advantages and drawbacks, and there are often trade-offs between a method's physical motivation and its simplicity. Our choice to use the NN and FA methods is based on the fact that these two methods are purely observational, and have a clear and intuitive definition. Sections 4.3.1–4.3.3 below contain a detailed description of the methods' implementation in the context of the ALFALFA sample.

4.3.1 An external reference catalogue for environment characterisation

The simplest way to find neighbouring galaxies for the ALFALFA sources would be to search within the ALFALFA catalogue itself. This approach has been previously used by Zwaan et al. (2005) to measure the environment of galaxies detected by the HIPASS blind HI survey. Even though straightforward, this methodology

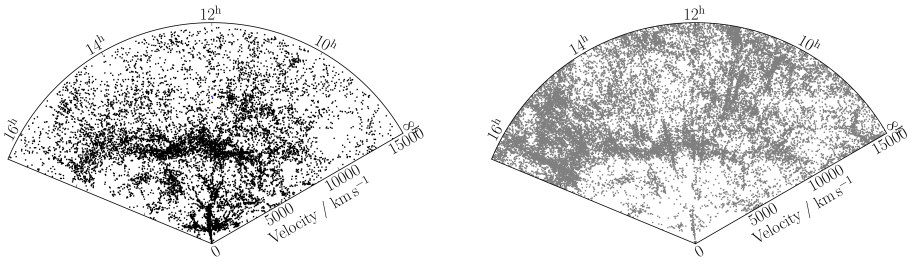

Figure 4.1: *Left panel*: Coneplot of ALFALFA galaxies in the Spring region of the sky. *Right panel*: Coneplot of the SDSS galaxies in the reference volume-limited catalogue, within the same volume as the ALFALFA sample. The environment of each ALFALFA galaxy in the left panel is calculated based on the position of neighbours in the reference catalogue shown in the right panel (refer to §4.3.1 for details).

comes with two important observational disadvantages. First, any blind HI survey produces a nearly flux-limited[ii] sample. As the left panel of Figure 4.1 shows, the number of detections in such a sample drops in the outer parts of the survey, since only the most HI massive galaxies remain visible at these large distances. Consequently, a bias is introduced in the measurement of environment, whereby galaxies appear systematically more isolated with increasing distance. Second, galaxies located in the central regions of clusters and rich groups are known to be HI-deficient with respect to their peers in the field (Haynes, Giovanelli & Chincarini, 1984, for a review). This means that HI-selected samples are biased against the highest density regions of the cosmic web. This effect can be clearly seen either directly in the spatial distribution of ALFALFA galaxies near clusters (see figure 6 in Haynes et al., 2011), or indirectly in the clustering properties and the colour-magnitude diagram of ALFALFA galaxies (see figure 20 in Papastergis et al., 2013

and figure 10 in Huang et al., 2012b, respectively).

In this article we remedy these shortcomings by defining the environment of ALFALFA galaxies based on an external reference catalogue. The catalogue we use has two important properties:

1. *It is optically selected.* In particular, we use galaxies from the spectroscopic database of the eighth data release of the Sloan Digital Sky Survey (SDSS DR8; Aihara et al., 2011). This property ensures that we trace the environment well even in high density regions where gas-deficiency becomes an issue.
2. *It is volume-limited.* We include in the reference catalogue only galaxies that are brighter than $M_r = -18.9$. Given the apparent magnitude limit for the SDSS spectroscopic sample ($m_r = 17.75$) and the maximum distance cut for the ALFALFA sample ($\approx$214 Mpc), these galaxies are bright enough to constitute a volume-complete sample within the ALFALFA volume. In turn, this ensures that environment is measured consistently regardless of the distance at which the ALFALFA galaxy is located.

The right panel of figure 4.1 shows the spatial distribution of the SDSS reference catalogue. As expected from its volume-limited nature, the number of objects in the reference catalogue grows steadily with increasing distance. Note that

[ii] In reality, the detection limit of a blind HI survey depends both on the integrated flux and the width of a galaxy's HI profile (see section 6 in Haynes et al., 2011). However, the width dependence of the detection limit is mild enough such that the detectability of a galaxy by ALFALFA depends primarily on its HI mass.

in order to avoid edge effects, the reference catalogue is slightly more extended in the radial direction than the ALFALFA sample, covering the distance range 500 – 15,500 km s^{-1}/H_0. We remind the reader that distance cuts are quoted in terms of recessional velocity, but they actually refer to distances that are estimated as described in §4.2. In order to avoid edge effects in the plane of the sky as well, the reference catalogue must have more than complete sky overlap with the ALFALFA sample. Figure 4.2 shows the footprints of the ALFALFA sample and the SDSS reference catalogue in the Spring region of the sky, and details the complicated sky mask that is necessary to maximise the number of ALFALFA galaxies while maintaining high levels of overlap with the reference catalogue. Keep in mind that, given the poor spectral coverage of SDSS in the Fall region of the sky, a different reference catalogue is necessary to study the 70% ALFALFA sample over its full sky extent (see §4.3.4).

Defining environment in this way, based on a volume-limited reference catalogue avoids the need to place harsh flux cuts on the ALFALFA sample (to make it volume-limited), as its sensitivity and completeness are well understood (Haynes et al., 2011) and can be corrected for independently of our external definition of environment, as will be described in §4.4.

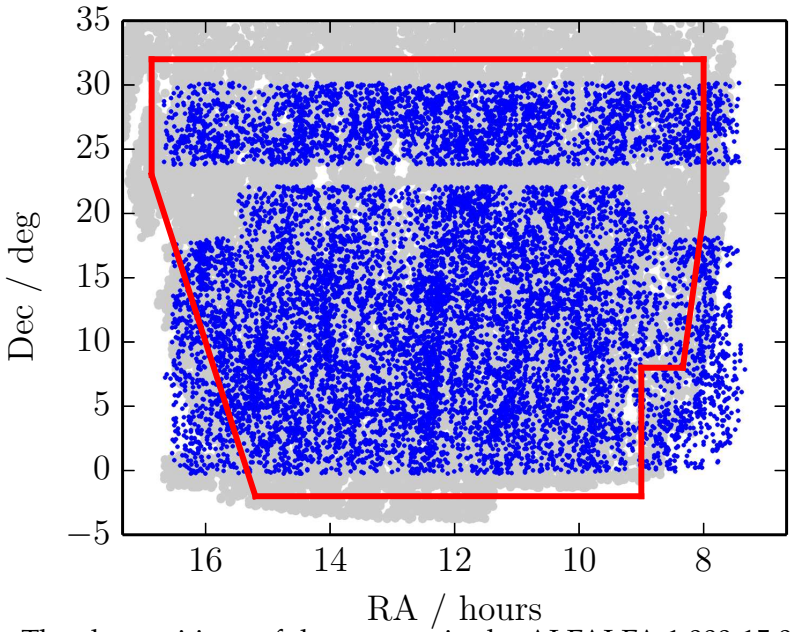

Figure 4.2: The sky positions of the sources in the ALFALFA 1,000-15,000 km s^{-1} sample (small blue points), and the 500-15,500 km s^{-1} SDSS reference catalogue (large, overlapping grey points). The thick red line is the cut that is applied to the ALFALFA sample when comparing with SDSS, in order to ensure there is more than complete overlap.

4.3.2 Nearest Neighbour Environment

We calculate a nearest neighbour density for each ALFALFA galaxy based on the projected distance to the third closest galaxy in the reference SDSS catalogue. First, we record the sky position of all objects in the reference catalogue that have a recessional velocity within ±500 km s^{-1} from the recessional velocity of the target ALFALFA galaxy. We then identify the third nearest object in the plane of the sky, and calculate its projected separation at the distance of the ALFALFA galaxy, R_3. The projected nearest neighbour density can then be calculated as

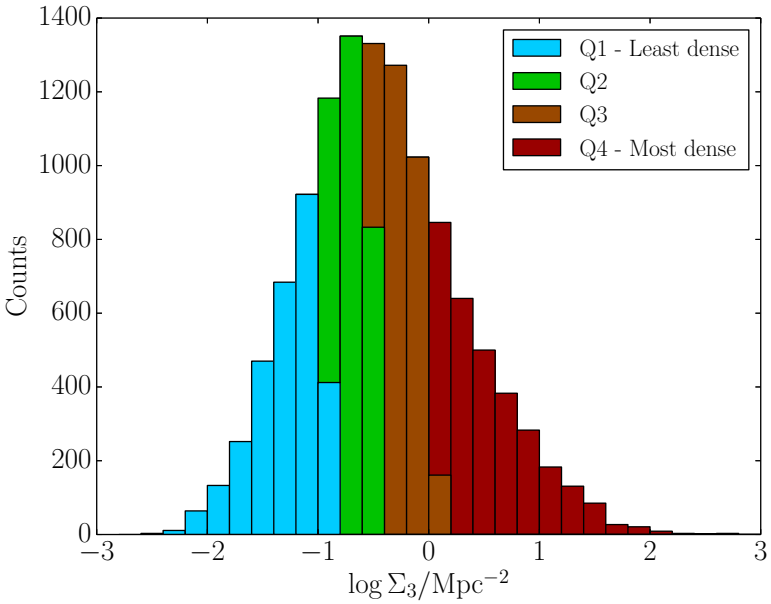

Figure 4.3: Histogram of the 3rd nearest neighbour density, Σ_3, for ALFALFA galaxies. The density of each ALFALFA galaxy is calculated based on the proximity of neighbouring objects in an SDSS volume-limited reference catalogue (refer to §4.3.1 & §4.3.2). Different colours and hatching styles mark the four quartiles of the distribution, which from light blue to dark red (light to dark colours, and left to right) contain galaxies situated in progressively denser environments.

$$\Sigma_3 = \frac{3}{\pi R_3^2} \quad . \tag{4.2}$$

When identifying neighbours, we exclude any object in the reference catalogue that is located within 5 arcsec and ± 70 km s^{-1} from the ALFALFA galaxy; such an object corresponds (almost always) to the counterpart of the ALFALFA galaxy in SDSS. Throughout this article, Σ_3 will be used to characterise the local environment via the NN method, and will often be referred to as simply 'the environment' or 'local density'.

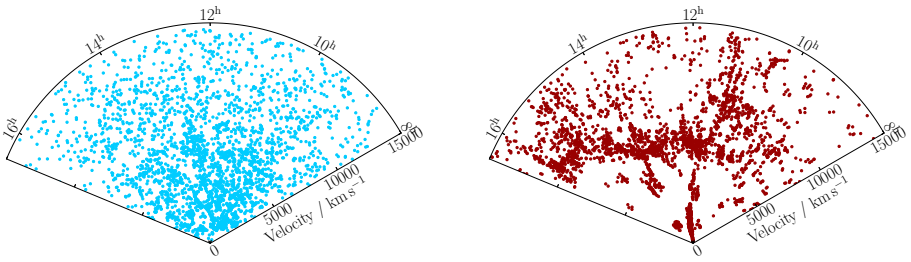

Figure 4.4: Coneplots of ALFALFA galaxies belonging to the lowest density quartile (*left panel*) and highest density quartile (*right panel*) of the nearest neighbour density distribution (see figure 4.3). Note the marked difference in clustering between these two environmental subsamples.

Figure 4.3 shows the distribution of Σ_3 for the ALFALFA galaxies. Based on the distribution's approximately lognormal shape, we divide the ALFALFA sample into four quartiles which contain objects residing in increasingly denser environments. Figure 4.4 shows coneplots of the ALFALFA galaxies belonging to the lowest and highest density quartile (left and right panel, respectively). Reassuringly, the difference in clustering between the two environmental subsamples is clearly visible by eye. Sources in the densest environment are grouped together in clumps and filaments, whereas the sources in the least dense environment are distributed almost uniformly in space. This is an excellent indication that the NN method is splitting the ALFALFA galaxies into environmental subsamples in a sensible way.

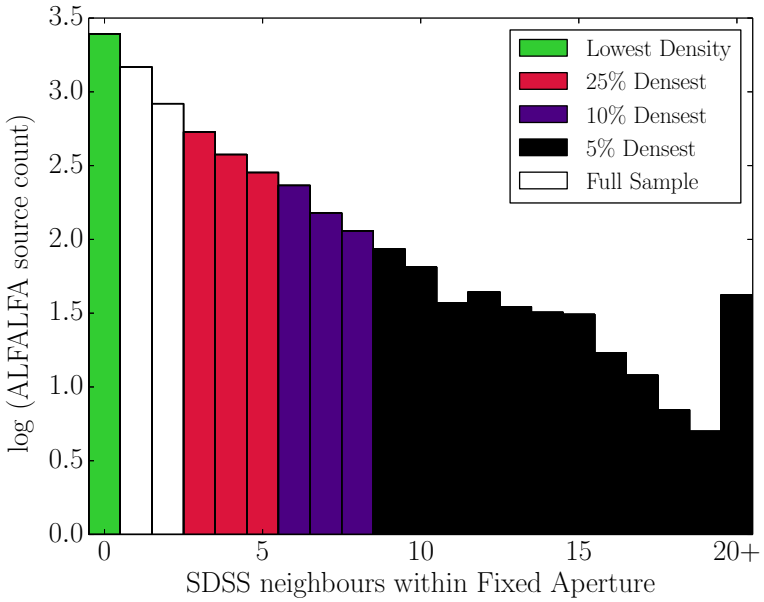

Figure 4.5: Histogram of the number of SDSS neighbours within the fixed aperture, N_{FA}, for galaxies in the ALFALFA sample (see §4.3.3). The green (leftmost) bar denotes the lowest density subsample, $N_{FA} = 0$. The crimson, purple and black bars (left to right) represent instead the ALFALFA galaxies located in the densest 25%, 10% and 5% environments, according to the fixed aperture method ($N_{FA} \geq 3$, $N_{FA} \geq 6$ and $N_{FA} \geq 9$, respectively). Note that these three all overlap as the densest 25% includes both the densest 10% and 5%. The final bin contains counts for all ALFALFA sources with 20 or more SDSS neighbours within the fixed aperture. The white bars correspond to galaxies with $0 < N_{FA} < 3$.

4.3.3 Fixed Aperture Environment

In addition to the NN method described above, we also adopt a fixed aperture approach as a complementary way to measure the environment of ALFALFA galaxies. In particular, we count the number of galaxies in the reference catalogue that lie within a radius of 1 Mpc and a velocity range of ±500 km s^{-1} from the position and velocity of our target ALFALFA galaxy. The fixed aperture environment is

thus characterised simply by a natural number, $N_{\rm FA}$. As with the nearest neighbour method, we exclude possible optical counterparts from the count (any object that is within 5″ and ± 70 km s^{-1} from the ALFALFA galaxy).

Figure 4.5 shows the distribution of fixed aperture environment, $N_{\rm FA}$, for the ALFALFA sample. Unlike in the case of nearest neighbour densities, the distribution of $N_{\rm FA}$ has a power law form. This means that the fixed aperture method provides a rather coarse description of environment at low densities; for example, the lowest FA density subsample ($N_{\rm FA}= 0$) contains already 38% of the total sample. On the other hand, the FA method is better for isolating the ALFALFA galaxies that reside in the highest density environments. The preceding points are visually demonstrated by the two coneplots in Figure 4.6: The left panel shows the lowest FA density subsample of ALFALFA. This sample is successful at tracing low density environments in general, but cannot discriminate between galaxies located in voids and galaxies located in parts of filaments with low local density. On the other hand, the right panel shows the top 5% of ALFALFA galaxies in terms of FA density ($N_{\rm FA}\geq 9$). This latter sample does an excellent job at tracing the locations of the largest clusters and groups in the survey volume.

4.3.4 2MRS Nearest Neighbour Environment

In order to study the environment of the 70% ALFALFA sample in both the Spring and Fall regions of the sky, we need a reference catalogue that covers the entire

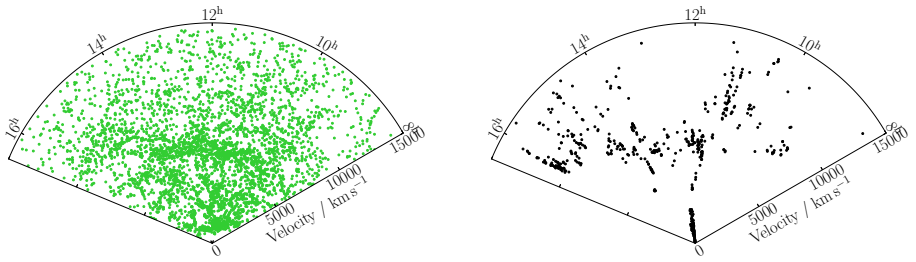

Figure 4.6: Coneplots of ALFALFA galaxies belonging to the lowest density subsample (*left panel*) and highest density subsample (*right panel*) of fixed aperture environment (refer to figure 4.5). The latter sample demonstrates that the fixed aperture method can be used to probe the largest groups and clusters in the survey volume.

celestial sphere. To this end, we follow the same approach described in §4.3.1, but now using the all-sky 2MASS Redshift Survey (2MRS) as reference. We select galaxies in the 2MRS that are brighter in the K-band than $M_K = -24.9$. Given the 2MRS apparent magnitude limit of $m_K = 11.75$, this cut makes the 2MRS catalogue volume-limited over the entire volume probed by ALFALFA out to 15,000 $\mathrm{km\,s^{-1}}/H_0$.

Compared to the SDSS spectroscopic survey, the 2MRS survey is much shallower. This means that the 2MRS-based reference catalogue is limited to much brighter objects than the SDSS-based one, and consequently it is much sparser in space. This fact affects the way in which environment is measured with the nearest neighbour method. In particular, the third nearest neighbour in the 2MRS catalogue is usually so far apart from the target ALFALFA galaxy that it does not provide a good measure of local environment. As a result, when using the 2MRS

catalogue as reference we calculate local densities based on the distance to the nearest neighbour, R_1; the corresponding density is then $\Sigma_1 = 1/\pi R_1^2$.

Figure 4.7 shows the distribution of Σ_1 for the full ALFALFA sample. We follow the same process described in §4.3.2 and split the distribution into four quartiles, containing galaxies located in progressively denser environments. Note that despite the change in nearest neighbour rank, the scale over which environment is probed by 2MRS is still larger than in the SDSS case. This is evident by the shift in the location of the distribution peak between figures 4.3 and 4.7; the former peaks at ~0.16 Mpc^{-2}, and the latter at ~0.01 Mpc^{-2}. The difference in scale over which environment is probed is also reflected in the spatial distribution of the 2MRS environmental subsamples. This is clearly visible in Figure 4.8, which plots the spatial distribution of the lowest and highest density 2MRS quartiles (left and right panel, respectively). By comparing with the corresponding panels in figure 4.4, one can immediately recognise that the 2MRS environmental subsamples follow more closely the cosmic LSS than their SDSS counterparts. For example, large filaments are more starkly defined in the highest density 2MRS sample than in the highest density SDSS sample. At the same time, galaxies in the lowest density 2MRS sample actively avoid the locations of large filaments, an effect that is not present in the corresponding SDSS sample (see figure 4.4).

4.4 Calculating HIMFs

The HI mass function (HIMF) is defined as the number density of galaxies as a function of their HI mass, $\phi(M_{HI})$. Galaxies span several orders of magnitude in terms of their HI mass, so the HIMF is customarily measured in logarithmic mass intervals as

$$\phi(M_{\rm HI}) = \frac{dN_{\rm gal}}{dV\, d\log_{10}(M_{\rm HI})} \quad . \tag{4.3}$$

In the equation above, $dN_{\rm gal}$ is the average number of galaxies in a cosmic box of volume dV, whose HI mass lies within a small logarithmic bin centred around $M_{\rm HI}$.

Since the ALFALFA sample is (roughly) flux-limited, the measurement of the HIMF is not a simple counting exercise. For example, there are many more detections in ALFALFA with $M_{\rm HI}$= 10^{10} $M_\odot$ than with $M_{\rm HI}$= 10^{8} $M_\odot$, but the former sources can be detected out to much larger distances than the latter. Once the sensitivity limits of the survey are known (Haynes et al., 2011, section 6), this effect can be compensated for by weighting each source according to the maximum volume over which it is detectable by the survey ('$1/V_{\rm max}$' method).

The $1/V_{\rm max}$ method has the advantage of being intuitive and simple to implement, but has one major limitation: it is unbiased only if the galactic population is distributed in an approximately uniform way within the survey volume. This

is definitely not the case for the ALFALFA survey, where large-scale structure is clearly present in the spatial distribution of galaxies (see figure 4.1). For this reason, we use in this article a more sophisticated method to calculate the HIMF, referred to as the '$1/V_{\rm eff}$' method (Zwaan et al., 2005). More specifically, the HIMF can be calculated within logarithmic mass bins as

$$\phi_i = \frac{1}{\Delta m_{\rm HI}} \cdot \sum_j \frac{1}{V_{{\rm eff},j}} \quad , \tag{4.4}$$

where the summation runs over all galaxies j that belong to mass bin i. Accordingly, the counting error on the HIMF can be calculated as

$$\sigma^2_{\phi_i} = \frac{1}{\Delta m^2_{\rm HI}} \cdot \sum_j \frac{1}{V^2_{{\rm eff},j}} \quad . \tag{4.5}$$

In the equations above, $\Delta m_{\rm HI}$ is the logarithmic width of the mass bin (i.e. $\Delta \log_{10}(M_{\rm HI}/M_\odot)$), while $V_{{\rm eff},j}$ is the 'effective volume' available to galaxy j. The effective volume is determined through a maximum-likelihood statistical technique, and takes into account both the survey sensitivity limits and the fluctuations of galaxy counts with distance induced by the large-scale structure in the survey volume. As a result, the $1/V_{\rm eff}$ method is fairly robust against bias caused by inhomogeneities in the spatial distribution of galaxies. Full details of the implementation of the $1/V_{\rm eff}$ method in the context of the ALFALFA survey can be

found in Martin et al. (2010, Appendix B) and Papastergis et al. (2011, §3.1), and references therein.

There are two important technical differences between the measurement of the HIMF of various environmental subsamples in this work, and the measurement of the overall HIMF of ALFALFA (Martin et al., 2010). First, it is very difficult to determine the actual survey volume occupied by each environmental subsample (see figure 4.4). As a result, we do not attempt to compute absolute normalisations for the environmental HIMFs, but rather we compare the HIMF shape among the various subsamples. Second, the spatial distribution of different environmental subsamples can be drastically dissimilar (see e.g. figure 4.6). As a result, the effective volumes for galaxies that belong to a specific subsample are computed based on the spatial distribution of the other subsample members only (rather than the whole ALFALFA sample).

The method described above for the measurement of the HIMF is fully non-parametric. However, previous studies (e.g. Zwaan et al., 2003, 2005; Martin et al., 2010) have shown that the HIMF can be described very well by a specific functional form, referred to as the 'Schechter function' (Schechter, 1976):

$$\begin{aligned} \phi(M_{\rm HI}) &= \frac{dN_{\rm gal}}{dV\, d\log_{10}(M_{\rm HI})} = \\ &= \ln(10)\, \phi_* \left(\frac{M_{\rm HI}}{M_*}\right)^{\alpha+1} e^{-\left(\frac{M_{\rm HI}}{M_*}\right)} \quad . \end{aligned} \tag{4.6}$$

The Schechter function describes a power law of logarithmic slope $\alpha + 1$ at the low-mass end ($M_{\rm HI} \ll M_*$), which transitions to an exponential drop off at the high-mass end ($M_{\rm HI} \gg M_*$). The parameter M_* is therefore the value of mass corresponding to the transition 'knee' of the HIMF, while ϕ_* controls the normalisation of the HIMF. In this work, we determine the best fit Schechter parameters for the measured HIMFs by ordinary least squares minimisation[iii]. As explained in the previous paragraph, the value of ϕ_* in the environmental HIMFs is arbitrary, and only the two shape parameters (M_* and α) are physically relevant in this case. Note that the two shape parameters are covariant, such that the fit error is best depicted as an ellipse in the $\{M_*, \alpha\}$ plane. Lastly, keep in mind that the errors on the fit parameters depend on the errorbars of individual HIMF datapoints. These errorbars are computed through Eqn. 4.5, and represent the statistical counting error only. As a result, systematic uncertainties are not included in the fit error values quoted in this article. The robustness of the $1/V_{\rm eff}$ method is discussed further in appendix B.3.

[iii] The best fit parameters are determined by the `scipy.optimize.curve_fit` routine written in the `Python` programming language. The minimisation is performed in linear space, assuming Gaussian errors with a magnitude determined by Eqn. 4.5.

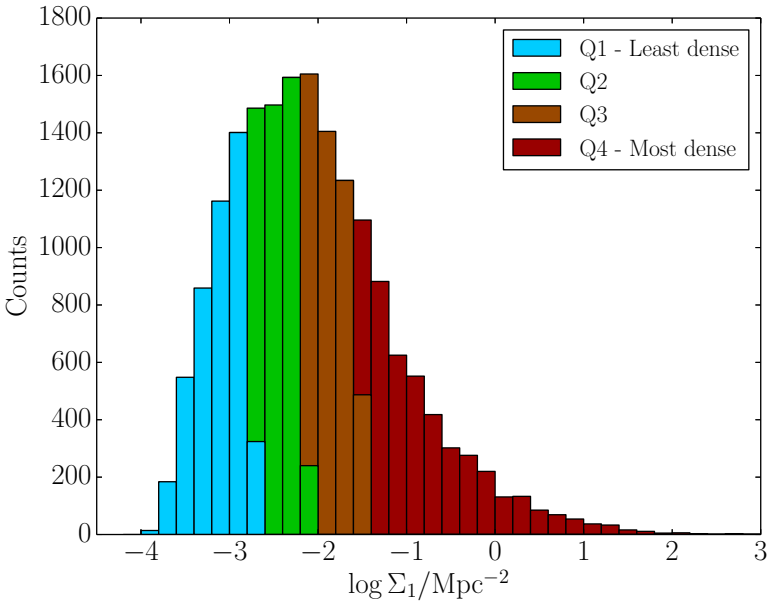

Figure 4.7: Similar to figure 4.3, but referring to the environment as defined by the 2MRS reference catalogue. Keep in mind that in the case of 2MRS the nearest neighbour density is calculated based on the distance to the closest neighbour (§4.3.4). Once again, different colours (shades) mark the four quartiles of the distribution, increasing in density left to right.

4.5 Results

4.5.1 SDSS Reference Catalogue

The following subsection is concerned with the results obtained when defining an ALFALFA galaxy's environment based on the SDSS reference catalogue that extends from 500-15,500 km s^{-1}/H_0, this includes both the NN and FA methods for defining environment (see §4.3).

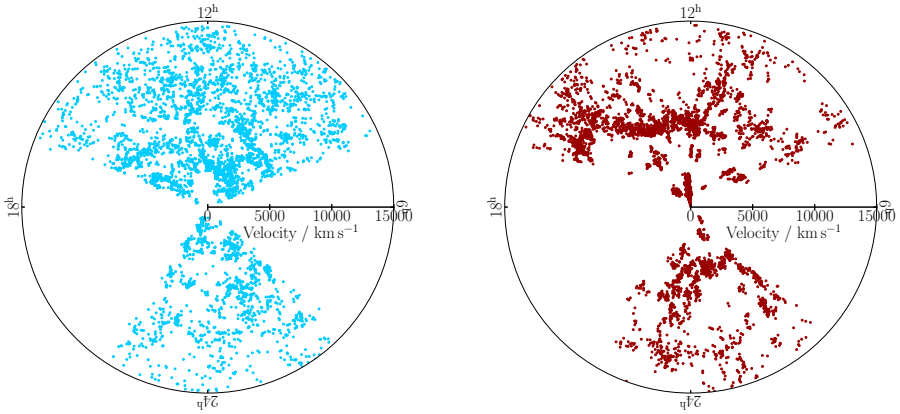

Figure 4.8: Same as figure 4.4, but showing coneplots of the lowest (*left panel*) and highest (*right panel*) density quartiles of the 2MRS nearest neighbour environment (see figure 4.7). Note that the 2MRS is an all-sky survey, and therefore it can be used to measure the environment in both the Spring and Fall portions of the ALFALFA footprint.

Nearest Neighbour Density

The nearest neighbour density calculated by the 3rd SDSS neighbour above the volume limiting absolute magnitude cut was used to define quartiles of environment for the ALFALFA galaxies. The galaxies from each quartile were used to calculate the HIMF for that environment (as described in §4.4) and were compared to the HIMF calculated from all four quartiles combined.

Figure 4.9 shows the HIMF for each of the four ALFALFA quartiles (left) and the 2-σ errors ellipses of the fit to the Schechter function parameters of each quartile (right).[iv] There is a clear trend of the lowest environmental density quartile

[iv]The reduced χ^2 values for these fits are 1.6, 0.8, 1.5 and 57 for for four quartiles (lowest to highest density). The anonymously large value for the highest quartile is caused by the first bin, which is so low that it might be confused with the quartile below. The source counts in this first

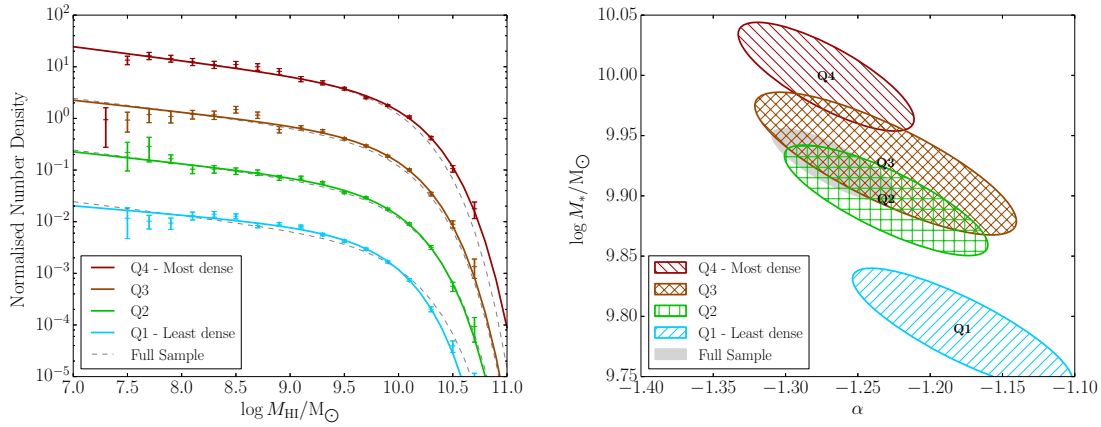

Figure 4.9: *Left panel*: The HIMFs of each environment density quartile in the ALFALFA sample. The solid coloured lines represent Schechter function fits of each quartile in nearest neighbour density, calculated using the 3rd nearest neighbour in the associated SDSS catalogue. In order of most to least dense they are dark red, gold, green, light blue, or equivalently, top to bottom (or dark to light shades). The dashed grey lines show the HIMF of the full sample, and are offset to aid readability. The error bars represent the counting errors only, and neglect errors in the input masses and velocity widths. *Right panel*: The 2-σ error ellipses of the Schechter function fit parameters of the HIMFs in the left plot. The colour scheme is identical to the left plot and the hatching styles are as follows: positively sloped, vertical cross, diagonal cross, negatively sloped, in order of increasing density quartiles. The grey filled ellipse represents the fit to the full sample.

(light blue) HIMF function falling below that of the full sample at the high mass end, and this switches to lying above it for the highest density quartile (dark red), with the middle two quartiles falling between the two extremes. There is also a much weaker dependence on the low-mass slope, with the quartiles appearing to produce a marginally flatter slope as the local density decreases.

Theses results seem to indicate that the 'knee' mass of the HIMF is indeed a function of nearest neighbour environment (as defined by the SDSS reference

bin are likely very incomplete because the completeness cut-off mass occurs part way across the bin. Removing this data point makes the reduced χ^2 value 0.9.

catalogue in §4.3.2) with the value of $\log M_*/M_\odot$ changing from 9.81 ± 0.02 to 10.00 ± 0.03 between the lowest and highest density quartiles (of the ALFALFA sample). There is also a suggestion of a trend in the low-mass slope, although this is much less pronounced. The error ellipses in figure 4.9 appear to move progressively further right (flatter low-mass slope) with decreasing density. However, this trend is not statistically significant as all the ellipses overlap in α, indicating that they are consistent within 2-σ. Fitting a vertical line (fixed α value) to the ellipses results in a reduced χ^2 value of 1.2, indicating that assuming no change in α is a reasonable model for the data (the equivalent χ^2 value, assuming no change in M_*, is 13). It should also be noted that the Schechter fit is based only on the counting errors when calculating the HIMF, thus the error ellipses are likely underestimates of the true errors, as they do not include distance uncertainties (probably the largest single source of error). Furthermore, this apparent shift is in the direction that you would expect α to be driven by the change in M_*, due to the covariance between the two parameters. This is also opposite to the trend between environment and α that is expected (steeper in low density environments).

Fixed Aperture Environment

In Figure 4.10 we show the measured HIMFs and error ellipses for four environmental subsamples defined via the fixed aperture method (refer to §4.3.3). In particular, the four sub-samples correspond to galaxies that belong to the lowest density FA environment (zero neighbours within the fixed aperture), and galaxies that

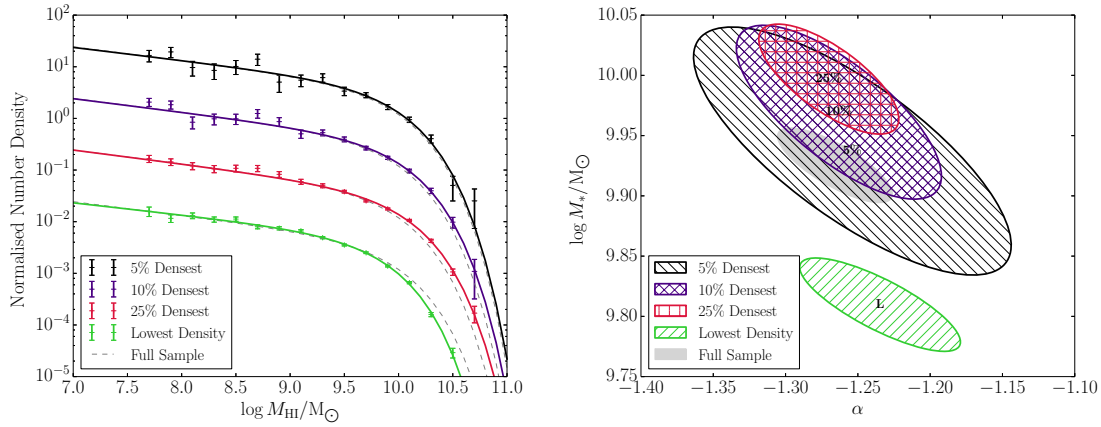

Figure 4.10: *Left panel*: The HIMFs of each environment defined by the fixed aperture method in the ALFALFA sample. The solid coloured lines represent the Schechter function fits of the four different environments, those with 0 neighbours within the fixed aperture, with 3 or more, 6 or more, or 9 or more. The respective colours are green, crimson, purple, and black or equivalently, bottom to top (or light shades to dark shades). The last three of these samples approximately corresponds to the 25, 10 and 5 percent most dense environments. The dashed grey lines show the HIMF of the full sample, and are offset to aid readability. The error bars represent the counting errors only. *Right panel*: The 2-σ error ellipses of the Schechter function fit parameters of the HIMFs in the left plot. The colour scheme is identical to the left plot and the hatching styles are as follows: positively sloped, vertical cross, diagonal cross, negatively sloped, in order of increasing density quartiles. The grey filled ellipse represents the fit to the full sample.

belong to the 25%, 10% and 5% densest environments in terms of FA neighbours. Figure 4.10 shows that there is no clear dependence of the low-mass slope on environment, in agreement with the findings of §4.5.1. However, the environmental dependence of the 'knee' mass is more complicated than before. In particular, we do observe a shift in the value of M_* between the lowest density and 25% densest FA sub-samples, that is compatible with the trend seen in figure 4.9. However, the trend does not extend consistently to the two highest density FA sub-samples; instead the value of M_* for the 10% and 5% densest FA sub-samples is actually

slightly lower than for the 25% sub-sample.

At first glance, the results of figures 4.9 and 4.10 regarding the environmental dependence of M_* may seem inconsistent with each other. However, this is most probably not the case, because the two densest FA subsamples probe a higher density regime than the fourth quartile of NN environmental density (refer to §4.3.3). We therefore interpret the observed M_* trend with FA environment as the result of HI-deficiency affecting galaxies in the highest density regions of the ALFALFA volume. According to this interpretation, the extrapolation of the environmental M_* trend observed for the NN subsamples into the highest density environments fails, because the processes responsible for HI-deficiency inhibit the formation of galaxies with high HI masses in these crowded environments.

4.5.2 2MRS Reference Catalogue

The 1st nearest neighbour in the volume-limited 2MRS catalogue was used to define quartiles of environmental density for the ALFALFA galaxies (refer to §4.3.4). The ALFALFA sample that can be used in the 2MRS analysis contains about 50% more galaxies than the sample used in the SDSS analysis, as 2MRS is all sky survey. Figure 4.11 shows the HIMF Schechter parameters calculated for each quartile of neighbour density (in 2MRS). Despite having a greater number of sources to compute the HIMFs, and therefore smaller error ellipses, no consistent trend in either M_* or α is evident; all four quartiles are consistent with the global sample at

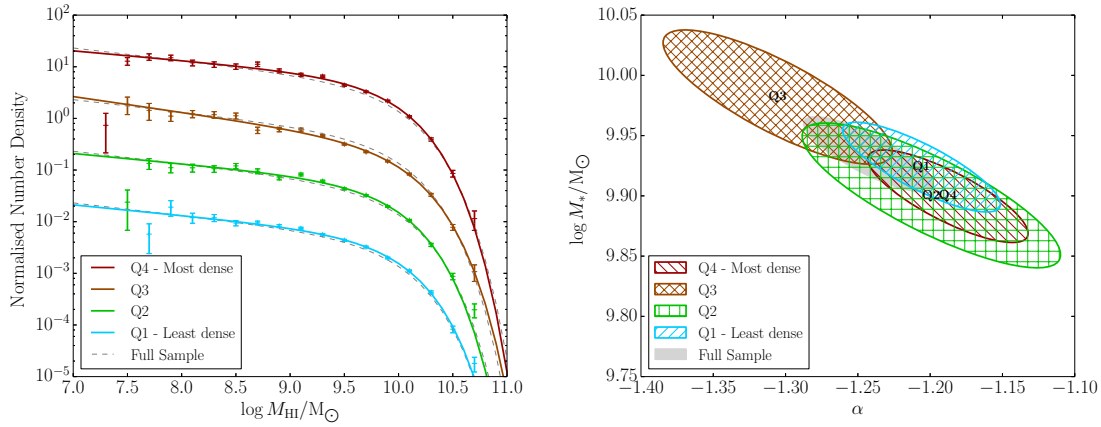

Figure 4.11: Identical to figure 4.9 except that here nearest neighbour environment quartiles are defined using the first neighbour in the 2MRS reference catalogue.

2-σ confidence. This result has been checked to be robust against cosmic variance and the colour of the reference sample (see appendix for details).

The fundamental difference between the SDSS-based and 2MRS-based environmental measures is the scales that they probe. As argued in §4.3.4, the environment defined using 2MRS is probing a larger scale than that defined using SDSS. This is because 2MRS is a shallower survey, which leads to larger separations between sources. In addition, using the 2MRS catalogue to define the environment results in a better separation of our ALFALFA sample based on the position of galaxies in the LSS. For example, filaments and clusters are starkly defined in figure 4.8 (right panel), while in the left panel there are clear gaps in the corresponding positions. Given these differences between environment defined using SDSS and 2MRS, and the fact that a trend between environment and M_* is only measured when using SDSS, the most straightforward interpretation of our results is

that an HI-selected galaxy's characteristic HI mass (M_*) increases with the density of its local environment, but is independent of its position relative to large scales structures. In addition, we find that the faint end slope of HI-selected galaxies is universal, having no significant dependence on any measure of environment we explored.

4.6 Discussion

The notion that local environment is the primary factor for determining a galaxy's properties is not a new idea, in fact it is the fundamental assumption underlying the very successful HOD formalism. There are also optical based experiments which have found similar results: Berlind et al. (2005) compared simulations and the SDSS to demonstrate that galaxy properties are strongly correlated with the host halo mass, and that this is the parameter that most environment measures based on local galaxy density, are tracing; Blanton et al. (2006) studied the environment of SDSS galaxies on different scales and found that only environment within ~1 Mpc is important for determining a galaxy's star formation rate and colour. Our results fit well with these theoretical and optical results, however there are still a number of tensions with theory and other HI observations. Below we review some literature results regarding the environmental dependence of the HIMF and discuss cases where there exists tension between these studies and the results of this work.

4.6.1 Comparison with previous HI survey results

The first study on the environmental dependence of the HIMF based on a large-area blind HI survey was performed by Zwaan et al. (2005), using the HIPASS dataset. Contrary to our results, they found that the low-mass slope, α, becomes steeper with increasing environmental density, while the 'knee' mass, M_*, is roughly independent of the environment (see their figure 3). The comparison between the HIPASS result of Zwaan et al. (2005) and the ALFALFA result obtained in §4.5 is not straightforward, because the two studies define the NN environment in different ways. In particular, Zwaan et al. (2005) find neighbours for the HIPASS galaxies in the HIPASS catalogue itself. This decision was dictated by the fact that there is no large-area spectroscopic survey at optical wavelengths that covers the HIPASS footprint. As explained in §4.3.1, this neighbour definition makes the consistent computation of environmental density throughout the survey volume very difficult to achieve in practice. In Appendix B.2 we show that if an environmental trend in α, equivalent to that found in HIPASS by Zwaan et al. (2005), was present in the ALFALFA dataset, it would have been easily detected by the current analysis.

Another important difference between the HIPASS and ALFALFA nearest neighbour definitions is the scale over which they probe the environment. More specifically, the HIPASS catalogue is much sparser than the SDSS reference catalogue used for environment definition in this work. If not due to the observational limitations therefore, the HIPASS trend should be driven by the large-

scale environment of galaxies, rather than the local environment probed in this article. However, this interpretation of the HIPASS result is also open to question. For example, Moorman et al. (2014) have recently measured the HIMF separately for the ALFALFA galaxies that reside in voids and for those that reside in walls/filaments. They find a difference in the HIMF measured for the two environmental samples that is similar to the environmental trend found in §4.5.1. In particular, the wall/filament HIMF has a higher 'knee' mass than the void HIMF, but only a marginally steeper low-mass slope (refer to their figure 8). Given that the Moorman et al. (2014) environment definition also refers to large scales (~10 Mpc), their result seems to contradict the HIPASS finding.

Our results make an intriguing addition to those of Moorman et al. (2014) because we detect a very similar trend in M_*, but associated with local, rather than large scale, environment. The reason for this apparent contradiction is not clear, however we note that it could be resolved if the separation of galaxies between void and wall objects in Moorman et al. (2014) is correlated with the local environment of the galaxies more than naively expected based on the size of these cosmic structures; in that case, it would be natural for the Moorman et al. (2014) result to be closely related to the result obtained by considering SDSS-based local densities.

An additional complication is added by the fact that the Moorman et al. (2014) trend is not detected in the present work when environment is defined on relatively large scales with 2MRS-based densities (see §4.5.2). Again, the reason for

this tension is not entirely clear, although (as above) if the void and wall samples of Moorman et al. (2014) were sufficiently correlated with local density, then a trend associated with local environment could be masquerading as one with large scale environment – a false trend that we would not necessarily expect to see with 2MRS neighbour densities. Alternatively, it is possible that 2MRS could be missing the large scale component of a real trend associated with both local and large scale. 2MRS clearly separates out the densest LSS into the 4th quartile of neighbour density, but if the separation between the remaining 3 quartiles was extremely noisy, then trends could be suppressed.

4.6.2 Comparison to the HIMF in groups

Verheijen et al. (2001); Kovac, Oosterloo & van der Hulst (2005); Freeland, Stilp & Wilcots (2009); Pisano et al. (2011) studied the HIMF in galaxy groups and all came to essentially the same conclusion; that the low-mass slop is flat in groups. Given these consistent findings, it is perplexing that we see no evidence for variation of the low-mass slope, as in the field it has been shown by both HIPASS (Zwaan et al., 2005) and ALFALFA (Martin et al., 2010) that it is not flat (both surveys measure $\alpha \approx -1.3$).

Assuming that a non-negligible fraction of ALFALFA's detections are galaxies in groups (Hess & Wilcots, 2013, find that approximately 25% of ALFALFA galaxies are in groups), such that any trend would not be drowned out, then the

findings above suggest that the nearest neighbour definition of environment is not consistently separating groups from the rest of the sample. If this were not the case, then there would need to be an inconsistency in how the wide field and targeted surveys are calculating the HIMF, in order to explain these seemingly contradictory findings.

This apparent shortcoming in the nearest neighbour method could be explained if the surface number density of galaxies in groups is approximately independent of group size. As our method cannot distinguish regions of the same surface density, under these assumptions, it would be incapable of separating groups of different sizes and we would be blind to any trend associated with group size. Therefore, if the low mass slope varies with group size, our analysis might not reveal this. Alternatively, as the surveys which have measured a flat low-mass slope in groups are mostly interferometric surveys (that resolve many of their sources), an uncertain detection threshold associated with HI surface density could result in an erroneous slope. A more detailed study of the HIMF in groups is required to test these hypotheses and compare the two existing methodologies.

4.7 Conclusions

We have used the 70% ALFALFA sample to search for dependence of the HIMF on galactic environment. In particular, we defined the environment of ALFALFA galaxies based on the neighbours found in both SDSS and 2MRS volume limited

reference catalogues. We find that the Schechter function 'knee' mass ($\log M_*/\mathrm{M}_\odot$) is dependent on environment, with its value shifting from 9.81 ± 0.02 to 10.00 ± 0.03 between the lowest and highest density quartiles. However, this dependence was only observed when defining environment based on the SDSS reference catalogue, not 2MRS. Using a fixed aperture measure of environment with SDSS, we also found tentative evidence for a decrease in M_* in the highest density environments, in agreement with the notion that galaxies in clusters should become HI-deficient.

In §4.3 we demonstrated that using our approach, 2MRS both measures environment on a larger scale than SDSS, and is more effective at separating large scale structures into different environment density quartiles. This strongly suggests that the dependence we are seeing is on local environment, rather than large scale, supporting the fundamental assumption of the HOD formalism, that a galaxy's properties are only dependent on the mass of its host halo. However, this is in tension with a previous ALFALFA-based study (Moorman et al., 2014) which found a similar trend in M_*, but based on separating galaxies which reside in walls and voids.

Although the true resolution remains unclear we offered two potential explanations for this discrepancy between our results and those of Moorman et al. (2014). If void and wall environments are sufficiently correlated with local densities such that trends are expected with either definition of environment, then the results would be in agreement. Alternatively, if the 2MRS densities used in this chapter were to be incapable of distinguishing low density environments then

trends associated with large scales might be hidden from our analysis.

In all of the tests we performed we detected no significant dependence of the the low-mass slope (α) on environment. Again, this appears in conflict with existing results, both from HIPASS (Zwaan et al., 2005) and from several studies of galaxy groups (which measure $\alpha \sim -1$). The steepening of α with denser environments that was observed in HIPASS is not directly comparable to this article due to different methodology (see §4.3.1), and in appendix B.2 we demonstrate that we would be capable of detecting an equivalent trend if it existed in our data. As an explanation to resolve the tension with the findings of group HI studies, we suggest that the inability of the nearest neighbour environment to separate different sized groups of the same projected surface density, might be responsible for our null result. If the low-mass slope was a function of group size and most groups had similar surface densities, then this would explain the observations. An alternative explanation could be inconsistent methodologies resulting from uncertain surface brightness limits in narrow field surveys. A more complete understanding of the HIMF in groups is needed to test these hypotheses.

CHAPTER 5

THE ARECIBO PISCES-PERSEUS SUPERCLUSTER SURVEY

5.1 Introduction

The existence of the 'cosmic web', crisscrossing linear overdensities stretching vast distances that form galaxy clusters and groups where they cross, has become central to our understanding of the formation of structure in the Universe, and cosmological simulations can now clearly show how these structures form from the collapse of primordial density fluctuations (e.g. Springel et al., 2005). There are numerous studies of galaxy clusters ranging from local studies looking at individual galaxies, to surveys of X-ray clusters, to strong and weak lensing studies, and now clusters have even been observed through the Sunyaev-Zel'dovich effect (both thermal and kinetic). All this means that galaxy clusters, and their relation to the cosmic web, are relatively well understood when compared to filaments, which are much harder to study, and thus much more poorly understood observationally. However, results from the *Illustris* simulation show that almost half the matter (dark and baryonic) in the Universe presently resides in filaments (Haider et al., 2016), clearly demonstrating that understanding this portion of the cosmic web is a key step in the understanding the population of galaxies and the environment they form and evolve in. In particular, with APPSS (Arecibo Pisces-Perseus Supercluster Survey) we aim to use the Pisces-Perseus Supercluster (PPS) filament as a test of whether the filaments produced in simulations, and the population of

galaxies within them, are consistent with what exists in the nearby Universe.

A poor approximation of a filament's linear density can be made based on the velocity dispersion of the galaxies it contains (Eisenstein, Loeb & Turner, 1997). However, to obtain a more precise measurement, and to constrain the filament's structure sufficiently to simulate its formation, requires mapping of the impact that the filament's mass has on the surrounding velocity field. Galaxies between the Milky Way and the PPS overdensity will have higher than expected recession velocities, due to their infall motion onto PPS, whereas those on the far side of PPS will have recession velocities lower than expected, due to the backflow. To use the galaxies as a tracer of the velocity field requires redshift independent distance measures such that the expected Hubble flow velocity can be removed, leaving just the contributions from the infall or backflow, plus random motions.

There have been numerous works that map the local velocity field (da Costa et al., 1996; Tonry et al., 2000; Branchini et al., 2001; Masters, 2005; Theureau et al., 2007; Hoffman, Courtois & Tully, 2015; Springob et al., 2016), however these generally aimed at mapping the bulk motions over the whole sky, and as a result typically had very few galaxies in PPS. To obtain redshift independent distances for 100s or 1000s of galaxies in very challenging. Obtaining distances based on the stellar population (e.g. the tip of the red giant branch or horizontal branch location) is only possible within ~10 Mpc, limited by the resolution and sensitivity of the Hubble Space Telescope, while other methods, such as Surface Brightness Fluctuations, are not applicable to the late-type galaxies that are found in the field.

This leaves as the best available method for a large sample, the Tully-Fisher Relation (TFR).

The TFR is the observational result that the luminosity of a late-type galaxy is proportional to its rotation velocity to some power (Tully & Fisher, 1977). While the exact reason for this tight relation, which spans many orders of magnitude, is still somewhat unclear, it undoubtedly stems from the fact that both of these properties (the luminosity and rotation velocity) are proxies for the total mass of the galaxy. It has become common for estimates of the stellar mass to be used in place of the luminosity, while a whole range of different estimates of the rotation velocity are used depending on what observational data is available for a given source catalogue. Use of the Baryonic Tully-Fisher Relation (BTFR), where the combination of a galaxy's stellar and HI mass is used as a proxy for its total mass, is becoming more common and is particularly important for low-mass star-forming galaxies as HI, not stars, is their dominant baryonic component (see Figure 5.1).

While the TFR (and BTFR) are consistent over many orders of magnitude, the relation is not without substantial scatter. A proper accounting of this scatter is essential to understand the uncertainty on the peculiar velocities derived using the relation. Masters et al. (2006) (following the methodology of Giovanelli et al., 1997) calculated the *I*-band TFR based from a sample of 807 spiral galaxies in and around clusters and groups. This "basket-of-clusters" approach allows the distance to all the galaxies in each cluster to be assumed to be the same, and in turn, they should all fall on the same TFR. The global TFR can then be calculated by

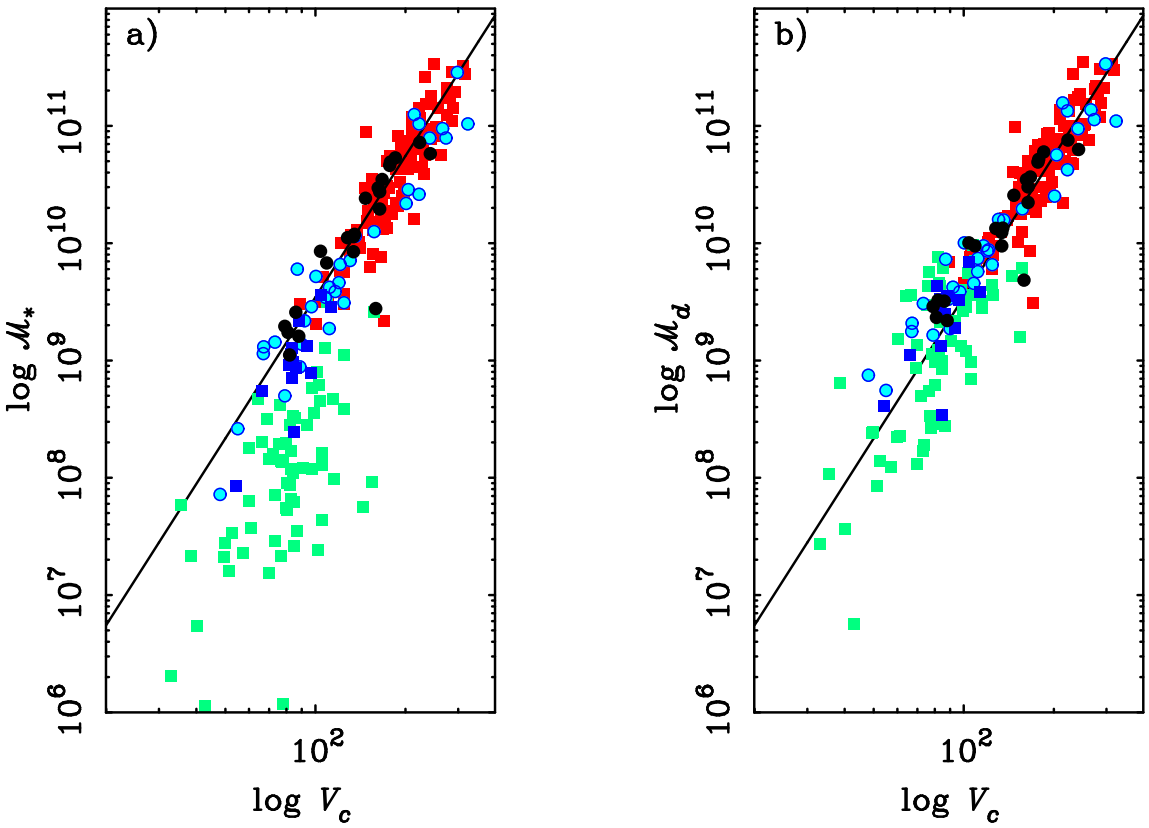

Figure 5.1: The Tully-Fisher relation (*panel a*) and the Baryonic Tully-Fisher relation (*panel b*) for the sample of late-type galaxies compiled in (McGaugh et al., 2000). The TFR compares the stellar mass of a galaxy to its rotation velocity, whereas the BTFR uses the stellar mass plus the gas mass. The trend in the left panel clearly has a break at stellar mass of $\sim 10^9$ $M_\odot$, whereas the right panel maintains a consistent slope for all masses in the sample. The break occurs at this mass because this is mass below which neutral gas overtakes stellar mass as the dominant baryonic component, hence the stellar mass is no longer a reliable proxy for the galaxy's total mass. Different symbols indicate different methods used to estimate the circular velocity (V_c). (Figure from McGaugh et al., 2000).

shifting the assumed distance to each cluster (while constraining there to be no large scale bulk peculiar motion) until all fall on a single relation. In this way a very precise TFR can be derived without the need for a large sample of primary distances. Masters et al. (2006) also estimated the error budget associated with scatter in the relation, finding the uncertainty in the absolute magnitude of a given source to be between about 0.2 and 0.7, depending on its velocity width (or equivalently, uncertainty in the distance between about 10% and 40%). Using this relation they estimated the peculiar velocity of each cluster to with ~5% of it's total recessional velocity.

Due to the relatively cheap observational cost of obtaining a TFR distance estimate combined with its wide range of applicable distances (compared to other distance measures), the TFR is a popular estimator when creating large samples for use in mapping the local peculiar velocity field. Recently Springob et al. (2016) used ~2000 galaxies from the 2MASS Tully-Fisher survey to map the peculiar velocity field out to approximately 140 Mpc, based on the combination of the H, J, and K-band TFRs. As 2MASS is an all sky survey, uniformly covering almost all 4π of the sky, it is ideally suited to measure any bulk flow motions, which was the main aim of Springob et al. (2016). Despite greatly improving the sky coverage they found results that are consistent with existing results, and no evidence of additional attractors in the local Universe.

Velocity field maps can also be used to constrain the initial density fluctuation of cosmological simulations in order to produce a more accurate model of

a particular environment. Sorce et al. (2016) used the cosmicflows-2 catalogue of ~8000 extragalactic distances (Tully et al., 2013, with HI measurements mostly from Springob et al., 2005; Meyer et al., 2004; Haynes et al., 2011), a large fraction of which are TFR distances, to create a suite of constrained simulations of the local volume out to 150 Mpc. This work demonstrated that these simulations were substantially more representative of the local volume when compared to random realisations. Although PPS is present in these simulations, due to the small number of tracers in the direction of PPS and the coarse smoothing length of the velocity field, the PPS filament does not appear strongly in these simulations.

Unlike the TFR, the BTFR has not been widely used to map peculiar velocities, however it is increasing in popularity, in particular for low-mass field galaxies. A number of authors have calculated the slope of the BTFR (McGaugh, 2012a; Zaritsky et al., 2014), most recently Papastergis, Adams & van der Hulst (2016), who made an accurate measurement of the BTFR based on 97 ALFALFA galaxies, found a perpendicular scatter of 0.055 dex in the relation, which corresponds to a distance uncertainty of about 25%. In the case of APPSS this highlights the need for a large sample such that $\sqrt{N}$ gains will be possible in multiple redshift bins on either side of the filament. With approximately 250 hr of Arecibo observing time, and through the use of the BTFR and constrained simulations, the APPS survey will enable the total linear density of the PPS filament to be measured, as well as providing a sample of low-mass galaxies in and around this exceptional structure.

5.2 Survey Overview

APPSS is an ongoing ~250 hr survey with the Arecibo telescope[i], which aims to expand the number of HI detections around the Pisces-Perseus filament by approximately 500 and enable the detection of infall onto the filament through the use of the BTFR. The Pisces-Perseus Supercluster (PPS) is the most dominant extragalactic feature in the Arecibo Fall sky, stretching more than 50° across the sky at a distance of ~70 Mpc (Figure 5.2). It is fortuitously oriented almost perpendicular to the line of sight (Wegner, Haynes & Giovanelli, 1993), making it an ideal location to observe infall and backflow onto a filament, as these motions will be aligned with the line of sight. Furthermore, PPS is conveniently placed between foreground and background voids meaning that the velocity field around it should be relatively clean of contaminants and dominanted by the presence of the filament itself. The cosmic web is full of filamentary structures, but these are much less well studied observationally than other large scale structures, such as clusters. By obtaining peculiar velocity measurements for the APPSS and ALFALFA sources in this region with the BTFR we will be able to measure the infall velocity and make a direct constraint on the filaments dynamical mass.

There have been numerous previous studies of the PPS region which have claimed low significance detections of infall (Han & Mould, 1992; Freudling et al.,

[i]I am the PI of this project, but members of the Undergraduate ALFALFA Team have contributed to numerous aspects of the project including source selection, scheduling, observing, and data reduction. The full APPSS proposal author list can be found at http://egg.astro.cornell.edu/alfalfa/docs/prop.mar16.authorlist.html.

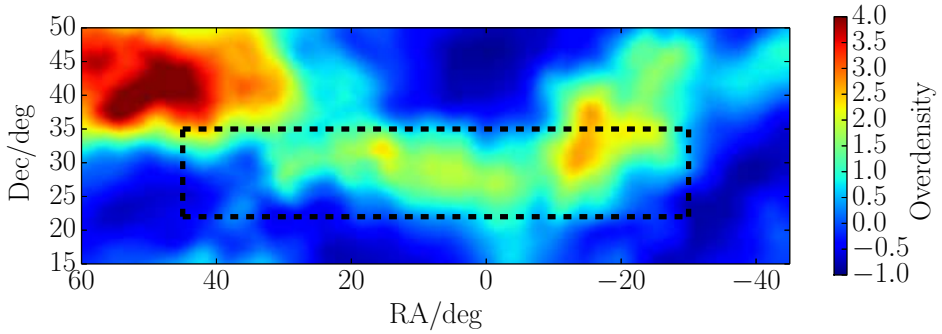

Figure 5.2: Mean matter overdensity between heliocentric velocities of 4000 and 8000 km s^{-1}, produced by interpolating between 2MRS overdensity map points (Erdoğdu+ 2006). The APPSS region is outlined in black.

1995; da Costa et al., 1996; Theureau et al., 1998; Hanski et al., 2001; Springob, 2006). However, these studies suffered from small sample size (a few hundred sources or less in the PPS region) and did not all produce consistent results. APPSS targets sources of unknown redshift with photometry that suggests they are gas-rich galaxies at approximately the distance of PPS, but were too low-mass for ALFALFA to detect. With the APPSS and ALFALFA PPS samples combined we expect ~1,000 sources suitable for use with the BTFR, which will allow a robust detection of infall and backflow.

5.3 Methodology

The APPSS targets were selected based on their SDSS and GALEX photometry. We specifically target objects that appear to be low-mass galaxies, as the detection limit of ALFALFA means that sources above $\log M_{\rm HI}/{\rm M}_\odot = 9$, at the distance of

PPS, have already been detected. Several authors (e.g. Zhong et al., 2008; Galaz et al., 2011; James et al., 2015) have used the magnitude, colour, surface brightness, concentration and 'diskiness' of photometric objects in SDSS to identify low optical surface brightness, star forming galaxies. We follow a similar procedure with the inclusion of GALEX UV photometry as an indicator of star formation (important as virtually all star forming galaxies have HI, Huang et al., 2012a). First a sample is identified automatically using an SQL query, before each source is checked by eye for complications that might impact the photometry, such as a bright foreground star, or for confusion within the Arecibo beam. A final cut is then made based on the axial ratio of the targets in SDSS. This eliminates the face-on sources that would be inappropriate for use with the BTFR. The selection method has been verified to have a high success rate, with a preliminary survey detecting ~70% of the targeted sources.

Although the orientation of the PPS filament suggests that a drift scan observing strategy with ALFA would be optimal, we estimated that to achieve the desired sensitivity over the whole field would require approximately 2,000 hr of telescope time, and due to Arecibo's pointing restrictions and scheduling constraints, this would take at least 5 years. An equivalent detection threshold can be achieved using 5 min ON-OFF pairs with the LBW (L-Band Wide) instrument for each target. Thus far we have observed for 126.5 hr and detected 68% of our targets, the locations on the sky and in redshift space for these detections (and non-detections) are show in Figure 5.3.

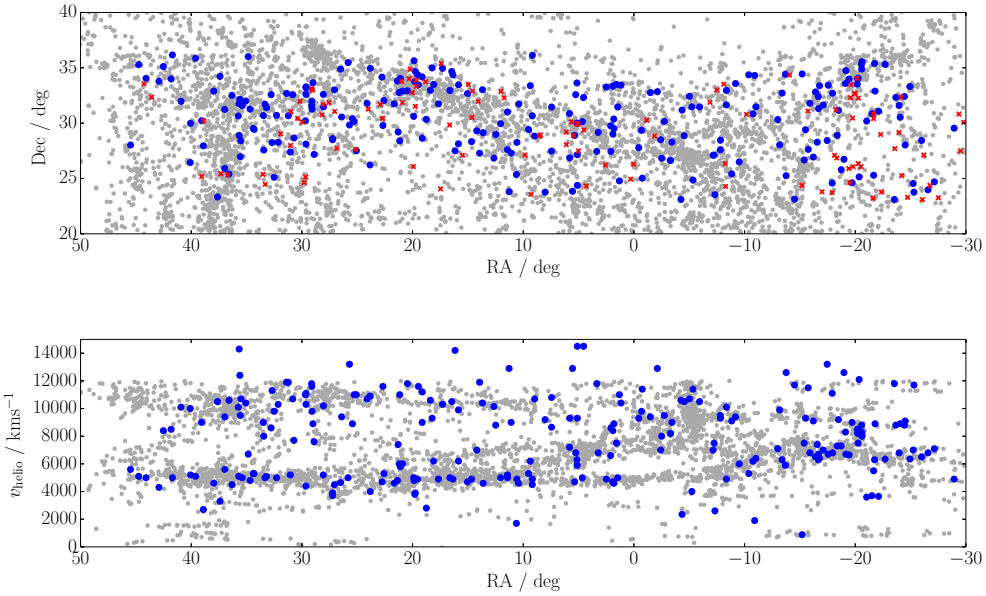

Figure 5.3: *Top:* Preliminary detection (blue points) and non-detection (red crosses) locations of the APPSS observations, with all galaxies of known redshift (grey points) in the background. The two former categories appear to be equivalently positioned on the sky. *Bottom:* Preliminary velocities of detections thus far (blue points) with all galaxies of known redshift in grey. Approximately half of the detections fall around the main ridge and the other half are in the near-background structure, suggesting that, because of the foreground void, the backflow may be easier to quantify than the inflow.

As can be seen in Figure 5.3 approximately half of the current detections lie in and around the PPS filament itself, with the other half mostly residing in background structures, and a small number in the deep foreground void. These preliminary detections indicate that it may be easier to detect the backflow than to detect the inflow. Hanski et al. (2001) estimated that a galaxy 40 Mpc away from the centre of the filament should have a peculiar velocity of 500 km s^{-1}. To detect such an extended influence will require sources covering the redshift range in front or behind the filament. Therefore, even though the uncertainty in the esti-

mated peculiar velocities will be smaller at smaller distances, the relative dearth of detections in the void in front of the filament will likely mean that the backflow is significantly easier to constrain. It should also be noted here that although Figure 5.3 included many background sources (grey points), that is, all galaxies in the field with known redshift, most of these objects do not have HI detections or would not be suitable for use with the BTFR, hence the need for APPSS.

A crude estimate of the total linear mass density of a filament can be made just based on the velocity dispersion of the galaxies it contains (Eisenstein, Loeb & Turner, 1997). However, to obtain a more precise measure will require the calculation of galaxy peculiar velocities and eventually a constrained DM simulation. The peculiar velocities of each galaxy will be estimated by using the BTFR to calculate a redshift independent distance such that the observed recession velocity can be compared to the expected velocity assuming pure Hubble flow. The BTFR is favoured over the TFR because for low-mass, star-forming galaxies HI is the dominant baryonic component (Huang et al., 2012a), and therefore the stellar mass alone is a poor proxy for a galaxy's total mass, thus the BTFR results in a more consistent relation across all masses (McGaugh, 2012b; Papastergis, Adams & van der Hulst, 2016). To accurately map the velocity field a substantial sample is required as the uncertainty in the BTFR means that for an individual galaxy the error in the peculiar velocity will likely be several hundred $\mathrm{km\,s^{-1}}$or more.

To understand exactly what signature we expect to see we must make comparisons with similar structures in simulations. In collaboration with Laura Sales

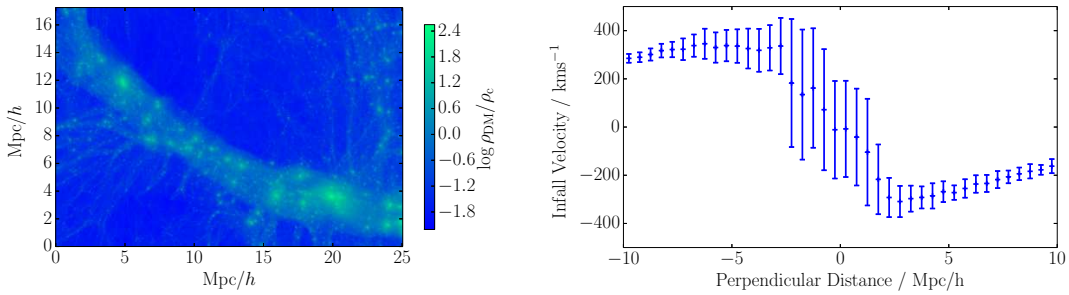

Figure 5.4: *Left:* Mean dark matter density (relative to the critical density) in a 10 Mpc/h deep cut-out from the *Illustris* simulation showing a large filamentary structure that we use as a comparison for PPS. While substantially smaller and less massive than the PPS filament, infall can clearly be seen in the velocity field (right). *Right:* The peculiar velocity (relative to the filament centre) of halos in the *Illustris* simulation. The bins are in perpendicular distance from the filament centre, moving approximately diagonally up and to the right from the bottom-left corner of the left-hand plot. This clearly indicates a ~300 km s^{-1} infall and backflow onto the filament that extends at least 10 Mpc.

(UC Riverside) I am currently identifying a sample of APPSS-like targets in the *Illustris* simulation (Vogelsberger et al., 2014). Due to the limited volume of *Illustris* (~100 Mpc on a side) and the exceptional size of PPS, which would stretch across the entire *Illustris* volume, a directly comparable structure is not possible to find. Figure 5.4 shows the largest filament that we have identified in *Illustris*, which has a linear density of approximately 10^{13} M$_\odot$/Mpc, compared to 8×10^{13} M$_\odot$/Mpc estimated for PPS (Eisenstein, Loeb & Turner, 1997). However, despite being much smaller and less massive than PPS, the density map show that (like PPS) it is sandwiched between two voids, and the velocity field shows very clear infall with a maximum amplitude of around 300 km s^{-1}. With an APPSS-like population identified around this simulated structure we will be able to assess how well our observations are expected to trace the velocity field of the DM halos and what corrections for observational biases will be needed.

While the peculiar velocities of the galaxies we are observing will allow us to fit a parametric model of the expected velocity field and gain an improved estimate of the filament linear density, to fully exploit the dataset will likely require a constrained DM simulation. A constrained simulation (e.g. the CLUES project, Gottloeber, Hoffman & Yepes, 2010) generates the galaxy velocity field from the observed galaxies using a filter function. This field is then approximated by a constrained Gaussian random field which, by assuming all the constrained scales evolve linearly, can be used to generate initial perturbations that when evolved to the present day with an N-body code, will produce a structure that is similar to the one observed. In collaboration with Miguel Aragon-Calvo (UC Riverside) we aim to construct such a constrained DM simulation when we have the final dataset. This will not only give the best understanding of the DM content of the filament but will also reveal how such a massive structure forms and evolves over cosmic time.

5.4 Summary

The APPS survey is an ongoing observing project with Arecibo that will make HI detections of hundreds of low-mass galaxies of previously unknown redshift, in and around the PPS filament. This targeted survey has selected galaxies based on SDSS and GALEX photometry to minimise the observing time and maximise the detection rate. At the survey's halfway point we have made approximately 250

detections, corresponding to 68% of our observed targets. Once the survey is complete the peculiar velocity of these new sources, along with the existing ALFALFA sources in the region, will be estimated using the BTFR. This velocity field will be compared to analogous structures in existing hydrodynamic simulations in order to estimate the total linear density of the filament, as well as used as the input for constrained DM simulations to reveal how PPS has evolved over cosmic time.

CHAPTER 6

CONCLUSIONS

The ALFALFA survey has dramatically brought forward the standing of blind HI surveys, increasing the number of HI sources detected by almost an order of magnitude (compared to previous blind HI surveys). The rich dataset produced by this survey is what enabled most of the work presented in this thesis. Previously much of the analysis based on the statistical properties of the HI population would have been considerably more uncertain, both due to the number of sources and the low mean redshift of past surveys. In this section we present brief conclusions of our work based on the HI population detected in ALFALFA, before discussing possible future directions for this research in the final chapter.

6.1 Confusion in present and future HI surveys

In chapter 2 we showed that we can simultaneously reproduce both the observed number counts of ALFALFA and HIPASS as a function of redshift, and their observed rates of confusion with redshift using mock catalogues. Using these mocks we demonstrated that the maximum possible shift in the Schechter function fit parameters of the HI mass function (HIMF) were at the level of the random errors, and were therefore not a major concern for existing surveys. Furthermore, we found that the rate of confusion will be lower in upcoming shallow and medium-deep SKA precursor surveys, as their improved resolution is sufficient to offset

the increased confusion that would be expected by having a more sensitive survey that probes to higher redshift.

HI surveys generally have fine frequency resolutions, such that two sources are only confused in redshift space if the frequency of their emission genuinely overlaps, therefore the only way to suppress the confusion rate is to improve angular resolution. This highlights the point that single dish telescopes will not be competitive at performing high redshift ($z > 0.1$) HI galaxy surveys, and so should focus on the local Universe where their low resolution, and corresponding high surface brightness sensitivity, is an advantage and not a hindrance.

In chapter 3 we focused on confusion in stacking experiments, where it contributes a non-Gaussian component to the resulting spectrum's noise. We developed an analytic expression to estimate the amount of confusion in the stacked spectrum of a generic HI survey. Stacking will be a vital tool for surveys aiming to detect HI galaxies out to $z = 1$ and beyond, and our results indicated that confusion may be a concern unless these surveys can achieve their initially intended angular resolutions.

In the cases where confusion dominated our mock stacks we had limited success in attempting to correct for the confused emission. The traditional method of assuming a double Gaussian profile, with a broad component from confusion and a narrow one from the targets, was inadequate as the confusion signal itself was approximately a double Gaussian profile. These ultra-deep HI surveys will likely need to explore and test potential mitigation strategies for confusion, which

will require more sophisticated simulations than the simple mocks created here. Without this, any measurements of changes in the HI population as a function of redshift, may be vulnerable to considerable systematic biases.

6.2 Environmental dependence of the HIMF

In chapter 4 we used the ALFALFA 70% catalogue to explore the dependence of the HIMF on a galaxy's environment, as defined by its neighbour density in SDSS and 2MRS. We found that the 'knee' mass of the HIMF does increase by approximately 0.2 dex going from the ALFALFA sources in the lowest to highest quartile of SDSS neighbour density. However, this shift was not apparent at all when the environment quartiles were defined using 2MRS. 2MRS is a shallower and more sparsely populated survey than SDSS, and mostly detects large, red, early-type galaxies which better trace the densest regions. Therefore, we interpreted these results as indicating that the trend in the 'knee' mass was associated only with a galaxy's local environment and not its large scale environment.

Unexpectedly, we found no robust evidence of a shift in the low-mass slope of the HIMF using either definition of environment. Such a shift is expected because studies of individual groups have generally found flat low-mass slopes, whereas the HIMF in the field has a much steeper slope, and has been observed directly that galaxies falling into groups and clusters have their neutral gas stripped. This strongly suggests there should be a flattening towards denser environments, how-

ever this anticipated trend is yet to be found.

CHAPTER 7

FUTURE WORK

The research presented here has primarily been focused on predicting the effects of potential issues for future HI surveys and exploring the impact of environment on the HI population. This chapter outlines some future directions in which this work could proceed.

7.1 The HI mass function of group galaxies

As discussed in chapter 4 the lack of environmental dependence in the low-mass slope of the HIMF appears to be in tension with the findings of surveys that targeted individual groups. Group surveys have typically found flat low mass slopes, whereas blind surveys find substantially steeper slopes in the field (and see no variation with source density). There are two apparent possible causes for this discrepancy: 1) as most of the targeted surveys were carried out with interferometers (not single-dish telescopes) it's possible that the surface brightness completeness for the group samples is not handled in a way that is consistent with that of the blind surveys, or 2) the measure of environment used in chapter 4 may be unable to effectively separate different group environments (for example, rich and poor groups), which could have differing HIMFs.

To attempt to resolve this discrepancy the two types of survey need to be compared in a common way, that is, we must estimate the HIMF of group galaxies

from a blind survey. There are hundreds of groups contained in the ALFALFA volume, however, most of these groups will have too few detections in ALFALFA to make a precise estimate of the HIMF's shape. To do this the average HIMF of all the groups in ALFALFA would need to be made. This would require an external reference group catalogue, such as from 2MRS (Crook et al., 2007) or SDSS (Berlind et al., 2006), because ALFALFA cannot detect most red galaxies (as they are so gas deficient) and so would not produce reliable groups by itself.

Irrespective of the result, this work would represent an important step for the study of the HIMF: if a flat slope were to be observed it would confirm the results of surveys of individual groups, likely indicating the current tension is due to differing definitions of environment; however, a slope consistent with that of the field would demonstrate that the slope is truly universal. Either result would act as an important new constraint for galaxy formation models and simulations. At present these models are constrained to produce a population of gas bearing galaxies which reflects the global properties of the real galaxy population, however there is very little constraint on how the neutral gas varies with galaxy environment. As many important evolutionary effects in the simulations depend on a galaxy's environment (e.g. the UV and AGN radiation field, tidal stripping, and stellar feedback), it is not sufficient to merely match the global population because certain environments could be misrepresented while the global population remains consistent.

The next generation of surveys will further enhance our knowledge of the

changes in the HI population both with environment and with redshift. Wide-field surveys such as WALLABY and WNSHS will provide a much larger sample of nearby group galaxies as well as sampling the full range of galaxy environments in the nearby Universe. Deeper surveys like the APERTIF medium-deep survey and DINGO will begin to measure galaxy groups outside the nearby Universe and start to assess how the HI population varies with redshift. When complete the SKA will carry this field yet further, making wide-field surveys possible that are simultaneously capable of probing redshift evolution in detail. Due to the complexity of galaxy evolution models and simulations, in order to gain a complete understanding of this process it is essential to add these additional dimensions (environment and redshift evolution) to the constraint on the resulting HI galaxy population. With a single end goal the simulations and models are sufficiently complex that there is a large degeneracy in how that end goal can be achieved, potentially with physical processes being modelled differently in each.

7.2 An improved method for estimating the HIMF

The HIMF is of central importance to understanding the HI population, however the present methods used to calculate its form have a number of known shortcomings (Willmer, 1997). The $1/V_{\rm max}$ method is known to be very susceptible to systematic errors caused by large scale structure (LSS) and therefore the $1/V_{\rm eff}$ (or 2D Stepwise Maximum Likelihood) method is the principle estimator used in the

literature. While simulations have demonstrated that the $1/V_{\rm eff}$ method is robust to LSS variations it does still harbour small systematic biases. At present these biases are not significant as they are below the level of the Poisson counting errors for the currently available HI galaxy samples. However, as the next generation of surveys will detect an order of magnitude more galaxies, these biases have the potential to become a major source of uncertainty in the calculations.

The $1/V_{\rm eff}$ method is also a non-parametric method, which means that rather than assuming the Schechter function form a priori, it estimates the height of the HIMF in bins, which a Schechter function is then fit to. While this method is appropriate to use with a population for which it is not known if the Schechter function is a good approximation, it is inefficient to first calculate a non-parametric estimator and then fit a parametric form. Furthermore, the non-parametric nature of the estimator means that the height of the mass-width function must be estimated in over 200 bins (in mass and velocity width). Effectively the $1/V_{\rm eff}$ method involves a few hundred parameter model, whereas a parametric estimator would require approximately 10 total parameters, and would thus be capable of estimating a tighter constraint on the Schechter function fit to the HIMF, with the same data.

In addition to these problems, the present methods also suffer from an incomplete handling of observational errors and a poor characterisation of correlations between the fit parameters. Typically errors are quoted as simply the fit uncertainty associated with the Poisson counting error from each mass bin, or as the

scatter in fit values from multiple realisations of the data (where the mass and width are adjusted in each realisation to provide a more representative accounting of the uncertainty in these values). By developing a Bayesian method to perform this calculation these uncertainties could be included more robustly in the the method itself, which would also produce the full posterior distribution of the parameters, providing a complete accounting of the covariance between the fit parameters.

An improved method such as this will be required in the near future as the datasets will become large enough to expose the inadequacies of the present methods. Furthermore, a clearer understanding of the biases in the method and covariance between parameters will be required in order to study the redshift evolution of the HIMF, a key goal of the next generation of HI surveys.

7.3 Surface brightness sensitivity limits

The next generation of blind HI surveys will be carried out with interferometers rather than single-dish telescopes. While this provides a great improvement in angular resolution it also complicates a survey's sensitivity limit. A typical nearby galaxy is on the order of an arcmin across, which, for either Arecibo or Parkes, fits comfortably in a single beam. However, with MeerKAT, ASKAP, or the VLA such a source would be spread out over somewhere between 4 and over 100 synthesised beams. As the background noise grows like the square root of the number

of pixels summed together, this means that the integrated flux sensitivity is poorer when a source is resolved. In other words an interferometric survey's completeness limit is not just a function of HI flux and velocity width (as for single-dish surveys), but also of angular size.

An accurate understanding of a survey's completeness limit is an essential component for any statistical analysis of the HI population. In order to probe the underlying HI population the observational biases due to a survey's sensitivity must first be corrected for. Duffy et al. (2012) estimated the impact of resolving sources on future survey detection counts, predicting that approximately 15% of the detections that WALLABY is expected to make would actually be below the detection threshold due to the sources being resolved. However, that paper did not explore how the nominal completeness limit could be adjusted to account for this effect, and only simulated sources with more than $10^{8.5}$ $M_{\odot}$ of HI, and therefore could not probe the lowest mass range of nearby dwarfs where these effect are likely to be most severe.

In order to produce mock catalogues (used in chapter 2, 3 and 4) we developed a computationally cheap method to generate realistic mass and velocity width values of the underlying HI galaxy population. By extending this method to also include a prescription for the extent of the HI disc, the impact of resolving targets on sensitivity limits could be further explored, potentially leading to a new expression for the form of the anticipated completeness limits of the next generation of HI surveys.

APPENDIX A

APPENDIX OF CHAPTER 2

A.1 Detection Limit

In order to develop a general expression for the detection threshold of a survey given its predicted rms noise per channel, channel width, and redshift range; we follow Giovanelli et al. (2005), which made a prediction for ALFALFA's detection limit, and make changes where appropriate.

The peak flux from an HI source (Jy) can be approximated as

$$S_{\rm peak} = \frac{M_{\rm HI}}{2.356 \times 10^5 d^2 W(1+z)} \frac{\rm Mpc^2\,km\,s^{-1}}{\rm M_\odot}, \tag{A.1}$$

where $M_{\rm HI}$ is the HI mass of the galaxy in $M_\odot$, W is its velocity width in $\rm km\,s^{-1}$ (corrected for cosmological expansion), and d is the comoving distance (using WMAP9 cosmology from Hinshaw et al., 2013) to it in Mpc. The factor of $(1+z)^{-1}$ results from competing effects due to the cosmological expansion (Peacock, 1999; Abdalla & Rawlings, 2005).

For a given telescope and frontend one can measure (or model) the system temperature and gain, in order to predict the rms noise per channel. Assuming this number ($S_{\rm rms}$) is available, the only aspects left to consider are the fraction of the source contained within the beam or synthesised beam (f_b), and the effect of smoothing to maximise signal to noise (S/N). This leaves us with the following

expression for S/N

$$S/N = \frac{M_{\rm HI} f_b \sqrt{f_{\rm smo}}}{235.6\, d^2 W S_{\rm rms}} \frac{\rm mJy\, Mpc^2\, km\, s^{-1}}{\rm M_\odot}, \tag{A.2}$$

where $f_{\rm smo}$ is the number of channels that the signal can be smoothed over. Here an additional factor of $(1+z)$ enters, which cancels out the previous factor, due to the fact that a uniformly tiled (or drift scan) survey effectively integrates a given point in the sky for longer at higher redshift, because the beam area grows in proportion to $(1+z)^2$, resulting in a factor of $(1+z)$ increase in expected sensitivity. As noted in Duffy et al. (2012), ASKAPs PAFs are designed to maintain approximately constant overlap between synthesised beams, regardless of redshift, which will negate this second effect. Therefore, equation A.2 will have a factor of $(1+z)^{-1}$ when considering ASKAP's HI surveys.

As long as smoothing occurs over regions containing signal, it will give a $\sqrt{f_{\rm smo}}$ increase to the S/N; as the signal increases linearly with the number of channels smoothed over, but the noise only increase like the square root. However, in practice very broad HI profiles have much less flux at their centre frequency than in the two horns, thus at some point smoothing will give diminishing returns. Haynes et al. (2011) found that for ALFALFA the transition width (W_c) occurs at $\log W_c/{\rm km\, s^{-1}} = 2.5$, and we adopt this value throughout. Thus the maximum number of channels a source can be smoothed over, is just the ratio of the larger of W or W_c, to the channel width.

$$f_{\rm smo} = \frac{1}{\Delta v_{\rm ch}} \begin{cases} W & \text{if } W \leq W_c \\ W_c & \text{if } W > W_c \end{cases} \tag{A.3}$$

Where $\Delta v_{\rm ch}$ is the channel velocity width (at $z = 0$). No redshift dependence is included for $\Delta v_{\rm ch}$ as W is the intrinsic velocity width, that is, it is already corrected for cosmological redshift.

In order to set the threshold value of signal to noise for an HI detection, we compare this model to the 50% completeness limit found by Haynes et al. (2011) for the $\alpha.40$ sample, which has an $S_{\rm rms}$ of 3.4 mJy per 24.4 kHz channel. A signal to noise threshold of 5.75 gives a very close approximation to the measured completeness limit. In practice the completes of any survey will depend on the data reduction and extraction process. As ALFALFA implements both an automated extraction algorithm (Saintonge, 2007), and visually inspects every potential source, it is unlikely that a purely automated process will recover an equivalent threshold, and in this sense it can be considered a lower limit.

We adopt a S/N threshold of 5.75 to simulate ALFALFA's extraction process, and apply this to all other simulation, with the exception of HIPASS, where we used the published completeness surface (Zwaan et al., 2004). Also for simplicity, we assume $f_b = 1$ for all sources within all simulated surveys. This is essentially always true for single dish surveys, but interferometric surveys are likely to resolve a significant fraction of HI galaxies, which will somewhat degrade their detection capabilities.

A.2 2D Correlation Function

The correlation function gives the excess probability (compared to random) that at a given velocity and angular separation from a source, there is another source. To find the probability that a given source will be confused, we need to know what the probability that at least one other source is within a certain projected separation perpendicular to the line-of-sight, $\kappa_{\rm sep}$ (dependent on the telescope beam, and distance), and velocity separation, $\beta_{\rm sep}$ (dependent on the velocity widths of the two galaxies). This scenario is best described by an inhomogeneous Poisson process; a Poisson process where the occurrence rate varies with position. Using this framework gives the probability of another source being within $\kappa_{\rm sep}$ and $\beta_{\rm sep}$ as

$$p(\kappa_{\rm nearest} < \kappa_{\rm sep} \cap \beta_{\rm nearest} < \beta_{\rm sep}) = 1 - e^{-\left\langle N(\kappa_{\rm sep},\beta_{\rm sep})\right\rangle}, \tag{A.4}$$

where subscript 'nearest' denotes the values of the central source's nearest neighbour, and $\langle N\rangle$ was defined in section 2.2 as:

$$\begin{aligned}\langle N\rangle \;=\; & 2\int_{W_{\rm min}}^{W_{\rm max}}\int_{M_{\rm lim(}d,W_2)}^{M_{\rm max}} \phi(M_2)p(W_2|M_2) \\ & \int_0^{\frac{W_1+W_2}{2H_0}}\int_0^{\Theta_{\rm beam}d} 2\pi\kappa\,(1+\xi(\kappa,\beta))\;\mathrm{d}\kappa\,\mathrm{d}\beta\,\mathrm{d}M_2\,\mathrm{d}W_2,\end{aligned} \tag{A.5}$$

where here $\kappa_{\rm sep}$ corresponds to $\Theta_{\rm beam}d$, and $\beta_{\rm sep}$ is $(W_1 + W_2)/2H_0$.

In order to evaluate $\langle N\rangle$ we must first fit an expression to the 2D CF Papastergis et al. (2013). We take the simplest form that is not axisymmetric, a function that is

elliptical in the $\kappa\beta$-plane:

$$\xi(\kappa,\beta) = \left(\frac{1}{r_0}\sqrt{\frac{\kappa^2}{a^2} + \frac{\beta^2}{b^2}}\right)^{\gamma}, \tag{A.6}$$

where $ab = 1$ and the best fit gives $r_0 = 9.05$ Mpc, $a = 0.641$, and $\gamma = -1.13$. This fit and the data are shown in figure 2.2. This fit demonstrates that there is a slight 'finger of god' effect present in the data, as the velocity axis is stretched relative to the angular axis. On scales larger than 10 Mpc, the apparent contraction of structure along the line-of-sight becomes the more obvious effect, however we do not see this in our fit because we only fit the CF for separations smaller than 10 Mpc, as larger separations are not relevant to the study of confusion.

Now to calculate $N(\kappa,\beta)$ we must evaluate the spatial integrals in equation A.5, which gives

$$2\int_0^{\beta_{\rm sep}}\int_0^{\kappa_{\rm sep}} 2\pi\kappa\,(1+\xi(\kappa,\beta))\,{\rm d}\kappa{\rm d}\beta = 2\pi a\left[\frac{\beta_{\rm sep}\kappa_{\rm sep}^2}{ba^2} + I\right], \tag{A.7}$$

where

$$I = \frac{2\frac{\beta_{\rm sep}}{b}\left(\frac{\kappa_{\rm sep}}{a}\right)^{\gamma+2}(\gamma+3)}{(\gamma+2)(\gamma+3)r_0^{\gamma}}\left[{}_2F_1\left(\frac{1}{2},-\frac{\gamma}{2}-1;\frac{3}{2};-\frac{a^2\beta_{\rm sep}^2}{b^2\kappa_{\rm sep}^2}\right) - 2\left(\frac{\beta_{\rm sep}}{b}\right)^{\gamma+3}\right] \tag{A.8}$$

and ${}_2F_1$ is the Gaussian hypergeometric function. A similar solution to this integral was derived in DMS12, however that solution was found to be unstable over the relevant parameter space. The solution above was compared against numerical integration for a range of physical parameters and gave consistent results in all cases.

A.3 Conditional Velocity Width Function

Once the HI mass of a given galaxy, and its position relative to its neighbours, has been determined via the HIMF and the CF, its velocity width must also be determined before it is possible to assess whether it is involved in a spectroscopic blend with a neighbour. To calculate the mass conditional velocity width function (MCWF) we follow a similar approach to Martin et al. (2010), where a Gumbel distribution is fit to the velocity width distribution within narrow mass bins, however here we weight each data point by $1/V_{\rm eff}$ (see Zwaan et al., 2005; Papastergis et al., 2011). The trend in the parameters of the Gumbel fits is then modeled to produce a simple analytic expression for the probability of a galaxy of mass 10^m $\mathrm{M}_\odot$ having a velocity width 10^w $\mathrm{km\,s^{-1}}$.

$$p(w|m) = \frac{1}{\beta(m)} \frac{e^{-\left(z(m)+e^{-z(m)}\right)}}{e^{-e^{-z_{\rm min}}} - e^{-e^{-z_{\rm max}}}}, \tag{A.9}$$

where $z = \frac{\mu(m)-w}{\beta(m)}$, $z_{\rm min}$ and $z_{\rm max}$ correspond to the minimum and maximum allowed values of w, μ is the distribution center, and β is its width, which are given by

$$\mu = 0.322m - 0.728 \tag{A.10}$$

and

$$\beta = \begin{cases} -0.0158m + 0.316 & \text{if } m \leq 9.83 \\ -0.0578m + 0.729 & \text{if } m > 9.83 \end{cases} \tag{A.11}$$

Additionally the above distribution is only valid for $\log 15 < w < 3$, and is set to zero beyond these to prevent the production of unphysical velocity widths.

APPENDIX B

APPENDIX OF CHAPTER 4

B.1 Robustness of Results

B.1.1 Impact of Confusion

In Jones et al. (2015) we warned that source confusion acts to increase the observed value of M_*, and that as confusion is undoubtedly a function of environment, caution must be used when looking for environmental trends in that parameter. The shift observed here is approximately 0.2 dex, whereas in Jones et al. (2015) the maximum shift created by confusion in an ALFALFA-like survey was estimated to be 0.06 dex. This indicates that confusion is very unlikely to be the source of the trend detected.

B.1.2 Testing Cosmic Variance

To test whether the results were biased by the particular directions the ALFALFA survey mapped we carried out two additional tests. The first was to simply eliminate the Virgo cluster. The Virgo cluster is the most dominant nearby, large scale feature in the Spring sky (where there is also SDSS coverage), and due to its proximity it raises the question of whether we can detect systems there that we would

never see if it were at a distance more typical of the other clusters in the survey, and whether this might bias our results. By removing all sources with recession velocities less than 3,000 $\mathrm{km\,s^{-1}}$, we remove almost all those objects associated with Virgo, and repeat our analysis.

Though clipping the inner 3,000 $\mathrm{km\,s^{-1}}$ of the data severely impacts our ability to constrain the low-mass slope, the trend in the 'knee' mass is still preserved, indicating that the exceptional location of Virgo is not the driving force behind this result.

The second test of cosmic variance involves comparing the Spring and Fall skies. As there is little spectroscopic SDSS coverage in Arecibo's Fall sky, this must rely on comparison with 2MRS. As shown in §4.5.2 when all of ALFALFA 70% is considered with environment defined using 2MRS there is no apparent trend in M_* or α with environment. This could either be due to the previous trend being a property only of the Spring sky (cosmic variance) or due to the differences between 2MRS and SDSS as reference catalogues. To assess which it was the same analysis was repeated again, but now only considering ALFALFA sources in the Spring sky. As before, when environment is defined by 2MRS, there is no apparent trend in M_* or α, suggesting that the trend observed with SDSS is indeed real and not due to cosmic variance, and that that apparent lack of such a trend with environment define by 2MRS is due to differences in the galaxies detected in those two surveys.

B.1.3 Independence and Covariance

In order to ensure that our findings are not dependent on the exact magnitude limits we set to make the SDSS and 2MRS catalogues volume limited, we repeated our analysis with three additional samples with ranges of 1,000-6,000, 1,000-8,000, and 1,000-12,000 km s^{-1}/H_0 in ALFALFA, and an additional 500 km s^{-1}/H_0 at either edge in SDSS and 2MRS. The trend in M_* shown in figure 4.9 appears in all three additional samples when compared to SDSS (but not any 2MRS reference sample), although the error ellipses become progressively larger as the samples get smaller. The apparent shift in α is also persistent across all the different ALFALFA samples, suggesting that it is statistically significant. However, not only should caution be used because α and M_* are highly covariant (and the assumed Gaussian errors likely do not fully encompass this dependence), but the four samples themselves are not independent because the galaxies in the 1,000-6,000 km s^{-1} catalogue are contained within the other three. While this latter point is unimportant for fitting M_*, as those galaxies are detectable by ALFALFA throughout all the samples, the galaxies in the 1,000-6,000 km s^{-1} catalogue dominate the low-mass population. Therefore if the trend in α with environment is not significant in the main sample (as was shown in §4.6), then it is not significant.

We also wished to check that the difference between the SDSS and 2MRS definitions of environment were due to the scale probed and not the colour of the reference population. To do this the SDSS catalogue was split into blue and red subcatalogues, with the division occurring at $u - r = 2.2$. The third nearest neighbour

environment was then re-calculated for the red and blue reference catalogues separately. The trend in M_* remained significant in both samples, though the range of M_* was marginally larger when environment was defined by the blue population. The modal values of the neighbour densities were equivalent between the red and blue nearest neighbour environments, with the distribution of densities defined by the red population showing a slightly longer tail towards high density.

B.2 HIPASS Low-mass Slope Trend

Other than studies based on ALFALFA, the largest sample used to study the variation of the HIMF with environment was carried out with the HIPASS dataset (Barnes et al., 2001). In particular, Zwaan et al. (2005) found that the HIMF low-mass slope, α, becomes steeper in higher density environments (see their figure 3). On the other hand, they found no trend of M_* with environmental density. In this section, we try to assess whether the presence of such an environmental trend would be detectable in the 70% ALFALFA sample. In order to do that, we first divide the sample into five equally spaced logarithmic bins in local density. We quantify the local density as described in §4.3.2, i.e. by considering the 3$^{\rm rd}$ nearest neighbour in the SDSS reference catalogue. Note that the environmental division scheme considered here tries to reproduce the one used in Zwaan et al. (2005), and it is not the same as the one used to create our Figure 4.3. In particular, here we split galaxies into five logarithmic density bins of equal width, while Figure

4.3 refers to four environmental sub-samples defined such that each contains the same number of objects.

We then create five mock samples, each consisting of approximately the same number of objects as one of the five real environmental subsamples in ALFALFA. The five mock samples are further created to reproduce the large-scale structure observed for their corresponding ALFALFA subsample. The mock samples mimic the environmental dependence of the HIMF found by HIPASS: the low-mass slope ranges from $\alpha = -1.2$ for the lowest density subsample to $\alpha = -1.52$ for the highest density one, while the 'knee' mass is kept fixed at $\log(M_*/M_\odot) = 9.94$.

We measure the HIMF in each of the five real and each of the five mock environmental subsamples, always using the same methodology (refer to Sec. 4.4). The result is shown in Figure B.1: The upper row shows the five HIMFs for the real environmental subsamples in ALFALFA, while the bottom row shows the HIMFs measured for the five mock samples. As expected based on the results of §4.5.1, we see in the top row a clear trend of increasing M_* value in higher density environments, and no significant environmental trend in α. On the other hand, the bottom row reproduces very well the HIPASS-like environmental trend used to create the five mocks; the low-mass slope becomes steeper with increasing environmental density, while there is no significant environmental dependence of M_*. Figure B.1 demonstrates that if an environmental dependence of the HIMF similar to what measured by HIPASS were indeed present in the 70% ALFALFA catalogue, it would have easily been detected in our current analysis.

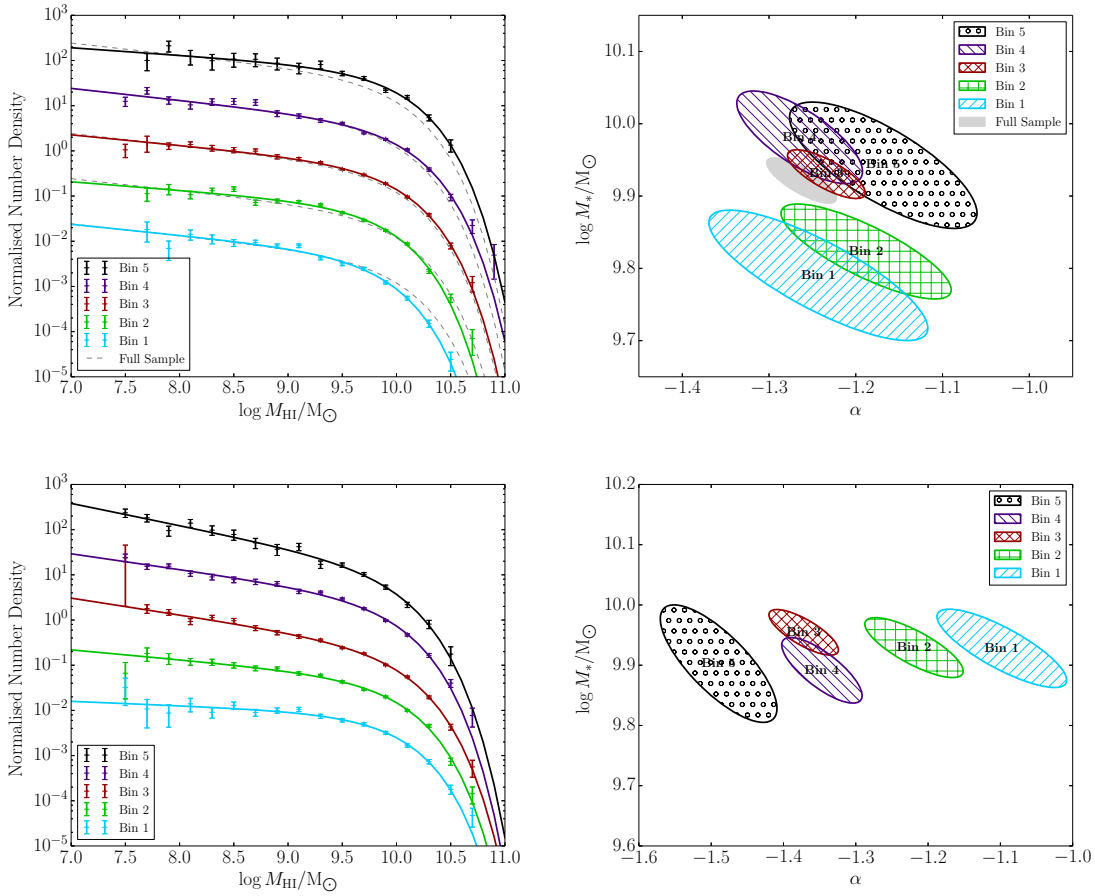

Figure B.1: *Top row*: HIMFs (*left panel*) and Schechter parameter error ellipses (*right panel*) for the five environmental ALFALFA subsamples defined in Appendix B.2. The layout of the figure follows the layout of figure 4.9, where HIMF colours from black to light blue (dark shades to light shades, and HIMF positions from top to bottom) correspond to subsamples of progressively lower environmental density. *Bottom row*: Same as the top row, but for the five mock environmental subsamples, which are created to mimic the HIMF trends reported by Zwaan et al. (2005) based on the HIPASS dataset (see Appendix B.2 for details). The figure demonstrates that, if the HIMF trend claimed by Zwaan et al. (2005) were present in the ALFALFA sample, it would have been easily detected.

At the same time, keep in mind that the comparison between the HIPASS and ALFALFA results is subject to one caveat. In particular, the HIPASS trend was detected when the environment was defined in terms of the 3rd, 5th and 10th nearest HIPASS neighbour (Figure 4 in Zwaan et al., 2005). However, the HIPASS HI-selected sample is much sparser than the SDSS reference catalogue used to calculate 3rd nearest neighbour densities for ALFALFA galaxies. It cannot be excluded therefore that the trend observed by HIPASS is present only when environment is defined on very large scales, but is absent when local environment is considered. Please refer to §4.6.1 for a more thorough discussion of the tension with the HIPASS result.

B.3 Robustness of the HIMF to LSS

There is substantial deviation from a uniform distribution of galaxy positions in the ALFALFA sample due to the LSS in the nearby Universe, therefore it is important to confirm that the $1/V_{\rm eff}$ method for calculating the HIMF (see §4.4) is robust to such deviations. To check this we used the methodology of Jones et al. (2015) to create a uniform mock catalogue of approximately 15,000 HI sources. A second catalogue was produced by adding Gaussian overdensities of sources at distances of 20 and 100 Mpc, in order to simulate the Virgo cluster at the Great Wall, two major structures in the ALFALFA footprint. Finally, a third catalogue was made with sources removed from around 100 Mpc to create an effective void. Each of

these three mocks was generated 30 times with input Schechter function shape parameters $\alpha = -1.30$ and $M_* = 9.95$. The mean values derived from the samples using the $1/V_{\rm eff}$ method were $\alpha = -1.28 \pm 0.01$ and $M_* = 9.96 \pm 0.01$, $\alpha = -1.27 \pm 0.01$ and $M_* = 9.96 \pm 0.01$, $\alpha = -1.27 \pm 0.01$ and $M_* = 9.96 \pm 0.01$, for the uniform mock, mock with overdensities, and the mock with a void, respectively. Similar experiments were carried out for a variety of input parameters (α and M_*) and gave equivalent results.

These results illustrate two important points: a) the $1/V_{\rm eff}$ method appears to be very robust against density deviations along the light of sight, b) the method has a slight systematic bias towards flatter low-mass slopes at the level of the second decimal place. This bias in the maximum likelihood methods has been known for some time (e.g. Efstathiou, Ellis & Peterson, 1988; Willmer, 1997) and is not presently a major concern given our level of precision, however for future surveys with larger datasets a different estimator may be required.

BIBLIOGRAPHY

Abazajian K. N. et al., 2009, ApJS, 182, 543

Abdalla F. B., Rawlings S., 2005, MNRAS, 360, 27

Ahn C. P. et al., 2014, ApJS, 211, 17

Aihara H. et al., 2011, ApJS, 193, 29

Barnes D. G. et al., 2001, MNRAS, 322, 486

Berlind A. A., Blanton M. R., Hogg D. W., Weinberg D. H., Davé R., Eisenstein D. J., Katz N., 2005, ApJ, 629, 625

Berlind A. A. et al., 2006, ApJS, 167, 1

Binggeli B., Sandage A., Tammann G. A., 1985, AJ, 90, 1681

Blanton M. R., Eisenstein D., Hogg D. W., Zehavi I., 2006, ApJ, 645, 977

Branchini E. et al., 2001, MNRAS, 326, 1191

Carollo C. M. et al., 2013, ApJ, 776, 71

Chang T.-C., Pen U.-L., Bandura K., Peterson J. B., 2010, Nature, 466, 463

Crook A. C., Huchra J. P., Martimbeau N., Masters K. L., Jarrett T., Macri L. M., 2007, ApJ, 655, 790

da Costa L. N., Freudling W., Wegner G., Giovanelli R., Haynes M. P., Salzer J. J., 1996, ApJL, 468, L5

Delhaize J., Meyer M. J., Staveley-Smith L., Boyle B. J., 2013, MNRAS, 433, 1398

Duffy A. R., Battye R. A., Davies R. D., Moss A., Wilkinson P. N., 2008, MNRAS, 383, 150

Duffy A. R., Meyer M. J., Staveley-Smith L., Bernyk M., Croton D. J., Koribalski B. S., Gerstmann D., Westerlund S., 2012, MNRAS, 426, 3385

Duffy A. R., Moss A., Staveley-Smith L., 2012, Publ. of the Astron. Soc. of Australia, 29, 202

Efstathiou G., Ellis R. S., Peterson B. A., 1988, MNRAS, 232, 431

Eisenstein D. J., Loeb A., Turner E. L., 1997, ApJ, 475, 421

Erdoğdu P. et al., 2006, MNRAS, 373, 45

Fabello S., Catinella B., Giovanelli R., Kauffmann G., Haynes M. P., Heckman T. M., Schiminovich D., 2011a, MNRAS, 411, 993

Fabello S., Kauffmann G., Catinella B., Giovanelli R., Haynes M. P., Heckman T. M., Schiminovich D., 2011b, MNRAS, 416, 1739

Fabello S., Kauffmann G., Catinella B., Li C., Giovanelli R., Haynes M. P., 2012, MNRAS, 427, 2841

Fernández X. et al., 2013, ApJ, 770, L29

Freeland E., Stilp A., Wilcots E., 2009, AJ, 138, 295

Freudling W., da Costa L. N., Wegner G., Giovanelli R., Haynes M. P., Salzer J. J., 1995, AJ, 110, 920

Freudling W. et al., 2011, ApJ, 727, 40

Galaz G., Herrera-Camus R., Garcia-Lambas D., Padilla N., 2011, ApJ, 728, 74

Giovanelli R. et al., 2013, AJ, 146, 15

Giovanelli R., Haynes M. P., Herter T., Vogt N. P., da Costa L. N., Freudling W., Salzer J. J., Wegner G., 1997, AJ, 113, 53

Giovanelli R. et al., 2005, AJ, 130, 2598

Giovanelli R., Haynes M. P., Salzer J. J., Wegner G., da Costa L. N., Freudling W., 1994, AJ, 107, 2036

Gottloeber S., Hoffman Y., Yepes G., 2010, ArXiv e-prints

Haider M., Steinhauser D., Vogelsberger M., Genel S., Springel V., Torrey P., Hernquist L., 2016, MNRAS, 457, 3024

Han M., Mould J. R., 1992, ApJ, 396, 453

Hanski M. O., Theureau G., Ekholm T., Teerikorpi P., 2001, A&A, 378, 345

Hartley W. G. et al., 2010, MNRAS, 407, 1212

Haynes M. P., Giovanelli R., Chincarini G. L., 1984, ARA&A, 22, 445

Haynes M. P. et al., 2011, AJ, 142, 170

Hess K. M., Wilcots E. M., 2013, AJ, 146, 124

Hinshaw G. et al., 2013, ApJS, 208, 19

Hoeft M., Yepes G., Gottlöber S., Springel V., 2006, MNRAS, 371, 401

Hoffman Y., Courtois H. M., Tully R. B., 2015, MNRAS, 449, 4494

Holwerda B. W., Blyth S.-L., Baker A. J., 2012, in IAU Symposium, Vol. 284, IAU Symposium, Tuffs R. J., Popescu C. C., eds., pp. 496–499

Hoppmann L., Staveley-Smith L., Freudling W., Zwaan M. A., Minchin R. F., Calabretta M. R., 2015, MNRAS, 452, 3726

Hoyle F., Rojas R. R., Vogeley M. S., Brinkmann J., 2005, ApJ, 620, 618

Hoyle F., Vogeley M. S., 2002, ApJ, 566, 641

Hoyle F., Vogeley M. S., 2004, ApJ, 607, 751

Huang S., Haynes M. P., Giovanelli R., Brinchmann J., 2012a, ApJ, 756, 113

Huang S., Haynes M. P., Giovanelli R., Brinchmann J., 2012b, ApJ, 756, 113

Huchra J. P. et al., 2012, ApJS, 199, 26

James B. L., Koposov S., Stark D. P., Belokurov V., Pettini M., Olszewski E. W., 2015, MNRAS, 448, 2687

Jones M. G., Haynes M. P., Giovanelli R., Papastergis E., 2016a, MNRAS, 455, 1574

Jones M. G., Papastergis E., Haynes M. P., Giovanelli R., 2015, MNRAS, 449, 1856

Jones M. G., Papastergis E., Haynes M. P., Giovanelli R., 2016b, MNRAS, 457, 4393

Kovac K., Oosterloo T. A., van der Hulst J. M., 2005, in IAU Colloq. 198: Near-fields cosmology with dwarf elliptical galaxies, Jerjen H., Binggeli B., eds., pp. 351–354

Lah P. et al., 2007, MNRAS, 376, 1357

Maddox N., Hess K. M., Blyth S.-L., Jarvis M. J., 2013, MNRAS, 433, 2613

Martin A. M., Giovanelli R., Haynes M. P., Guzzo L., 2012, ApJ, 750, 38

Martin A. M., Papastergis E., Giovanelli R., Haynes M. P., Springob C. M., Stierwalt S., 2010, ApJ, 723, 1359

Masters K. L., 2005, PhD thesis, Cornell University, New York, USA

Masters K. L., Springob C. M., Haynes M. P., Giovanelli R., 2006, ApJ, 653, 861

McGaugh S. S., 2012a, AJ, 143, 40

McGaugh S. S., 2012b, AJ, 143, 40

McGaugh S. S., Schombert J. M., Bothun G. D., de Blok W. J. G., 2000, ApJL, 533, L99

Meyer M., 2009, in Panoramic Radio Astronomy: Wide-field 1-2 GHz Research on Galaxy Evolution, p. 15

Meyer M. J. et al., 2004, MNRAS, 350, 1195

Moorman C. M., Vogeley M. S., Hoyle F., Pan D. C., Haynes M. P., Giovanelli R., 2014, MNRAS, 444, 3559

Muldrew S. I. et al., 2012, MNRAS, 419, 2670

Nan R., 2006, Science in China: Physics, Mechanics and Astronomy, 49, 129

Nguyen H. T. et al., 2010, A&A, 518, L5

Papastergis E., Adams E. A. K., van der Hulst J. M., 2016, ArXiv e-prints

Papastergis E., Giovanelli R., Haynes M. P., Rodríguez-Puebla A., Jones M. G., 2013, ApJ, 776, 43

Papastergis E., Giovanelli R., Haynes M. P., Shankar F., 2015, A&A, 574, A113

Papastergis E., Martin A. M., Giovanelli R., Haynes M. P., 2011, ApJ, 739, 38

Peacock J. A., 1999, Cosmological Physics. Cambridge University Press

Peebles P. J. E., 2001, ApJ, 557, 495

Pisano D. J., Barnes D. G., Staveley-Smith L., Gibson B. K., Kilborn V. A., Freeman K. C., 2011, ApJS, 197, 28

Press W. H., Schechter P., 1974, ApJ, 187, 425

Prochaska J. X., Wolfe A. M., 2009, ApJ, 696, 1543

Rao S. M., Turnshek D. A., Nestor D. B., 2006, ApJ, 636, 610

Rhee J., Zwaan M. A., Briggs F. H., Chengalur J. N., Lah P., Oosterloo T., van der Hulst T., 2013, MNRAS, 435, 2693

Rojas R. R., Vogeley M. S., Hoyle F., Brinkmann J., 2004, ApJ, 617, 50

Rosenberg J. L., Schneider S. E., 2000, ApJS, 130, 177

Rosenberg J. L., Schneider S. E., 2002, ApJ, 567, 247

Saintonge A., 2007, AJ, 133, 2087

Schechter P., 1976, ApJ, 203, 297

Skrutskie M. F. et al., 2006, AJ, 131, 1163

Solanes J. M., Sanchis T., Salvador-Solé E., Giovanelli R., Haynes M. P., 2002, AJ, 124, 2440

Sorce J. G. et al., 2016, MNRAS, 455, 2078

Springel V. et al., 2005, Nature, 435, 629

Springob C. M., 2006, PhD thesis, Cornell University, New York, USA

Springob C. M., Haynes M. P., Giovanelli R., 2005, ApJ, 621, 215

Springob C. M., Haynes M. P., Giovanelli R., Kent B. R., 2005, ApJS, 160, 149

Springob C. M. et al., 2016, MNRAS, 456, 1886

Stierwalt S., Haynes M. P., Giovanelli R., Kent B. R., Martin A. M., Saintonge A., Karachentsev I. D., Karachentseva V. E., 2009, AJ, 138, 338

Theureau G., Hanski M. O., Coudreau N., Hallet N., Martin J.-M., 2007, A&A, 465, 71

Theureau G., Rauzy S., Bottinelli L., Gouguenheim L., 1998, A&A, 340, 21

Tinker J. L., Conroy C., 2009, ApJ, 691, 633

Tonry J. L., Blakeslee J. P., Ajhar E. A., Dressler A., 2000, ApJ, 530, 625

Toribio M. C., Solanes J. M., Giovanelli R., Haynes M. P., Martin A. M., 2011, ApJ, 732, 93

Tully R. B. et al., 2013, AJ, 146, 86

Tully R. B., Fisher J. R., 1977, A&A, 54, 661

Verheijen M. A. W., Trentham N., Tully B., Zwaan M., 2001, in Astronomical Society of the Pacific Conference Series, Vol. 240, Gas and Galaxy Evolution, Hibbard J. E., Rupen M., van Gorkom J. H., eds., p. 507

Vogelsberger M. et al., 2014, MNRAS, 444, 1518

Walter F., Brinks E., de Blok W. J. G., Bigiel F., Kennicutt, Jr. R. C., Thornley M. D., Leroy A., 2008, AJ, 136, 2563

Wechsler R. H., Zentner A. R., Bullock J. S., Kravtsov A. V., Allgood B., 2006, ApJ, 652, 71

Wegner G., Haynes M. P., Giovanelli R., 1993, AJ, 105, 1251

Willmer C. N. A., 1997, AJ, 114, 898

York D. G. et al., 2000, AJ, 120, 1579

Zaritsky D. et al., 2014, AJ, 147, 134

Zhong G. H., Liang Y. C., Liu F. S., Hammer F., Hu J. Y., Chen X. Y., Deng L. C., Zhang B., 2008, MNRAS, 391, 986

Zwaan M. A., Meyer M. J., Staveley-Smith L., Webster R. L., 2005, MNRAS, 359, L30

Zwaan M. A. et al., 2004, MNRAS, 350, 1210

Zwaan M. A. et al., 2003, AJ, 125, 2842